University of Nevada, Reno

Surface and Sub-Surface Analyses for Bridge Inspection

A dissertation submitted in partial fulfillment of the
requirements for the degree of Doctor of Philosophy in
Computer Science and Engineering

by
Habib Ahmed

Dr. Hung Manh La/Dissertation Advisor

December 2022

THE GRADUATE SCHOOL

We recommend that the dissertation prepared
under our supervision by

HABIB AHMED

Entitled

Surface and Sub-Surface Analyses for Bridge Inspection

be accepted in partial fulfillment of the requirements for
the degree of

DOCTOR OF PHILOSOPHY

Hung Manh La, Advisor

Sushil Louis, Committee Member

Monica Nicolescu, Committee Member

Khiem Tran, Committee Member

Gokhan Peckan, Graduate School Representative

Markus Kemmelmeier, Ph. D., Dean, Graduate School

December 2022

Abstract

by Habib Ahmed

The development of bridge inspection solutions has been discussed in the recent past. In this dissertation, significant development and improvement on the state-of-the-art in the field of bridge inspection using multiple sensors (e.g. ground penetrating radar (GPR) and visual sensor) has been proposed. In the first part of this research (discussed in chapter 3), the focus is towards developing effective and novel methods for rebar detection and localization for sub-surface bridge inspection of steel rebars. The data has been collected using Ground Penetrating Radar (GPR) sensor on real bridge decks. In this regard, a number of different approaches have been successively developed that continue to improve the state-of-the-art in this particular research area. The second part (discussed in chapter 4) of this research deals with the development of an automated system for steel bridge defect detection system using a Multi-Directional Bicycle Robot. The training data has been acquired from actual bridges in Vietnam and validation is performed on data collected using Bicycle Robot from actual bridge located in Highway-80, Lovelock, Nevada, USA. A number of different proposed methods have been discussed in chapter 4. The final chapter of the dissertation will conclude the findings from the different parts and discuss ways of improving on the existing works in the near future.

Acknowledgements

I would like to formally acknowledge Dr. Hung Manh La, Dr. Sushil Louis, Dr. Monica Nicolescu, Dr. Kheim Tran, and Dr. Gokhan Peckan for being part of the committee.

This work is supported by the U.S. National Science Foundation (NSF) under grants NSF-CAREER: 1846513 and NSF-PFI-TT: 1919127, and the U.S. Department of Transportation, Office of the Assistant Secretary for Research and Technology (USDOT/ OST-R) under Grant No. 69A3551747126 through INSPIRE University Transportation Center (http://inspire-utc.mst.edu) at Missouri University of Science and Technology. The views, opinions, findings and conclusions reflected in this publication are solely those of the authors and do not represent the official policy or position of the NSF and USDOT/OST-R.

Contents

List of Figures

Chapter 1

Introduction

Inspection of civil infrastructure by means of NDE techniques has been a growing research area of interest in the recent past. Of the different types of civil infrastructure, the need for maintenance and evaluation of bridges has been stressed by studies in the recent past [14], [15], [16], [17]. Some of the major emerging themes in recent studies can be classified into research related to technological platforms, sensors and instrumentation modules for data collection, and algorithms for data analyses. The monitoring, maintenance and rehabilitation of critical civil infrastructure during their life-cycle is of paramount importance. Of the different components of civil infrastructure, the need for periodic assessment, evaluation and maintenance of highway bridges has been emphasized by studies in the recent past [14], [15], [16], [17].

1.1 Manual Inspection of Bridges

Traditionally, assessment of civil infrastructures has been performed manually by human inspectors, relying primarily on visual inspection [18]. However, visual inspection work is time-consuming and prone to errors. Even the NDE methods, like GPR, require extensive effort to manually process raw data and extract relevant information [19]. Lack of adequate attention towards maintenance and monitoring of bridges can lead to disastrous incidents. The issue of bridge-related accidents will be discussed in the next section. At the same time, a number of different bridge-related accidents in the US will be highlighted, which lead to considerable loss of lives, property and significant costs overhead.

The NDE of civil infrastructure has been a widely discussed research area in the recent past. Figure 1.1 highlights the chronological developments in the research field of the NDE of civil infrastructure, in particular bridge inspection. It can be seen from figure 1.1 that the beginning period (1950–1978) of this research area focused on the development of novel sensing technologies, for bridge inspection in particular, and civil infrastructure in general [20], [21], [22], [23], [24]. Some of the major sensing technologies developed include GPR, infrared thermography, electric resistivity sensors, impact-echo-based techniques and ultrasonic pulse propagation-based methods. After that time period, the focus was devoted towards using different sensor fusion techniques and their application towards bridge inspection and civil infrastructure evaluation [25], [26].

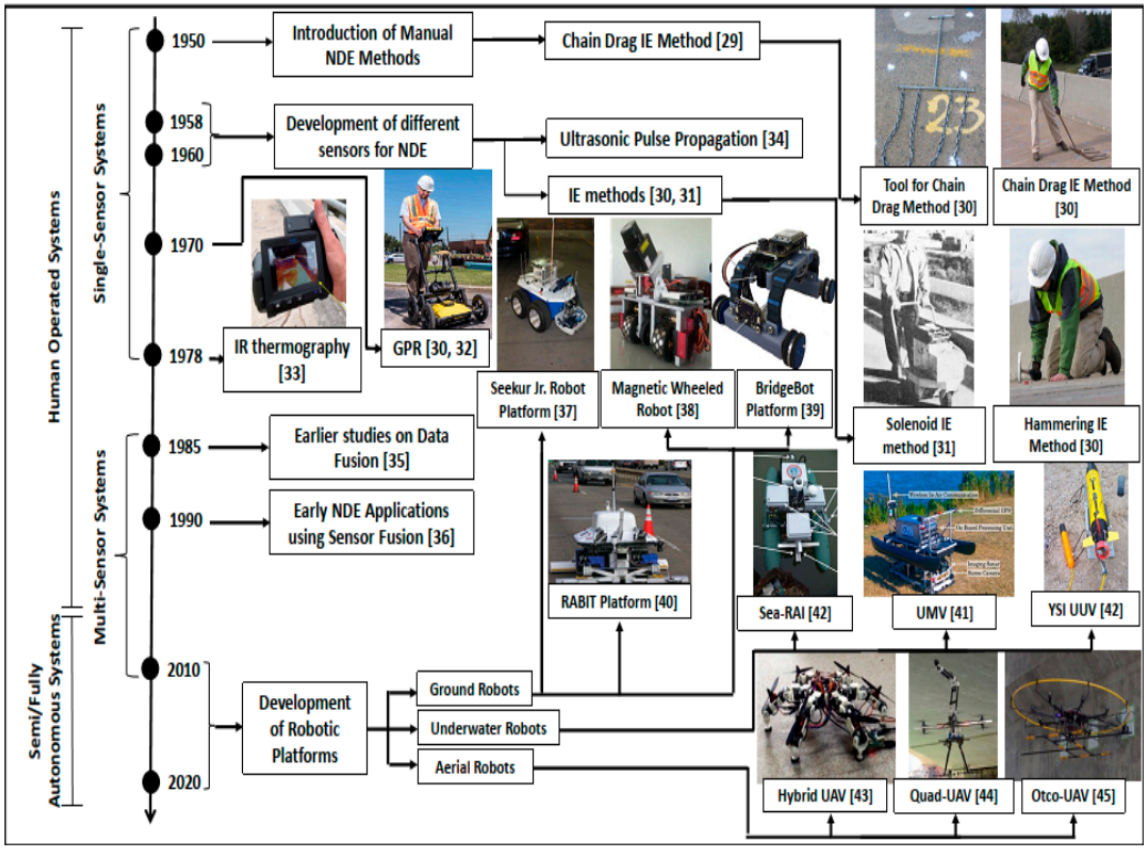

FIGURE 1.1: The development in the field of bridge inspection using NDE technologies

1.2 Bridge-related Accidents in the United States

According to the recent statistics in 2021 and 2022, there are more than 617,000 (620,000 by 2022 estimates) bridges in the entirety of the United States [27, 28]. A number of different factors contribute towards the partial or total destruction of bridges, ranging from design errors and construction defects to environmental degradation, scour, flood, collision and overloading [29], [30]. The impact of bridge destruction and collapse far exceeds the overall material and financial costs associated with the bridge construction, as it also includes the various direct and indirect costs,

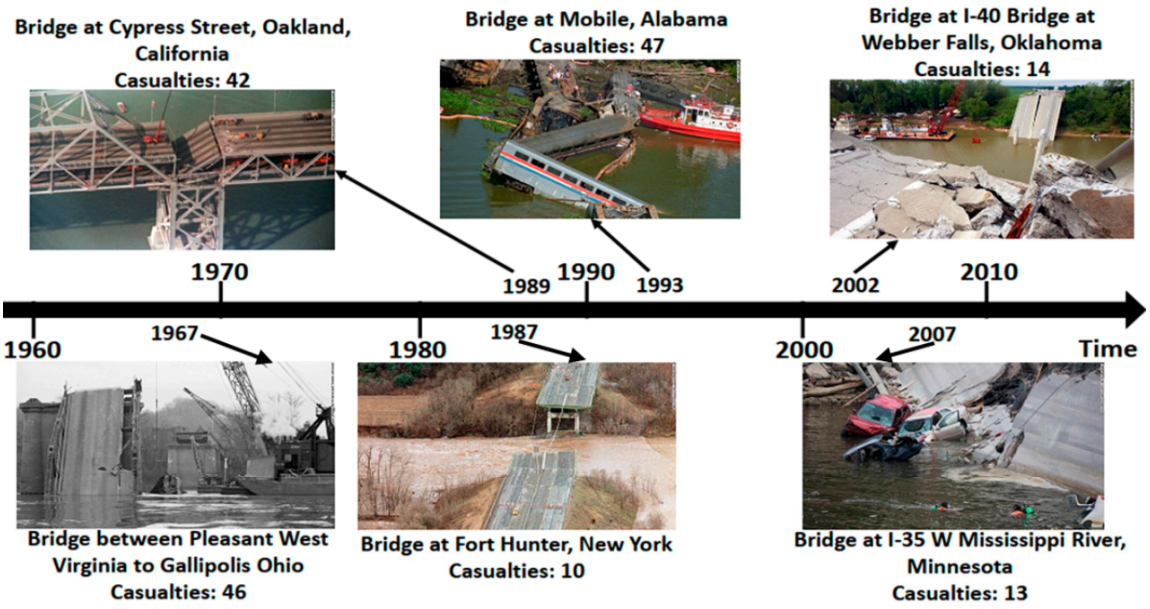

FIGURE 1.2: Bridge-related Disasters throughout the past decades in the United States, along with casualties reported for each incident

which include, but are not limited to loss of lives, user delays, planning for alternate routes, along with the greenhouse gas emissions linked to detours and delays in traffic [29], [31], [32], [33]. Some of the serious recent bridge accidents in the United States include a collapsed railroad bridge in Alabama that resulted in around 47 deaths and Collapsed bridge that connected Point Pleasant, West Virginia with Gallipolis, Ohio [14]. Figure 1.2 shows the major bridge-related incidents that took place in the past few decades in the United States. It can be seen that the bridge destruction is a recurring occurrence in the United States, which leads to devastating financial, economic, lass of lives and considerable incurred costs that could have been easily avoided.

1.3 Bridge Defect Statistics in the United States

The recent statistics (year 2020-2021) provided by the American Society of Civil Engineers (ASCE) on US infrastructure highlights that 46,154 bridges (out of total 617,000 bridges) have been categorized as structurally deficient in nature [27]. According to the US Department of Transportation [34], the number of bridges that can be categorized as "poor" or structurally deficient amount to 43,586 from a total of 619,622 bridges in the US. Another recent statistics from 2022 reveal that out of total 620,699 bridges in the US, 42,966 are labelled as having poor condition [28]. Although, the number of structurally deficient bridges has been declining over the past years (57,049 in 2012, 50,917 in 2015, 48,559 in 2018, 43,586 in 2021, 42,966 in 2022), rapidly ageing infrastructure (42% of bridges are more than 50 years old) and lack of adequate funding will cause a major backlog in bridges requiring repair and maintenance in the long-run [27, 28, 34]. For many decades, health and status assessment of these structures have been performed primarily through visual inspection using human inspectors. While this approach remains essential for structural health assessment, it presents significant limitations that hinder the detection of various defect types and extent of damage that may lead to undesired consequences. In addition to other types of inspection methods, non-destructive evaluation (NDE) techniques have the potential to streamline various forms of periodic inspections and to minimize the direct and indirect costs associated with failure of ageing bridges. Therefore, the timely evaluation, monitoring and rehabilitation of bridges can reduce

the overall direct as well as indirect costs and prevent loss of lives due to a possible structural failure and collapse. In the light of this realization, a number of national-level initiatives have been developed in the United States. One such example is the Long-Term Bridge Performance Program (LTBP) initiated by the Federal Highway Administration (FHWA) with the primary aim towards promoting the utilization of non-destructive evaluation technologies and techniques for regular bridge inspection and maintenance [35].

1.4 Costs of Bridge Repairs in the United States

In 2010, out of the $14.3 billion expenditure sanctioned for maintenance of existing bridges and construction of new bridges $12.8 billion was dedicated towards the maintenance of existing bridges [36]. According to the 2021 estimates, this amount of funding is insufficient and currently, $22.7 billion annual funding is required to improve the current situation in relation to bridge repair and maintenance [27]. It is being predicted that with the increase in climate change and frequency of adverse climate incidents (e.g. hurricane, floods, tsunamis) on a global scale, the overall costs related to bridge repair is also expected to accelerate from $140 billion to $250 billion annually [32] with direct and indirect losses amounting to more than 17% of the total costs [33]. Therefore, the timely evaluation, monitoring and rehabilitation of bridges can result in reduced overall direct costs as well as the indirect costs in terms of potential destruction of property and lives in the wake of bridge destruction.

For the purpose of bridge monitoring and evaluation, the different techniques for NDE have the potential towards minimizing the overall direct and indirect costs associated with destruction of bridges caused by internal deficiencies, construction deficits and maintenance-related issues. In the light of this realization, a number of national-level initiatives have been developed in the United States. One such example is the Long-Term Bridge Performance Program (LTBP) initiated by the Federal Highway Administration (FHWA) with the primary aim towards promoting the utilization of non-destructive evaluation technologies and techniques for regular bridge inspection and maintenance [37].

1.5 Objectives of this Dissertation

Prior sections have highlighted the different factors that act as motivation for development of systems for inspection of bridges. Therefore, the utilization of automation of inspections processes (e.g. rebar detection and localization system, steel defect detection system) will have broader, long-term objectives in relation to improving efficiency, reducing errors and costs of inspection. Since, these systems are currently in the developmental phases with constant efforts towards improvement in comparison with state-of-the-art systems, it will not be feasible to make estimations in relation to reducing costs and performance in comparison with human inspectors for a number of technical (the systems would need to operate regularly side-by-side with human

inspectors), economic and practical reasons. Therefore, the broad, long-term objective of research conducted in this dissertation is not to replace human inspectors, but to act as assistive technological systems that can reduce time, efficiency and performance of human inspectors. Due to the diverse nature of inspection on the different sections of the bridges, there is a need to clearly outline the scope and objectives of the dissertation. For example, bridges are large-scale structures with complex structures above and below the bridge deck with large-scale structural variations from one bridge to another. In this dissertation, the focus is not to provide inspection of the complete bridge structure. There are two prime aspects of this dissertation. Each aspect of this dissertation will focus on inspection of specific part of the bridge. It is for this reason, the objectives will be discussed separately for the two aspects of this dissertation, which are highlighted in the following sub-sections:

1.5.1 Sub-Surface-Level Analysis of Bridges for Rebar Detection and Localization System

The scope of sub-surface-level analysis performed in this dissertation will be limited to bridge decks. Even within bridge decks, there is a need to further limit the scope, as bridge decks can span for multiple miles with complex structures both above and below the bridge decks. Within the bridge decks, rebar detection and localization system deals with the detection and localization of parabola signals generated from GPR sensor with data collected from bridge decks, which contain steel rebars to

reinforce and support concrete bridge deck. For developing systems for rebar detection and localization, there is a need to improve on existing methods in terms of the approaches utilized with performance that is reliable after validation from real bridge dataset. Due to lack of available dataset and differences in proposed approaches, it is difficult to compare performance across different studies. Furthermore, different studies rely on diverging metrics for assessing system performance, which can further add to the challenges with respect to comparison between studies. Therefore, the major objective for developing rebar detection and localization system should be as follows:

(i). The proposed system should be novel in nature. It should not be a repetition of existing methods proposed in earlier studies for rebar detection and localization.

(ii). The proposed system should be trained, and validated on data from multiple real bridges. Using data from multiple bridges would ensure that the proposed system is robust and generalizable for developing practical bridge inspection systems with rebar detection and localization.

(iii). The proposed system should be able to provide reliable performance on data from multiple bridges. The selection of metrics can vary depending on the type of methods being utilized.

1.5.2 Surface-Level Analysis of Bridges for Steel Defect Detection System

The scope of surface-level analysis performed in this dissertation will be limited to steel structures in bridges. For developing steel defect detection system in bridges, there is no existing study in this regard. Consequently, there are no available approaches and benchmarks that can be used to compare the performance of the proposed system in defect detection system. Unlike the limited scope of rebar detection and localization to bridge deck, the steel defect detection system should be able to provide coverage to different steel parts of the bridges both above and underneath the bridge decks.

(i). The proposed system should be novel in nature. It should not be a repetition of existing methods proposed in earlier studies for defect detection system. Since, there are no existing approaches for defect detection systems for steel bridges, this aspect will not be an issue.

(ii). The proposed system should be trained and validated on data from multiple real bridges. Using data from multiple bridges would ensure that the proposed system is robust and generalizable for developing practical bridge inspection systems with defect detection system.

(iii). The proposed system should be able to provide reliable performance with data from robot platform equipped with high-quality visual sensor. The selection of metrics

can vary depending on the type of methods being utilized.

(iv). The proposed multi-directional bicycle robot is able to reach places on the bridge that are not easily accessible to human-inspectors. Due to the wireless operability of the robot platform, the inspectors can use the multi-directional robot to perform inspection tasks on inaccessible/hard to access areas of the bridge infrastructure without putting themselves in harms way.

1.6 Chapter Summary

In this chapter, a number of key motivation aspects related to automated solution for bridge inspection have been discussed. The earlier methods for non-destructive evaluation (NDE) are based on human inspectors. There are various issues related to the use of human inspectors to inspect bridges, which include human error, higher cost of inspection, and its time-consuming nature. As a result, it increases the chance of higher risk of bridge-related accidents, which usually are the result of small-scale errors and lack of proper judgments in inspecting different sections of the bridge. In the past few decades, it has been a regular occurrence in the United States that there are different bridge-related accidents leading to considerable costs, loss of lives and high amount of time taken to rebuilt the destroyed infrastructure. This further leads to increased costs towards maintaining and inspecting bridges in the United States. All of these factors act as catalysts towards developing algorithms, sensor deployment

and integration and implementation on a real-time multi-sensor, multi-robotic system for structural health monitoring and bridge inspection.

Chapter 2

Background

In this chapter, there are a number of different aspects of literature pertaining to automated systems for bridge inspection. surface and sub-surface analyses for bridge inspection. In light of this novel taxonomy, three key aspects of automated bridge inspection systems will be discussed, namely robot platforms, sensors and methods for surface-level and sub-surface-level analysis of bridges. The discussion regarding robot platforms for bridge inspection will be provided with respect to ground, aerial and underwater robots. At the same time, discussion regarding single sensor and multiple sensor system will be outlined. The discussion regarding methods will be divided into surface-level analysis and sub-surface-level analyses methods. In the context of surface-level analysis, the studies related to steel defect detection system and concrete crack detection system will be highlighted. In the context of sub-surface-level

analyses, the discussion regarding studies related to rebar detection and localization will be outlined.

2.1 Proposed Taxonomy for Automated Bridge Inspection Systems

In this section, a broad overview of the different automated solutions that have been proposed in the past few decades will be highlighted. The overall research area has been divided into three major streams with three major research aspects, namely the robotic platforms, sensors deployed on the robotic platforms, and the different algorithms developed for analyzing the different data from the wide-range of sensors deployed on the particular robot platforms. Each of these research streams will be separately discussed with considerable level of details, as given in the proceeding sub-sections.

2.1.1 Platforms

Different robotic platforms being used to assess the various physical characteristics of bridges. A taxonomy will be proposed, which will differentiate the different types of robot platforms for the NDE of bridges. Some of the essential components for bridge inspection will also be examined. Traditionally, infrastructure evaluation has been

considered a manual labor-intensive task, which is carried out by civil personnel using different sensors for data collection [38]. Despite recent technological advancements in this research area [38] [39] [40], a majority of the infrastructure evaluation is still performed by human operators using traditional modes for data collection, which are composed of standalone single sensor-based systems. In Figure 2.1, a better appreciation of the manner in which the available tools, techniques and platforms have evolved in recent years can be observed. It can be seen that there are fundamental divergences between the traditional methods and the innovative technological tools, techniques and platforms that have been employed for the NDE of civil infrastructure in the recent past.

Most of the traditional tools utilize single-sensor-based systems, which means that the overall hardware and software requirements and complexities are limited in nature. However, most of the traditional tools and techniques require human operators a considerable number of man-hours to collect the data for assessing the structural fitness for a particular type of infrastructure. In contrast, the technologically advanced tools and techniques are efficient, such that they can use a limited amount of time to collect data from a wide array of sensors to provide an in-depth and multi-faceted assessment of the different structural deficiencies within infrastructures. In recent decades, there has been an increased focus towards the development and usage of semi-autonomous and fully autonomous robots for the NDE of civil infrastructures in general and bridges in particular. A wide array of diverse robots have been developed ranging from climbing robots (e.g., legged robots, wheel-based sliding robots and

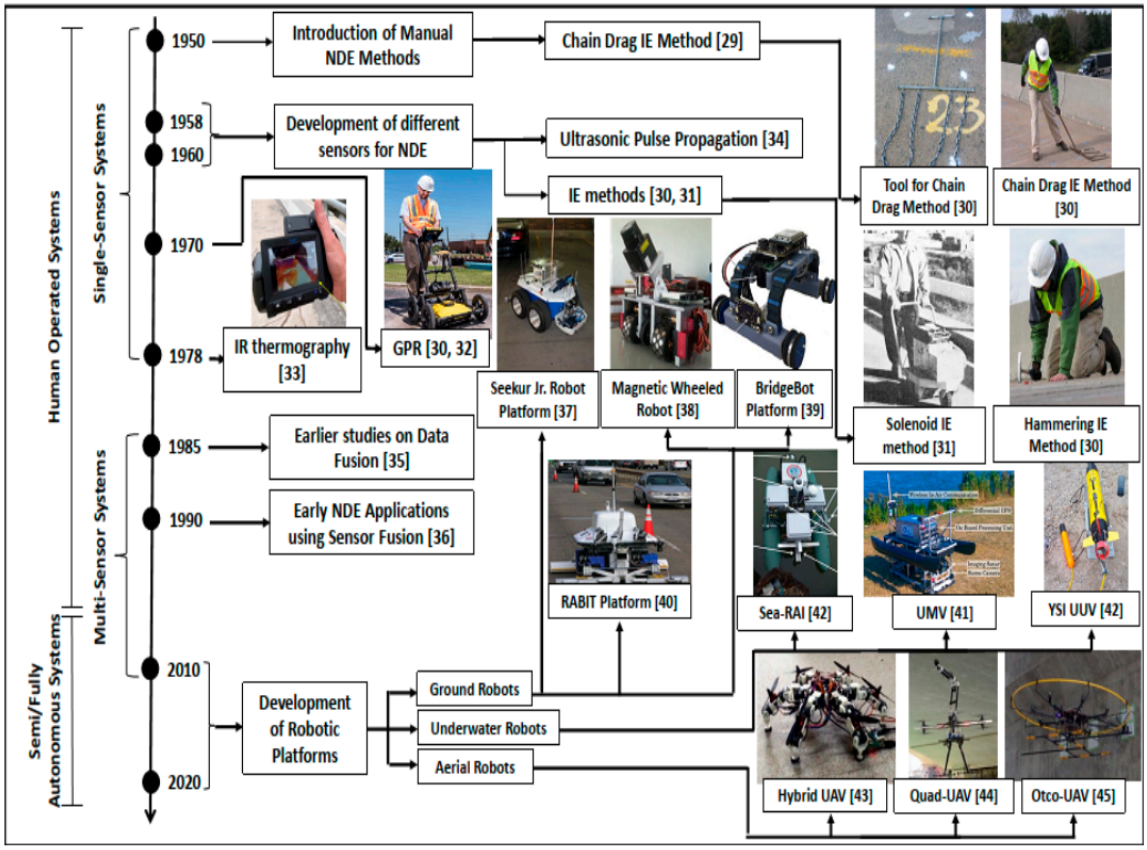

FIGURE 2.1: The development in the field of bridge inspection using NDE technologies

crawler robots) [41] [42] [30] [43] [38] [44] [45] [46] [47] [48] [49] [50] [51] [52] [53] [54] [55] [56], and multi-rotor unmanned aerial vehicles (e.g., quad-rotors and octo-rotors) [57] [58] [59] [60] [61] [60] [62] to unmanned ground vehicles (UGVs) (e.g., advanced robotics and automation (ARA) lab robot, robotic crack inspection and mapping (ROCIM), robotics-assisted bridge inspection tool (RABIT)) [5–9, 40, 63–68] and water-based robotic crafts (e.g., unmanned submersible vehicles (USVs), underwater marine vehicles (UMVs), underwater vehicles (UUVs)) [30, 69, 70].

Some of the recent studies have also focused towards developing hybrid robotic frameworks (e.g., wall-climbing unmanned aerial vehicles (UAVs), robots capable of flying and crawling and other multi-rotor flying robots capable of latching on to specific parts of infrastructure that require inspection), which are able to provide multi-functional roles and capabilities for the different types of inspection activities [10, 71–76]. A number of different types of robots (e.g., flying robots, walking robots, sliding robots, climbing robots, and underwater diving robots) have been leveraged for the NDE of bridges in order to gain access to different parts of the bridges. For example, evaluating and inspecting tall steel beams above bridges can be a hazardous task for human inspectors to perform during different environmental conditions (e.g., rain, snow, wind, day and night conditions). It is for this reason that different types of climbing and aerial robots have been used to facilitate these tasks. In particular, the versatility of the aerial robots has allowed their increased utilization for the inspection of the different parts of bridges, such as the inaccessible underside of the bridge decks, higher parts of the bridge beams and cables [30, 38, 47, 52, 59–61, 76]. Similarly, a number of different wheel-based and legged robots have also been used for inspecting concrete bridge decks, steel wires, concrete underside, and steel beams.

A number of different robot platforms are designed for inspection activities for specific types of bridges (e.g., cantilever, arch, suspension, truss, cable-stayed, beam, girder and tied-arch bridges) [30, 41–43, 45, 50, 52, 52, 53, 57–62, 65, 66, 77–79]. In order to provide some level of insight regarding the different robotic solutions for bridge inspection, the proceeding discussion will focus on the taxonomy provided in figure

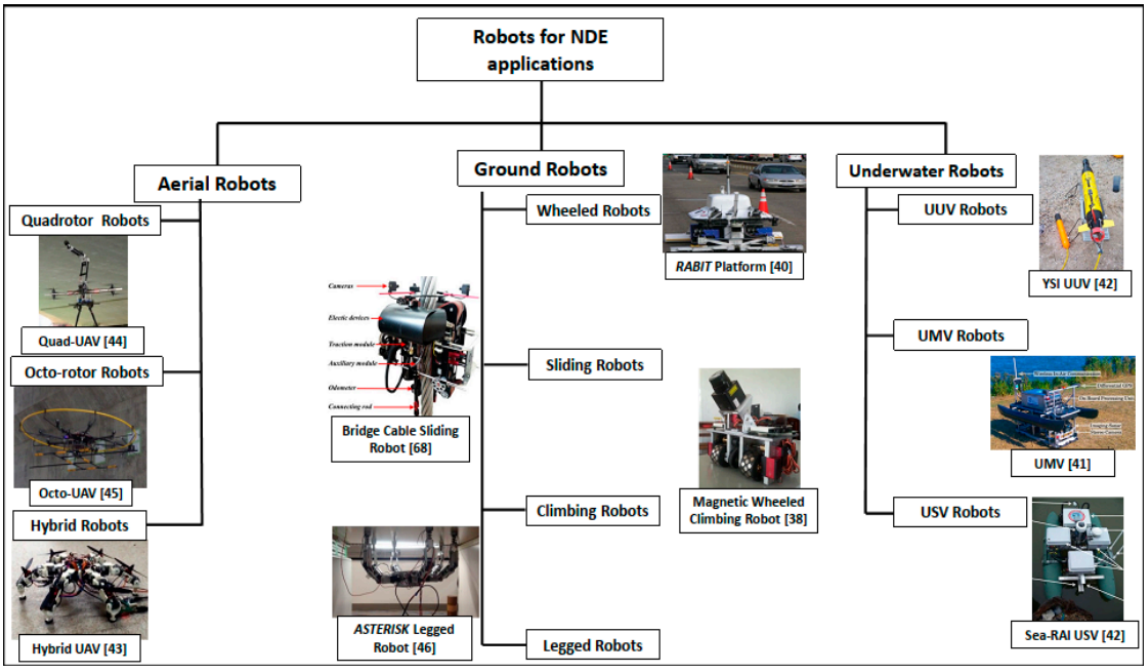

FIGURE 2.2: Taxonomy of different bridge robots, namely in the ground robots, aerial robots and marine robots categories

2.2, namely: (i) ground robots, (ii) aerial robots, and (iii) marine robots. Some details regarding the different platforms are outlined in the following sub-section:

2.1.1.1 Ground Robots

The majority of the robots developed for the NDE of bridges can be classified under the category of ground-based robots, in view of the taxonomy proposed in Figure 2.2. As it has been provided in Figure 2.2, the ground-based robots (these robots can also be termed as land-based robots, as they are developed to function on land) can be further classified based on the different types of locomotion capabilities developed, which allow them to inspect specific parts of the bridge infrastructure. ROCIM is a

robotic platform that has been developed for bridge deck inspection [45, 80]. Similarly, RABIT is another wheel-based ground robot with a wide array of sensors and autonomous navigational capabilities [35, 38, 40, 45, 68, 77, 80–82]. This particular robotic platform has been equipped with state-of-the-art sensor technologies (e.g., impact echo, ultrasonic surface waves, electrical resistivity and GPR), which enable the classification of some of the most common defects in bridge decks, such as concrete degradation, delamination and rebar corrosion [40, 82]. The ARA Lab Robot is also a wheel-based robotic platform that has been recently developed for bridge deck inspection. and maintenance [39, 44, 83]. With a similar array of sensors, another autonomous platform for infrastructural inspection was developed by La et al. [30], which provided a wide array of different functionalities related to the automated monitoring of civil infrastructure, using on-surface crack detection and bridge evaluation for signs of deterioration within the metal rebar and concrete slabs.

In this particular research, the overall effectiveness of the automated robotic inspection system was also assessed for the evaluation of actual bridges [38]. A climbing robot was leveraged for the inspection of the underside of the bridge deck [53]. The majority of these robots have primarily been used for bridge deck inspection applications. A number of climbing, walking and crawling robots have also been developed, which are able to scale the vertical surfaces of the bridge infrastructure. Some of these robots include the BRIDGE (Bridge Risk Investigation Diagnostic Grouped Exploratory) bot [42], chain-lIkeda robot [78], magnetic wheeled robot [55], and the vortex climbing robot [62]. Most of the climbing and sliding robots dedicated to the

inspection of different parts of the bridges are small-scale in nature, with a primary reliance on visual inspection methods using vision-based sensors.

Many bridges are equipped with cables to provide support and load balancing across the different parts of the bridge. To provide the automatic maintenance and inspection of these parts of the bridges, a considerable amount of studies focuses towards the mechanical design and development of different cable climbing robots [47–49, 51, 53, 57, 58, 58, 61, 78, 84]. The use of bipedal and quadruped legged robots has also been proposed for the inspection of civil infrastructures in general and the vertical structures of bridges in particular [76, 79, 85–90].

Table 2.1 summarizes some of the major characteristics of the different platforms for the NDE of bridges using a wide array of different robotic platforms and their respective sensory modalities. Due to the wide array of different sensors available for the NDE of bridges, the different sensory modalities are classified into radars (GPR sensors that employ EM waves of different frequency and wavelength), vision (all types of cameras and other sensors that provide visual information, e.g., red green blue (RGB), RGB-Depth (RGB-D), time-of-flight, thermal cameras, and sensors for infrared thermography), acoustic (all forms of sensors that employ sound for NDE, e.g., different IE methods and microphones, ultrasonic sensors) and electric (sensors that employ variations in current and voltage, e.g., ER, potential field mapping and Eddy current sensors) sensory modalities. When comparing the different ground-based platforms given in Table 2.1, it can be seen that the RABIT and ARA Lab

Platform	Type	Radar	Vision	Acoustics	Electric
RABIT-Bot	Wheeled	1 GPR	1 Camera	IE + USW	1 ER
ROCIM-Bot	Wheeled	N/A	1 Camera	N/A	N/A
ARA-Bot	Wheeled	1 GPR	2 Cameras	N/A	2 ER
ETH-Bot	Wheeled	N/A	N/A	N/A	1 HCPM
BridgeBot	Wheeled	N/A	1 ArduCAM	N/A	N/A
SBC-Bot	Climbing	N/A	2 Cameras	N/A	1 EC
ABI-Bot	Climbing	N/A	1 Camera	N/A	N/A
Caterpillar	Climbing	N/A	1 Camera	N/A	N/A
SkySweeper	Climbing	N/A	N/A	N/A	N/A
Cable-Bot	Sliding	N/A	4 CCD	N/A	N/A
CI-Bot	Climbing	N/A	3 Cameras	N/A	N/A
CCRobot-II	Climbing	N/A	N/A	N/A	N/A
MRC-IN-II	Sliding	N/A	1 Camera	N/A	N/A
Quadrotor	UAV	N/A	N/A	N/A	N/A
Manipulator	UAV	N/A	N/A	N/A	N/A
CP-Bot	UAV	N/A	N/A	N/A	N/A
FW-Bot	UAV	N/A	N/A	N/A	N/A
Octo-rotor	UAV	N/A	N/A	N/A	N/A
Quad-rotor	UAV	N/A	1 Camera	N/A	N/A
Hammer	UAV	N/A	N/A	1 IE	N/A
3D Mapper	UAV	N/A	1 3D LiDAR	N/A	N/A
DJIP	UAV	N/A	1 Camera	N/A	N/A
2D-LRF	UAV	N/A	2D LRF	N/A	N/A
Omni-Wheel	UAV	N/A	2 Cameras	N/A	N/A
II-Bot	UAV	N/A	IR + RGB	N/A	N/A
UROV	USV	N/A	1 Camera	N/A	N/A
Sea-RAI	USV	N/A	4 Cameras	N/A	N/A
MW-Bot	USV	N/A	2 Cameras	N/A	N/A
Videoray	USV	N/A	1 CI Sonar	N/A	N/A
YSIE	USV	N/A	1 SS Sonar	N/A	N/A

TABLE 2.1: Different Bridge Inspection Robots and their Sensory Modalities

Robot are the two robotic platforms with existing hardware and software capabilities that can allow them to function in an intelligent, autonomous fashion with regards to path planning, collision avoidance, trajectory planning, trajectory generation and sensor fusion techniques. As functional robots, they also have the ability to evolve over time, by equipping them with the state-of-the-art sensors for enhanced autonomous

capabilities and data collection. In comparison, the majority of the other ground-based platforms relied on a single form of sensory modalities with limited hardware and software capabilities.

2.1.1.2 Aerial Robots

The recent breakthroughs in the field of aerial robots has allowed the usage of various multi-rotor platforms (e.g., four-rotor and eight-rotor-based platforms) in the field of NDE, with various implementation focusing towards bridge inspection and maintenance. The majority of the studies for bridge inspection using UAVs rely on visual inspection methods [5–8, 66]. However, some of the recent studies have attempted to explore different ways in which aerial robots can be modified to provide perching and contact-based inspection capabilities [10, 63, 67, 73]. A number of recent studies have also proposed the development of hybrid robots, which are able to provide multiple functionalities (e.g., flying and walking mechanisms and a number of different flying and contact-based approaches) [71] [72] [73]. Some of these platforms have provided a proof-of-concept with considerable potential towards successful utilization for bridge inspection in the future. Some of the different aerial robots deployed for the visual inspection of bridges are outlined in Table 2.1. For example, a UAV platform developed in [72] provided contact-based bridge inspection capabilities. Similarly, research by [63] examined the effect of contact force on pitch angle and vertical thrust force using one degree of freedom manipulator to perform the hammering analysis for bridge

inspection. However, this platform did not rely on any NDE sensors, as the research is still in its initial stages. Another study focused on the position determination of UAV for the visual inspection of bridges using an on-board camera [8].This is a relatively new field of research and further research is required in order to fully exploit the flexibility and versatility of aerial robotic platforms towards the accessing and monitoring of different parts of the bridge infrastructures.

2.1.1.3 Undersea Robots

Marine robots primarily deal with the inspection of parts of the bridge infrastructure, which are submerged underwater. One of the earliest studies in this category emphasized the importance of examining and inspecting inaccessible or hard-to-access regions of the bridge infrastructure by human inspectors [70]. This platform made use of a camera for the visual inspection of submerged pier sections of the bridges [70]. However, the overall effectiveness of visual inspection is heavily affected by the clarity of the water and weather conditions, to name a few limitations of underwater standalone vision-based systems. Over the years, this area has expanded to receive attention with regards to post-disaster inspection as well as the regular inspection of bridge piers [91]. A number of unmanned marine vehicles (UMV), unmanned underwater vehicles (UUVs) and remotely operated vehicles (ROVs) have been deployed in the past, which include semi-autonomous sensory platform, Muddy Waters, sea-RAI, VideoRay and YSI Ecomapper [69] [91] [70]. The majority of the limited number

of robotic platforms deployed underwater rely on the visual sensory information for assessing the condition of bridge structure submerged under water, as it can be seen from Table 2.1. However, due to the various challenges associated with underwater inspection, there is a need for further research, which can provide improved sensory capabilities for data collection as well as tools and techniques for analyses, which can be used for the underwater inspection of bridges in the future. At the same time, there is also a need for performing the comprehensive feasibility of the developed and deployed robotic platforms within different underwater conditions for the inspection of different bridges. In the following section, the prime focus will be towards discussing some of the different algorithms and techniques developed for the NDE of bridges.

2.1.2 Sensors

An array of instrumentation modules used for data collection will also be discussed with specific distinction between the single sensor-based and multiple sensor-based systems for NDE of bridges. Data from multiple sources require an additional level of complexity with regards to specifying the appropriate sensor fusion techniques. This particular aspect will also be analyzed in sufficient details.

Sensors allow the different NDE platforms to collect data, which can be used to assess the overall conditions of the infrastructure in terms of its suitability and safety for humans in the near future without endangering their lives in any way. For studies in

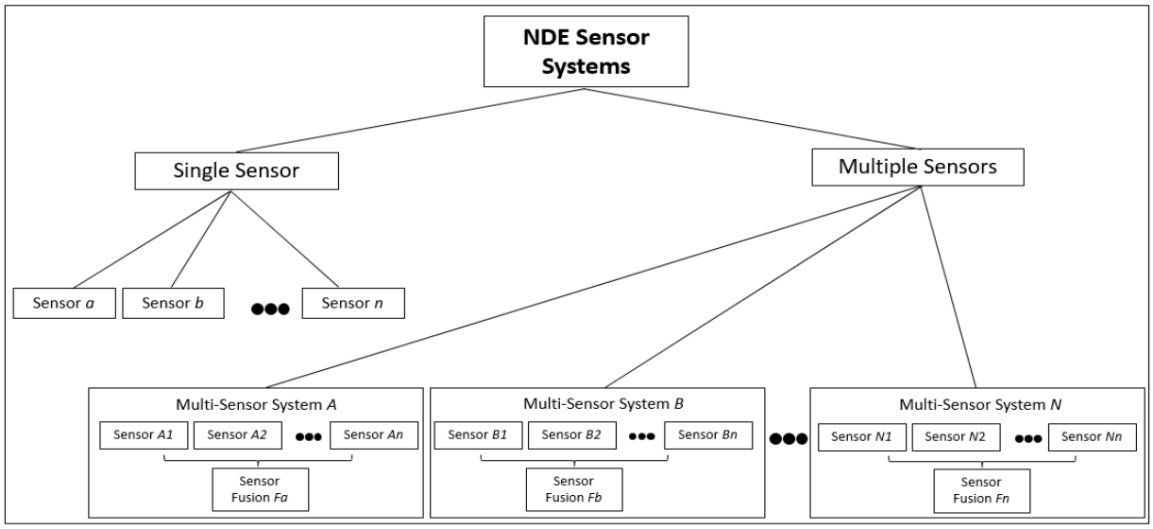

FIGURE 2.3: The different sensor configurations within the NDE literature

this particular field, it is important to incorporate sensors, which are able to analyze the overall internal and external conditions without physically tampering with the infrastructural materials (e.g., concrete, steel). In the previous section, it can be seen in Table 2.1 that the different types of sensors deployed on the various platforms had been classified into four main categories, namely vision, acoustics, radar, and electric sensors. The classification proposed in Table 2.1 was based on the different sensory modalities that were equipped in the different NDE platforms. However, in this section, the scope is broader than the usability and applicability of the variety of sensors on NDE-based robotic platforms. In this section, the primary discussion will relate to the different types of sensor-based systems utilized for infrastructure evaluation and structural health monitoring.

It can be seen in Figure 2.3 that NDE systems can be broadly classified into single-sensor and multi-sensor-based systems. Most of the single sensor systems, such as

Roadmap [92] and BYU (Brigham Young University) IE scanner [93] employ a single sensor each, namely GPR and IE respectively. Conversely, multi-sensor systems (e.g., RABIT [30, 35, 40, 45, 64] and Seekur Jr. [38]) make use of different types of sensors, which allows them to provide an accurate and multi-faceted evaluation of the infrastructure, such that the limitations of one sensor type (e.g., infrared thermography, which is limited in terms of providing information regarding near-surface delamination [82] can be mitigated by the use of other sensors (e.g., GPR, which is able to provide information regarding the structural defects present at sufficient depth underground [40]). However, this platform did not rely on any NDE sensors, as the research is still in its initial stages.

2.1.2.1 Single-Sensor Systems

It has already been discussed in the prior sections that many of the earlier studies in the field of the NDE of bridges deal with single sensor-based systems. At the same time, according to table 2.1, the majority of the existing robotic solutions developed can also be classified as single-sensor-based systems. However, there are a number of different sensory modalities available for the NDE of bridges and civil infrastructures in general, which will be discussed in sufficient detail in this section. For the case of impact-echo-based NDE techniques, metallic objects (e.g., metal chains, ball bearings) are used to create acoustic vibrations and contact sensors are employed to record the reflected sound waves from the different underground materials and the

defects within infrastructures. A number of studies in the field of the NDE of infrastructures have reported the utilization of impact-echo sensors in the recent past [93–98, 98–101]. These studies have focused towards examining the different types of defects present within civil infrastructures. For the case of the research proposed by Zhu and Popovics [95], an air-coupled impact-echo sensor and recording devices have been used to analyze the extent and depth of delamination within concrete structures. The effectiveness of the impact-echo sensors is dependent on the type of impactor used [95]. This particular tool for data collection has been extensively used for infrastructure evaluation in a number of recent studies [94, 95]. Another study validating the effectiveness and efficiency of air-coupled sensors was also validated [95]. However, for rapid scanning-based applications, the use of air-coupled sensors can pose challenges for real-time data collection [100]. To improve the overall efficiency of data collection for NDE-based applications, different NDE-based applications, different studies have developed automated IE systems with complicated electromechanical mechanisms for the repeated and consistent impacts on structure surfaces [31, 93, 97, 102]. Figure 2.4 provides details regarding the impact-echo method and its utilization for the NDE of civil infrastructures using different components, such as impactors (metal objects used to create sound vibrations), transducers (sensor used to detect the sound reflections), data acquisition module (hardware components used to filter sound vibrations) and the data analysis module (software used for analyzing and visualizing the signal output from the sensor over time).

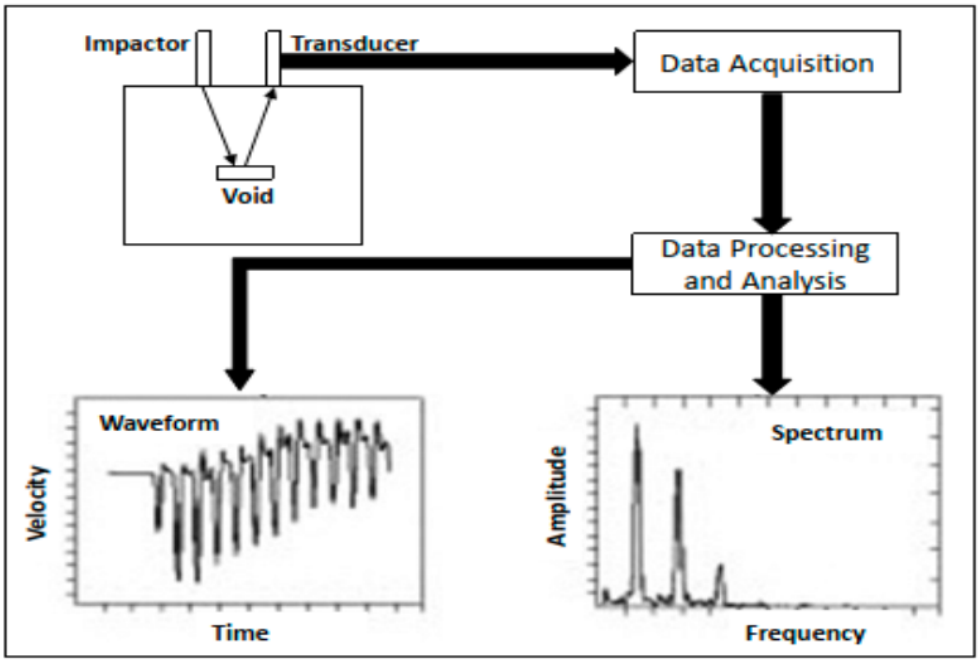

FIGURE 2.4: Different elements of the IE method for NDE of infrastructure

In the wake of technological improvements in commercially available infrared detectors, infrared (IR) thermography has gained considerable popularity in the past decade, specifically after being established as an American Society of Testing and Materials (ASTM)-certified method to detect delamination in bridges in 2003 [103, 104]. The use of infrared thermography has been discussed, not only in the context of infrastructure evaluation [103, 105–108], but also for tunnel excavation [109–111] and for the examination of different materials (e.g., metals, aluminum laminates, carbon fiber reinforced polymers and glass fiber-reinforced polymers), which is important towards assessing the structural integrity of different mechanical parts specifically developed for the aerospace industry [112, 113]. In comparison with other methods for the NDE of infrastructure, infrared thermography has been recommended to provide the real-time, objective assessment of infrastructural health, specifically for the case

of near-surface delamination detection [114–116]. However, with the increasing depth of the underground defects within infrastructures, the overall accuracy and reliability of the infrared thermography technique decreases substantially [117–119]. Some of the other factors which can impede on the accuracy of the data collected include the type of sensor equipment being used, shadows, moisture, surface debris, wind speed and sustained solar heat [107, 120, 121].

The governing principles underlying the usage of infrared thermography include conduction, convection and radiation. For the case of the near-surface delamination of the presence of underground void spaces, infrared thermography leverages the concept of variation of the temperature gradient between the defective and non-defective regions within infrastructures [1] [2]. Figure 2.5 (a,b) outline the ways in which heat conduction and radiation emission during day and night time, respectively, allow the infrared thermography sensors to differentiate between delaminated and non-delaminated regions [1]. It can be seen in Figure 2.4 (c,d) that the regions with potential underground structural defects are visible as bright regions on the thermogram [2].

Another widely utilized sensor is the ground-penetrating radar (GPR), which has been the focus of a number of recent studies related to the infrastructure inspection and evaluation of civil infrastructures and bridges [38] [39] [40] [39] [19] [122] [123] [124] [125] [126] [127] [128] [129] [130] [131]. Within civil engineering, GPR has been utilized for diverse applications, which include, but are not limited to, detecting and measuring pipes, mines, other underground utilities, the health monitoring of bridges,

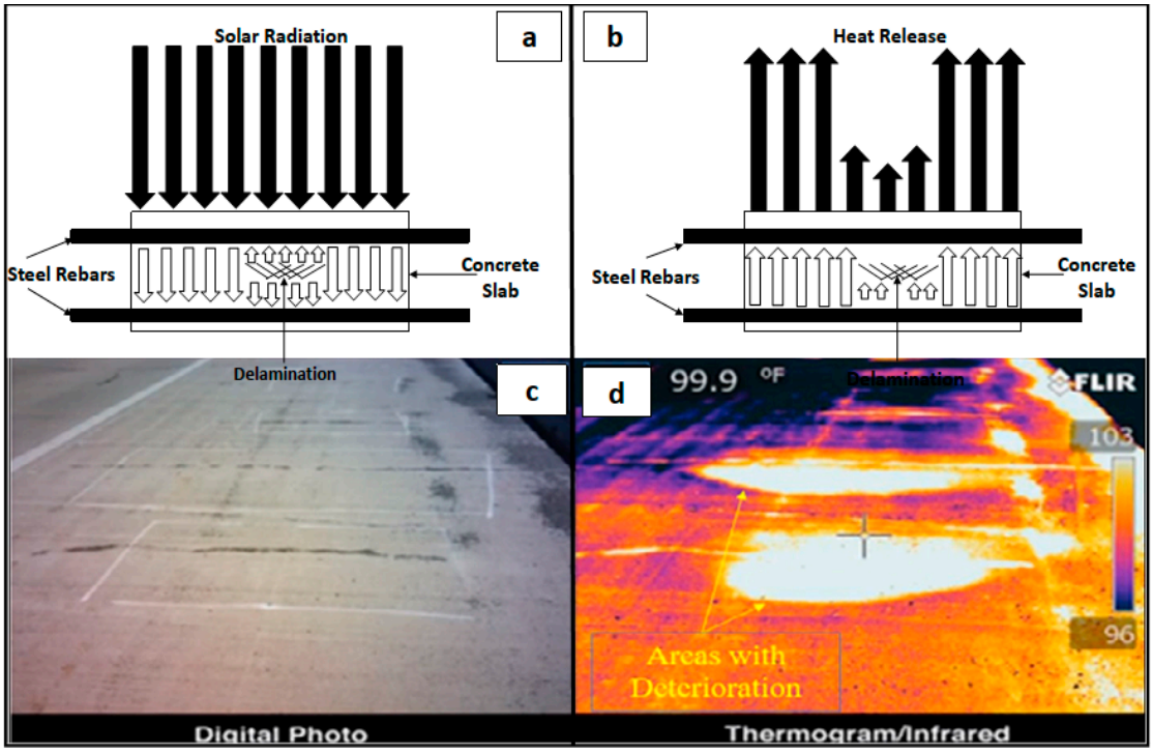

FIGURE 2.5: Data collection using a thermography sensor: (a) the absorption of solar radiation by the different parts of the infrastructure during the day time [1], (b) the emission of radiation from the different parts of the infrastructure during night time [1], (c) the output of the data collection unit in the form of a digital image [2], and (d) the output of the data collection unit [2]

railway tracks, tunnels, roads and pavements, as well as for the detection and localization of underground rebar [38] [39] [40] [19] [122] [123] [124] [125] [126] [127] [128] [129] [130] [131] [132] [133]. The B-scan data from GPR sensors provide a visual transformation of the radar waves reflected from different parts of the underground infrastructure (e.g., concrete, steel rebars, void spaces), which can be used to highlight the corrosion, delamination, presence of void spaces and structural damage to rebars [39] [19] [122] [123]. The details regarding different data analysis techniques will be discussed in the following sub-section. Figure 2.6 (a) provides information regarding the underlying principles for wave propagation using the fixed-offset-based method

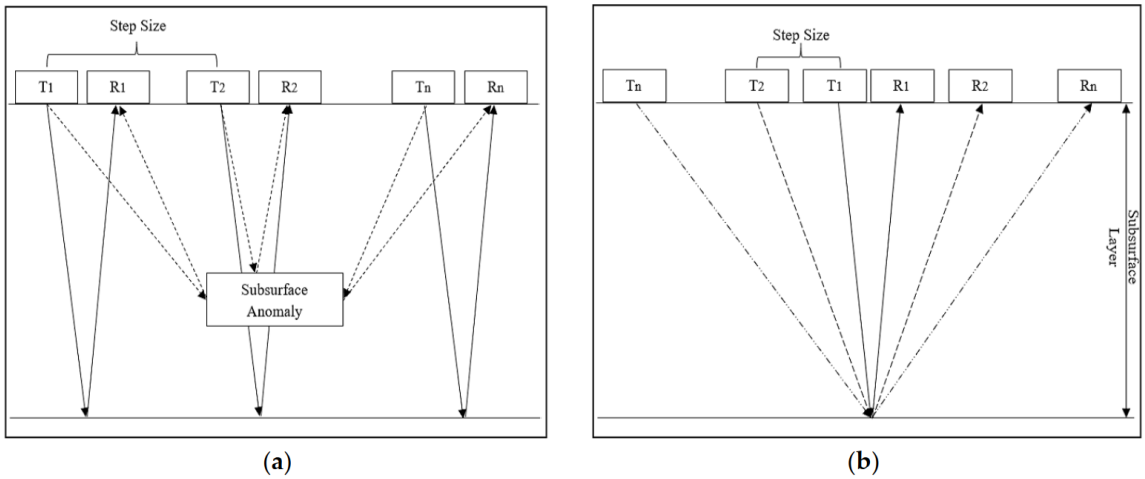

FIGURE 2.6: Principles for the GPR wave transmission: (a) wave transmission with the fixed-offset profiling method for data collection, (b) the use of a common midpoint method for data collection using GPR [3] [4] with different visual sensors to provide surface-level information to assess the structural health of bridges [5] [6] [7] [8] [9] [10]

for data collection using GPR [3] [4]. Similarly, the use of a common midpoint-based method has been shown in Figure 2.6 (b) [3] [4]. The radar waves from the transmitter penetrate the ground, and based on the different properties of the underlying construction materials and other artefacts (e.g., location, dimensions, density, depth), the intensity and signature of the waves reflected back from the different regions to the receiver can vary to a considerable extent.

Vision-based sensors have received considerable attention in the recent past towards the NDE of diverse civil infrastructures, ranging from sewers [134], tunnels [135] [136], structural ceilings [137], roads [138] [139] [140], dams [141], pavements [142] [143] [144] [145], and bridge decks [30] [43] [64] [146] [147]. The advent of state-of-the-art learning-based techniques for data analysis has facilitated the widespread usage of vision-based sensors within different robotic systems for the NDE of bridges [82] [39]

[30] [40] [64] [44] [45] [68] [119] [80] [83]. The visual inspection of infrastructure is important to provide information regarding the surface-level defects and damages in concrete. A number of vision sensors have been utilized to perform the inspection of civil infrastructures, namely the smartphone camera [137], digital cameras [30, 45, 82, 119, 135, 148], depth sensors [147] [91], time-of-flight cameras [149], closed-circuit television (CCTV) [134], laser-scanners [9, 90, 140, 147] and Visual SONAR (Sound Navigation and Ranging) sensor [69]. The vision-based sensors are dependent on the reflection of light from infrastructure surfaces to provide an assessment of surface-level NDE. Based on the data in Table 2.1, it can be seen that many of the aerial robots are equipped with different visual sensors to provide surface-level information to assess structural health of bridges [5–10, 66, 90].

A number of different electrical sensors have also been used for the assessment of bridge infrastructure [30, 35, 39, 39, 44, 45, 53, 64, 68, 78, 80, 82, 83, 119, 150, 151], which are primarily used in a ground-based robot. A half-cell potential sensor was used by the ETH (Eidgenössische Technische Hochschule) Zurich autonomous robot for potential mapping to detect a level of corrosion within the concrete structures (e.g., bridge deck underside and parking lots) [53]. Electrical Resistivity (ER) probes have been one of the most widely used electrical sensors, which have been incorporated within two of the most widely discussed ground robots for the inspection of bridge decks in the recent past, namely the ARA Lab Robot [39] [44] and RABIT platforms [30] [83] [150] [151]. The purpose of ER probes is to examine the level of sub-surface corrosion within bridge decks and other infrastructures [68]. The RABIT platform is

equipped with four Wenner-type ER probes; two outer probes generate an electrical current and the two inner probes measure the intensity of electrical field, which is used to calculate the electrical resistivity [68]. Another type of electrical sensor was used by the steel climbing robot, namely the Eddy current sensor [47, 150, 151], which is used to measure the level of corrosion, rust and crack within the steel structures of bridges.

2.1.2.2 Multi-Sensor Systems

For the case of traditional tools, techniques and platforms, any one of the aforementioned data collection methods (e.g., impact echo, GPR or infrared thermography) can be utilized for performing inspection of civil infrastructures. However, state-of-the-art platforms (e.g., Seekur Jr., RABIT) [38] [68] [30] [40] [45] [64] have utilized an array of different sensors, which provide an in-depth evaluation of the civil infrastructures. In this section, the primary purpose is to explore the different ways in which sensor fusion techniques can be used for different modalities (discussed in the previous section) to collectively allow the development of efficient and cost-effective systems for the NDE of bridges.

Sensor fusion within multi-sensor systems allows the improvement in the ability of those systems towards effectively obtaining insights from the available data. Prior studies have revealed that sensor fusion techniques also improve the overall accuracy and efficiency as well as reduce the data-level and system-level redundancy of

multi-sensor-based systems [152, 153]. Sensor fusion is being widely utilized in a wide array of applications, ranging from medical diagnostics [154], aerospace [155], plant inspection, and high-precision manufacturing [156] [157] to remote sensing [158] and the NDE of civil infrastructures [153]. One of the various functions of sensor fusion is to ensure that the data from multiple sources can be combined together to facilitate appropriate analyses, leading to the enhanced efficiency and effectiveness of the deployed practical systems [159] [160]. Some of the earlier studies have explored different types of fusion techniques, which can be broadly classified into the following:

1. Data-level fusion: Raw data from the different sensors are transformed and concatenated together. A single technique for data processing and analysis is applied collectively to the fused data from the different sensors [50] [117] [161];

2. Feature-level fusion: Feature from the multi-modal data are collated collectively. In order to ensure that data from different sensors are fused together effectively, different types of data transformation technique are utilized [50] [117] [161];

3. Classifier-level fusion: A number of different classifiers are used together to develop hybrid classifiers. The final performance of the hybrid classifier is based on the average of the individual classifiers chosen for analyzing multi-sensory data [50] [117] [161];

4. Result-level fusion: A number of techniques are employed to individually analyze data from individual sensors. The results from each method are combined together based on specified criteria [50] [117] [161].

It is important to understand that different sources provide varying classifications for understanding the different types of data fusion techniques. For example, a review of NDE sensor fusion techniques by Liu et al. [50] outlined the different approaches that can be broadly divided into signal-level, feature-level, pixel-level and symbol-level fusion techniques. Meanwhile, the survey of different data fusion techniques in another study developed a taxonomy in terms of the different underlying challenges, namely data imperfection, data correlation, data inconsistency and varying data forms [162]. For catering to the various technical requirements of multi-sensor-based systems, a major stream of literature related to NDE has focused towards developing the different techniques of sensor fusion [50] [117] [153] [163]. A common method for data fusion is the Dempster–Shafer Theory, which has been widely used for NDE applications ranging from data fusion between ultrasonic and X-ray imagery to the techniques developed from the data fusion between infrared thermography and GPR-based sensor modalities [152] [153] [164]. One of the earlier studies on the fusion of data from NDE sensors (e.g., GPR, portable seismic analyzer, and falling weight deflectometer) utilized a number of different fusion techniques, which include fuzzy logic, Bayesian, statistical weighted average and hybrid fusion techniques [165]. The use of adaptive fusion operators with customized decision criteria was employed by one of the relevant studies for performing the fusion of multi-modal data (e.g., electrical resistivity, ultrasonic waves, infrared thermography) represented in the form of possibility distributions and fuzzy sets [153]. The use of radar and ultrasonic sensory modalities was performed in another study by Maierhofer and colleagues [152], which

utilized data pre-processing, normalization, filtering and amplification techniques for data transformation before different fusion techniques (e.g., summation, subtraction and maximum amplitude-based methods) were performed on the multi-sensor data. In their research, Kee et al. [117] proposed the usage of tools related to infrared thermography and air-coupled impact echo, along with their fusion techniques, which was based on simple rule-based criteria to provide valuable insights towards effective infrastructural maintenance.

However, the data were not obtained from an actual bridge, but from a bridge test-bed specimen, which means that this method has not been tested on a practical system using data from actual bridges. Data from a wide array of different sensors were utilized within the RABIT platform in another study related to the NDE of bridges [30]. However, the use of sensor fusion techniques was not outlined to ensure that the data from different modalities could be effectively leveraged to provide an in-depth inspection of bridges. For the case of the deployment of the ARA Lab Robot for the NDE of bridges, a sensor fusion algorithm was deployed, which allowed the robot to optimize the duration of time taken to perform the necessary operations required for data collection using a camera, GPR and IE sensors across the different regions of the bridge deck infrastructure [39]. According to Brierley et al. [157], the questions related to the selection of an appropriate sensor fusion technique is application specific in nature. Some of the considerations in this regard are given as follows: (i) the type of problem being addressed, (ii) the type and scale of the sensory data being handled, and (iii) the assessment criteria for performance evaluation, as

the sensor fusion techniques can provide varying results in different contexts and applications [157].

2.1.3 Methods for Surface-level and Sub-Surface-level Analysis

In this section, the focus will be towards outlining the different analysis techniques using data from a wide array of NDE sensors for bridge infrastructural evaluation, which were highlighted in the previous sub-sections. The discussion in this section will be divided into two sub-sections, namely:

(i) Different techniques pertaining to analysis of the surface-level data for bridges and other civil infrastructures. The surface-level analysis for NDE is used to examine the level of cracks, and the corrosion of the concrete surfaces of civil infrastructures. Another stream of literature pertaining to surface-level analysis of bridges include steel defect detection. Although, there is a dearth of studies in this research area, but this dissertation has made some progress to extend the state-of-the-art.

(ii) Myriad of techniques developed for analyzing sub-surface-level data for bridge decks. The sub-surface-level analysis allows the evaluation of the steel rebars in the bridge decks. The research in this dissertation deals with the detection and localization of rebars. The condition assessment of bridge rebars is beyond the scope of this dissertation.

2.1.3.1 Surface-Level Analysis: Concrete Crack Detection

There is a considerable amount of research effort devoted towards concrete crack detection for the surface-level inspection of civil infrastructures in general and bridges in particular [39, 43, 45, 80, 101, 166–175, 175–195]. Due to the concrete-based composition of the majority of civil infrastructures (e.g., dams, roads, buildings, sewers, bridges, tunnels), the techniques developed for concrete crack detection within a particular type of concrete structure can also be generalized towards other civil infrastructures. Some of the earlier works focused on the utilization of basic-level image-processing techniques for crack detection in concrete structures [43, 45, 80], which included basic-level morphological approaches [149, 175–177, 196], digital image correlation techniques [178–180, 197] and different segmentation-based approaches [181].

A number of different image-based filtering techniques were also employed, namely Gabor filtering [182], median filtering[169] [183], texture filtering [172] [185] and data fusion-based filtering approaches [161] [186]. The efficacy of different image transformation techniques has also been discussed, ranging from the watershed transform [175] [177] [178], wavelet transform [183] [184] [187] [188], and randomized Hough transform [183] [189]. The use of fast Fourier and fast Haar algorithms with Sobel and Canny edge detectors was developed for the concrete crack detection in one of the earlier studies [190]. A block-based crack detection approach was developed for the bridge decks in another study. Another study made use of histogram-based method

for the extraction of crack features from the input images of bridge decks [43]. A genetic learning-based network optimization algorithm was also proposed with the application for concrete crack detection [168].

Data from the GPR sensor were used for sensitive concrete crack detection using a super high-frequency band system and time-variant deconvolution-based approach [191]. The use of different deep-learning frameworks has gained considerable attention in recent works related to concrete crack detection [140, 166, 167, 174, 192]. A deep-learning-based SSD Inception V2 and SSD MobileNet models for concrete road damage detection was developed in another recent study [138] [142, 193]. Similarly, the crack detection problem was solved using semantic segmentation with the help of deep residual neural networks (NNs) in a number of recent studies [194, 195]. A Faster-region-based CNN model (Faster R-CNN) was proposed towards the quasi-real-time system development for the detection of different types of defects (e.g., concrete crack detection, steel delamination, bolt corrosion, etc.) [135, 192]. Another recent study utilized a U-net-based fully connected CNN model for concrete crack detection [173]. Some of the most recent studies have made use of different encoder–decoder-based deep-learning architectures to improve the existing limitations of crack detection systems using a pixel-wise classification of concrete images [140, 159, 166, 167, 174, 198].

DeepCrack is the name proposed for a deep learning-based framework designed specifically for the crack detection using crack probability maps obtained with the help of

a deep-encoder–decoder-based network [199]. A comparison in the performance and techniques employed by the different studies in the past towards concrete crack detection have been outlined in Table 2.2. A number of other deep-learning frameworks have also been developed for crack detection, such as the CrackNet [199], CrackNet II [200] and CrackNet V [201] models, which have further improved the performance of the crack detection systems. Another study made use of multiple visual sensors (e.g., digital camera, laser scanner and distance sensor) for concrete crack detection and measurement with the help of the YOLO (You Only Look Once)-v3-tiny model [147]. An autonomous crack width-measurement system using medial axis transform and flexible kernel was also proposed in another recent study [202].

Study	**Struct.**	**Data**	**Img. Size**	**Method**	**Result**
Li	Bridge	1,000	N/A	IS	Acc.= 92.6%
Fujita	General	60	640 x 480	LAT	AuC=98.0%
Chen	Bridge	40	3,088 x 2,056	SOMO	Acc.=89-91%
Oh	Bridge	80	640 x 480	MO	Acc.=94.1%
Li	Bridge	1,200	4288 x 2848	ACM/SVM	Acc.=92.1%
Liu	General	84	512 x 512	U-Net	F1=90.0%
Ren	Tunnels	409	4032 x 3016	CSN	Rec.=85.54%
Dung	General	40,600	227 x 227	FCN/VGG	Prec.=90.0%
Zhou	Road	52,408	256 x 256	ResNet	F1=99.8%
Billah	Bridge	43,996	256 x 256	ResNet	Acc.=94.0%
Park	General	1,800	N/A	YOLO-T	Err.=0.09mm
Billah	Bridge	12,000	256 x 256	SegNet	F1=24.1%
Li	Sewer	18,333	224 x 224	ResNet/HS	Acc.=64.8%
Wang	Ceiling	1,953	400 x 600	DCNN	Acc.=86.22%

TABLE 2.2: Comparison between the state-of-the-art techniques for Concrete Crack Detection

2.1.3.2 Surface-Level Analysis: Steel Defect Detection

The research pertaining to the steel defect detection system for steel bridges has been a relatively under-studied area of research in the past [203–207]. In this respect, a handful of studies have been reported, which will be presented here to provide a brief overview of the state-of-the-art before highlighting the proposed methods developed in this dissertation. One of the earliest studies in this regard utilized a texture-based approach for detecting corrosion in steel bridge surfaces [203]. In this approach, the proposed system converted images into the RGB color space, calculated the statistical information (e.g. difference, mean, and standard deviation of each color component) [203]. Wilks' lambda and data range analysis was applied to the aforementioned metrics to calculate three indices (e.g. mean values in red, difference in green, and difference in blue) to assess whether steel bridge coating images contained corrosion or not [203]. This method [203] works effectively with blue-paint-coated steel bridge images. However, its effectiveness with other coating colors and coating images with background noise or non-uniform illumination or low-contrast has not been examined. A detection method for rust defects on steel bridge coatings was developed in [204].

An automated rust-defect-determination method that leverages aerial imagery has been presented in [207] with *image registration* (for which a binary information method is proposed to match the infrared images to their respective RGB images), *bridge component retrieval* (automated segmentation obtained by fusion of RGB and infrared images) and *rust region identification* (rust regions are identified in YCbCr

colorspace and rust percentage is calculated). The approach to corrosion detection in steel bridges developed in [206] was able to provide an unsupervised learning-based approach (e.g. K-means clustering). An automated steel bridge coating rust defect recognition method based on color and texture feature was developed in [205]. The proposed method performed color transformation on the original image, followed by the application of Fourier Transform and low-pass filters [205]. Another approach discussed in [208] make use of roughness analysis and color comparison on image patches to separate corrosion patches for steel images. Another study [209] made use of texture analysis with variables such as contrast, correlation and energy. Study by [210] is used for crack and corrosion detection, which made use of a supervised classification method with code-word dictionary consisting of stacked RGB histograms for image patches symmetric gray-level co-occurrence matrix for each patch.

Some of the studies in this respect tackle bridge steel defect detection as a bridge coating assessment problem (i.e. when paint coating removes from the steel surface of the bridge, followed by steel corrosion and rust formation. Therefore by examining the uniformity of coating, the percentage of corrosion and rust present on bridge surface can also be highlighted) [204, 211–221]. One of the earliest studies in this regard [211] was able to highlight the efficacy of color-based features as an effective approach for rust detection under varying light conditions. An image recognition technique for bridge coating assessment with multi-resolution pattern classification (MPC) and double sampling was developed in [212]. Another study [213] developed a neuro-fuzzy recognition approach (NFRA) to solve the non-uniform illumination

problem. A number of studies [214–218] selected the L*a*b* color space to develop an Adaptive Ellipse Approach (AEA), along with solution for non-uniform illumination problem. A Support Vector Machine-based Rust Assessment (SVMRA) was developed in [216] to tackle the issue of non-uniform illumination in outdoor images captured for bridge condition assessment. Another study [220] proposed a method for steel bridge maintenance with emphasis on accurate and rapid rust detection with consideration for current standards of practice (considering rust distribution type, e.g. spot, general or pinpoint rusting). A wavelet transform for rust detection with dimensionality reduction to improve computational efficiency was proposed in [221]. Another study [219] developed a wavelet-based de-noising method with wavelet-based edge detection methods to specify rust and its spatial distribution. [204] used ranges of H layers and the co-efficient of variation (COV) of grayscale to divide images into three groups. Three separate image recognition techniques were used in the different color spaces [204]. K-means clustering method was used in the H layer and Double-Center-Double-Radius (DCDR) algorithm was used in the Red-Green-Blue (RGB) and Hue-Saturation-Intensity (HSI) color spaces [204]. The Least Square Support Vector Machine (LS-SVM) was adopted to predict the radii in the DCDR approaches [204].

2.1.3.3 Sub-Surface-Level Analysis: Rebar Detection and Localization

One of the primary emphases of this section will be towards the algorithms proposed for rebar detection and localization, which is essential for the structural health monitoring of bridges. For the case of bridge monitoring, earlier studies utilized different pattern recognition and image-processing techniques for rebar detection and localization by hyperbola extraction from GPR radargrams [222] [164] [202]. Different hand-crafted features were employed by many of the earlier studies, such as the edge-based features [132] [133] [223] [163] [224] [225], texture-based features [164] [226], template matching [222] [222], histogram of oriented gradients (HOG) [40] [39] [126], feature transformation methods, e.g., Radon transform [128], and Hough transform [158, 227–229] and statistics-based methods, such as clustering-based approaches[202] [230], least-square methods [163], and higher-order moments [231, 232]. These features were trained using a wide range of different learning-based techniques towards developing effective rebar detection and localization algorithms in the past [19, 39, 40, 123, 124, 225, 233]. Research by Gibb and La [39] trained a Naïve Bayesian classifier using HOG features. Support Vector Machine (SVM) has also been used in prior studies [40, 131]. A number of different neural network (NN) frameworks have also been employed in earlier studies for rebar classification [133, 223, 225, 233]. Many of the earlier methods failed to effectively leverage the capabilities of NN models using edge-based features [133] [223] [225], which are not suitable for real-world systems dealing with GPR data that contain varying rebar

signatures and fluctuating noise levels. Some of the recent studies have made use of convolutional neural networks for rebar detection [19, 123, 124, 234, 235]. A study by Dinh et al. [19] proposed the usage of a 24-layer deep CNN model for rebar classification. The use of residual neural networks (ResNet-50) has also been proposed in recent studies related to rebar detection and localization [123, 124].

The preliminary examination of the results using GPR data from real-world bridges has shown that different ResNet models (i.e., ResNet-18, ResNet-32, ResNet-50, ResNet-101, ResNet-152) provide increased accuracy and generalizability [123, 124, 234]. Another study implemented the multi-objective genetic algorithm for the classification of rebar images [236]. Due to its critical importance, many of the studies focused on the development of rebar detection and localization systems in a collective fashion [40] [39] [19] [122]. The earlier studies made use of hand-crafted features with edge-fitting or curve-fitting algorithms to localize rebar signatures from GPR radargrams containing multiple rebar profiles [129] [133] [222] [230]. Hough transform fitting has also been leveraged with edge features to localize individual rebar profiles [230]. Yuan et al. [224] proposed the drop-flow algorithm using edge features to decompose individual hyperbolas and cater to over-segmentation. The edge-feature-based localization methods suffer from a lack of generalizability to rebar size, dimensions, location and variations in the noise levels. An expectation-maximization algorithm was proposed by Chen and Cohn [231], which has various limitations for implementation in real-time systems, in terms of computational complexity, difficulty in

Study	Feats.	Data	Detection Method	Detection Result	Localiz. Method	Localiz. Result
Dou	Edges	N/A	C3+NN	Rec.=70.4	OHF	Prec.=70.8
Kaur	HOG	3B	SVM	Acc.=91.98	RANSAC	Acc.=91.98
Gibb	HOG	4B	Naive Bayes	Acc.=95.05	PHL	t=32.4s
Dinh	HOG	26B	CNN	Acc.=99.6	RP	Acc.=99.6
Ahmed	N/A	6B	ResNet-50	Acc.=99.42	KMC	Acc.=94.53
Harkat	HOS	133RG	MOGA/CNN	Acc.=88.99	Hough	N/A
Ahmed	N/A	9B	Deep ResNet	Acc.=97.20	NRL	F1=95.58

TABLE 2.3: Comparison between the state-of-the-art techniques for Rebar Detection and Localization

convergence and sensitivity to the variations in configuration points. A column-connecting clustering algorithm with orthogonal hyperbola fitting was developed in [19]. Another study proposed a precise hyperbola localization algorithm, which made use of the hyperbola fitting and local maxima. However, this method has limitations towards providing results for real-time systems. In contrast to previous hyperbola-fitting methods, the study by Kaur et al. [40] made use of random sample consensus (RANSAC), which is an iterative method for robust hyperbola fitting with corrective capabilities, specifically with noisy data and outliers.

The different characteristics of the studies related to rebar detection and localization have been outlined in Table 2.3. There are various other studies utilizing GPR sensors with rebar detection and localization algorithms, which focus on other underground buried objects, such as landmines, void spaces, and pipes. These studies have not been included in the table, as they are beyond the scope of this discussion. Despite considerable research in this field, the effective acquisition of hyperbolic signature remains a complicated research problem with various challenges, such as the separation

of intersecting rebar profiles, the full/partial occlusion of hyperbolic signatures, and the complexities within the underground spatial configurations [124, 125, 224].

2.2 Challenges

There are a number of different challenges affecting the development of semi or fully autonomous systems for the NDE of civil infrastructures in general and bridges in particular. Most of the processes underlying NDE systems (e.g., manufacturing NDE, industrial NDE and civil infrastructure NDE) are time and resource intensive in nature. This means that NDE is performed only if the cost of failure (in terms of capital and loss of human lives) is greater than the costs associated with performing NDE, but with timely inspection and remedial measures, the probability of defect can be substantially reduced [157]. Over the years, a number of robotic platforms have been developed for performing the NDE of infrastructure [30] [82] [39] [40] [78]. However, there are a limited number of different initiatives towards the development of semi or fully autonomous systems that can reduce the overall time and resources taken to provide regular health monitoring services for civil infrastructures. It is for this reason that the current situation warrants the development of robust and cost-effective technological platforms for the inspection of civil infrastructures in general and bridge inspection in particular.

From a sensor and data fusion perspective, there are a number of challenges that have hindered the development of effective sensor fusion techniques for practical systems in the past. The deployment of contact-based sensors for the NDE of civil infrastructure is time-consuming in nature [39]. In this respect, there is a need for the development of stochastic, optimal path planning algorithms that utilize sensor fusion-based decision making to differentiate between areas of higher and lower priorities for inspection, depending on the input from different sensory modalities. At the same time, the majority of the existing studies related to sensor fusion do not provide reliable performance evaluation metrics [162]. Some of the other challenges towards the development of performance criteria for effective sensor fusion techniques include a lack of effective ground truth, multiple, often conflicting dimensions of different performance metrics, and the need for the modification of the performance criteria for sensor and data fusion in view of the underlying criteria, context and applications [162]. A similar issue has also been encountered with respect to the examination of studies related to rebar detection and localization. In table 2.3, only a handful of studies have been reviewed, as the majority of the studies related to rebar detection and localization do not provide reliable and effective performance evaluation metrics. Apart from that, there are many studies that do not provide any information regarding the performance criteria used to assess the quality of findings in their respective studies.

Many of the existing studies utilizing robotic platforms for the bridge inspection rely on single sensors, which can provide limited insight into the multi-faceted problem

related to bridge inspection in particular and civil infrastructures in general. In this regard, the increased utilization of vision-based inspection methods has been stressed in one of the recent studies [237]. A scientometric analysis of the relevant research field provided insight regarding the lack of multi-disciplinary research, which is hindering and limiting the development of effective solutions for the NDE of bridges [237]. A number of studies in other research domains related to robotics have extensively examined the human-level factors that affect the development of relevant systems. However, the use of civil infrastructure-based robotic systems has not examined the human factors, which include, but are not limited to, the civil inspectors' skills, trust in automation-based platforms, situation awareness, and the workload demands of civil inspectors [238]. There is also a need to assess the human–robot collaborative factors that can determine the effectiveness of deploying inspection-based robotic platforms in the different environments and contexts within the field of civil infrastructure evaluation.

Another limitation towards the development of effective real-time robotic solutions for the NDE of bridges is the lack of adequate funding towards the development of automated solutions to provide the regular inspection of bridges. In order to expedite the process of the regular maintenance of public infrastructure, there is a need for investment in the field of NDE of infrastructure, which can allow the development of effective autonomous and semi-autonomous platforms. One of the recent studies in this regard emphasized the high costs regarding development, the testing and practical deployment of on-ground robotic systems for facilitating the inspection

of civil infrastructure [239]. Earlier studies have emphasized the effectiveness and superiority of the robot-based NDE systems in comparison with the traditional maintenance techniques that have been in practice in the past [239] . Nevertheless, the overall advantages of developing autonomous/ semi-autonomous robotic platforms for inspection outweigh the underlying costs and challenges.

2.3 Performance Benchmarks

In this section, the primary focus will be towards highlighting the availability as well as the need and lack of widely-established and highlighted benchmarks in relation to the research in this dissertation. Since, the research in this dissertation can be divided into two separate streams, the discussion regarding benchmarks and its availability will also be discussed separately for the two research streams. These two sub-sections are given below:

2.3.1 Sub-Surface-Level Analysis of Bridges for Rebar Detection and Localization System

It has been highlighted in the prior section 2.1.3.3 that the studies developing parabola detection and localization systems in different contexts and environments (e.g. hyperbola recognition in GPR images [125], underground mines [126, 127] ,concrete bridge deck rebar [123, 124, 128] cylindrical objects [129], no apriori knowledge on medium

[131, 132], buried underground objects and utiliies [130, 133]). Unfortunately, some of the issues and limitations in the way of benckmark development include diversity of applications, lack of availability of open-source data for the different applications, type of algorithms leveraged (i.e. benchmark for one type of methods might not be valid for other types of methods), limited usage of real-world data for different studies, and lack of effective performance metrics for assessing the different systems developed. The manner in which the systems are developed and the results are presented and evaluated also varies from one study to another. This shows that despite studies in this field dating back to early 2000s, there has not been any established benchmarks or any attempts by studies to highlight any established framework for assessing the performance of the GPR rebar detection and localization systems. Many studies only focus on rebar detection system, while only a handful of studies provide details and performance analysis of rebar detection and localization systems both [39, 40, 125, 234, 236, 240].

In this respect, for the context of bridge decks, the proposed studies [234, 240, 241] have attempted to provide some benchmarks with regards to the performance metrics and the level of analysis to provide in order to guarantee comprehensive evaluation of the proposed approaches utilizing Deep Learning-based approaches. At the same time, an approach has been established for separately discussing the performance of rebar detection and localization system. Furthermore, the performance is also discussed from a qualitative and quantitative perspectives. The quantitative aspects deal with discussing the visual elements of the results (e.g. the parts of the result

images the proposed system was able to detect correctly and what limitations and issues of the proposed system can be detected visually).

2.3.2 Surface-Level Analysis of Bridges for Steel Defect Detection System

There are some relevant studies, which deal with different approaches towards steel corrosion detection [208–210]. Similarly, the steel defect detection systems exist for other applications. For example, for improving steel manufacturing process, steel sheet defect detection has received attention in the past [242–244]. However, these methods are not relevant or generalizable to this context (e.g. steel defect detection in bridges) due to a number of factors. These factors include *outdoor environment* (this comes with challenges with respect to change in lighting condition, shadows and other effects that can hinder accurate defect detection relying on vision-based sensors for data collection), *complex steel structures* (steel structures below and above the bridge decks are composed of complicated steel beams, trusses and other steel-based support structure), *large variance in bridge steel structures* (different bridges have varying level of steel above and underneath the bridge decks), and *robot-based application* (The system has to be ultimately be deployed in real-time on an actual robot for bridge inspection).

Due to lack of adequate attention in this field of study, there has not been any development of benchmark that can assist in the accurate evaluation of system performance.

Existing studies in this regard covered in this dissertation [245, 246] have proposed the utilization of novel framework for steel bridge defect detection using robotic platform. The development of benchmarks require a steady number of studies in a particular field. Future studies in this respect will focus towards benchmark development for robotic bridge inspection.

2.4 Novel Contributions of this Dissertation

The prior sections outlined careful assessment of the underlying literature pertaining to the inspection of bridges using different robots and sensors. In this section, the prime focus will be towards highlighting the novel contributions of this dissertation in the context of state-of-the-art. The novel contributions of this dissertation can be broadly classified into two folds, namely with respect to the development of novel methods for *sub-surface-level analysis* (i.e. rebar detection and localization systems) and *surface-level analysis* (i.e. steel defect detection system). To discuss the intricate details regarding the novelties in each of these two aspects of the literature, the following sub-sections will shed light on each of the individual parts.

2.4.1 Sub-Surface-Level Analysis of Bridges for Rebar Detection and Localization

As highlighted in section 2.1.3.3, it can be concluded that the research area pertaining to the development of rebar detection and localization has received considerable attention in the past. In relation to these studies, the novelty of the proposed approaches, which will highlighted as a successive series of five separate publications that will outline the evolution in the approach taken to provide more robust and effective systems for rebar detection and localization. The individual novel elements of each study developed for rebar detection and localization can be broken down into key parts that are given below:

1). **Dataset**: The GPR dataset that has been used in these studies is novel in the sense that it has not been used in any prior study. The data from a total of eight bridges (novel data not used in prior studies), along with one open-source GPR data [40] has been used in majority of the studies published. All of the data was collected using RABIT platform [81, 247, 248] in an automated fashion between 2013 and 2014 from diverse bridges from all across the United States. The use of data from multiple bridges ensured that the proposed rebar detection and localization is able to provide reliable performance for bridges with different physical properties. In terms of quantity, this dataset provides a reasonable amount of data, as quality and quantity of data is critical for development of robust and reliable Deep Learning-based algorithms for rebar detection and localization.

2). **Proposed Approaches**: A number of novel approaches have been developed in published work associated with this dissertation. In [123], a novel approach for rebar detection was developed that leveraged Deep Residual Networks (ResNet-50). The results were promising and the follow-up to this study were planned accordingly. This work [123] was extended from multiple perspectives in future studies. Firstly, [123] proposed a rebar detection system without any method for rebar localization. In order to mitigate that, [124] was able to provide a novel framework for rebar detection and localization. The rebar detection system proposed in [123] and rebar localization system proposed in [40] was extended in [234]. For rebar detection and localization system in [234], a combination of supervised (e.g. multiple Residual Frameworks and DenseNet framework (e.g. ResNet-18, ResNet-34, ResNet-50, ResNet-101, DenseNet-121, DenseNet-161)) and unsupervised (K-means clustering with sliding-window-based approach) methods were leveraged to provide a novel rebar detection and localization framework. In light of the various challenges and limitations of block-based approaches (e.g. [39, 40, 123, 124, 234]) highlighted in [234], thee was a need for developing a better way to provide more accurate detection and localization system. It is for this reason, the use of Deep Encoder-Decoder networks was adopted in [240, 241]. The difference between Deep Encoder-Decoder networks [240, 241] and earlier Deep Networks used in [123, 124, 234] is the manner in which data is annotated and analyzed, namely the block-based approach (regions within GPR B-scan images are either classified as belonging to rebar or background classes) in [123, 124, 234] and pixel-based approach (each pixel is either assigned a

class label of rebar or background) in [240, 241]. By leveraging the pixel-based approach in [240, 241], a fine-grained and more accurate analysis of rebar B-scan images can be performed. In [240], based on prior knowledge, a novel multi-stage framework leveraging deep encoder-decoder network was developed for rebar detection and localization with a unique approach towards tackling this research problem. In the first stage of the novel framework in [240], the goal is to separate rebar layer from background regions. In the second stage of the novel framework in [240], the goal is to separate rebar pixels from the background pixels. Using this approach, the effect of noise and reflective signals can be reduced in an effort to mitigate some of the challenges and issues highlighted in [234].

3). **Level of Analysis**: Earlier studies for rebar detection and localization were not able to appreciate the separate nature of the rebar detection and rebar localization. The manner in which results were outlined in [124, 234, 240], a clear distinction was maintained between the two tasks and benchmark for evaluating the rebar detection and localization from quantitative and qualitative analysis was developed in [124, 234, 240]. This approach to analyzing the performance of the rebar detection and localization system separately can allow the researchers to gain a better understanding of the underlying systems and the performance of rebar detection and rebar localization systems.

4). **Key Challenges**: Unlike earlier studies that merely provided results without shedding light on limitations and challenges of dealing with diverse GPR data, [234]

was able to spend considerable effort towards highlighting various issues and limitations that inhibit the development of an effective, robust system for rebar detection and localization. This can serve as guidance for researchers in this field as well as field experts in order to find effective ways to tackle various limitations and challenges outlined in [234].

2.4.2 Surface-Level Analysis of Bridges for Steel Defect Detection

In the context of steel bridges, the literature on steel defect detection is limited in nature. There are only a handful of studies that discuss steel crack and corrosion detection [203–210]. When comparing the other studies [203–210] with proposed studies in this dissertation, there are wide divergences in terms of: (i) depth of evaluation of system performance, and (ii) the metrics used for performance evaluation. It is for this reason, a need was felt to develop steel defect detection systems that can be practical, and provide greater coverage in terms of detecting defect in difficult-to-reach and remote regions of the bridge infrastructure. The individual novel elements of each study developed for steel defect detection can be broken down into key parts that are given below:

1). **Robot Platform**: A novel multi-directional bicycle robot has been designed and its performance has been discussed in [245]. The robot is novel in terms of its hardware

specifications and design. This robot has been used to collect data for validation of the steel defect detection system that has been discussed in this dissertation [245].

2). **Dataset**: There are two novel dataset used for the development and validation of steel defect detection system discussed in this dissertation [245, 246]. Colleagues of the Advanced Robotics and Automation (ARA) Lab located in Vietnam were able to collect around 5,000 high-resolution images with steel parts containing defects. Furthermore, in order to validate the robustness and real-time performance of the proposed steel defect detection system, the validation dataset was 1,500 high-resolution images collected from an actual bridge inspection performed in Lovelock, NV, USA. This dataset has also not been used in any other studies.

3). **Proposed Approaches**: In light of the benefits and improved gains from usage of Deep Encoder-Decoder networks in the context of rebar detection and localization [240, 241], decision was made to leverage Deep Encoder-Decoder networks for steel defect detection. This approach is novel in the context of steel defect detection systems, as existing methods have not leveraged Deep Neural Networks for defect detection. In this respect, a recent study leverage UNet as the primary architecture, along with different encoder modules were used for steel defect detection with promising results [246]. This was followed by another study that proposed a novel pipeline for real-time processing for steel defect detection in [245] with results highlighted for different set of Deep Encoder-Decoder frameworks and encoder modules.

4). **Real-Time Evaluation**: The novel pipeline for steel defect detection developed

in [240, 241] is able to provide real-time validation for defect detection in steel bridges. Two different systems with varying hardware and software specifications were used to validate the proposed system. The system was trained offline and the trained models were used for real-time validation in two systems. The results revealed real-time capabilities, which can be leveraged in the near-future to develop systems on board bridge inspection robots to provide real-time defect detection of steel regions.

2.5 Performance Metrics

This section will discuss the background regarding statistical metrics for performance evaluation used in this dissertation, along with developing a contextual understanding of the results for each metric used. Some of the metrics used to verify and validate the performance of the Machine Learning-based systems include accuracy, loss, precision, recall, F1-score (also known as Dice Loss), and mean-Intersection-over-Union (mIoU). Prior to discussing the mathematical foundation and contextual understanding, there are a few metrics relevant to the classification problem in Machine Learning systems that need to be understood. Figure 2.7 highlights the confusion matrix for a Machine Learning system that is used for binary classification (i.e. classification of images into two classes, here referred to as class 0 and class 1). For developing a multi-class classifier, the confusion matrix will have more row and columns identifying the different classes (i.e. ML-based classifier for 3 classes will have three rows and three columns in confusion matrix, ML-based classifier for 4 classes will have four

rows and four columns in confusion matrix and so on). Confusion matrix for two classes with four metrics given in the four boxes in relation to positive/positive, positive/negative, negative/negative, and negative/positive for the actual and predicted values are given in figure 2.7. Actual values correspond to the ground truth for the image classes. Predicted values are the results of prediction results provided by the ML-based classification system. With regards to True Positive (TP), it is the number of images that were correctly classified as belonging to the class 1. Similarly, for True Negative (TN), it is the number of images that were correctly classified as belonging to class 0. For False Positive (FP), this metric outlines the misclassification of images belonging to class 0 as inaccurately belonging to class 1. For False Negative (FN), this metric tells us about the quantity of the misclassification of images belonging to class 1 as inaccurately belonging to class 0.

These four metrics are important, as at the end of each training/validation session of the different ML-based models with binary classification, the output is in the form of TP, FP, FN, and TN (More classes means that there will be more pairs of positive and negative metrics for each class, i.e. three classes will lead to 9 metrics, four classes will have 16 and so on). These metrics are further leveraged to provide calculations regarding other more useful metrics that can be directly used to assess the performance of the proposed models. FP and FN are also referred to as Type-1 and Type-II error respectively. Equation 2.1 provides mathematical formula for calculating the accuracy of the proposed system, which is a ratio of sum of TP and TN and sum of TP, TN, FP, and FN. This basically means that the total number

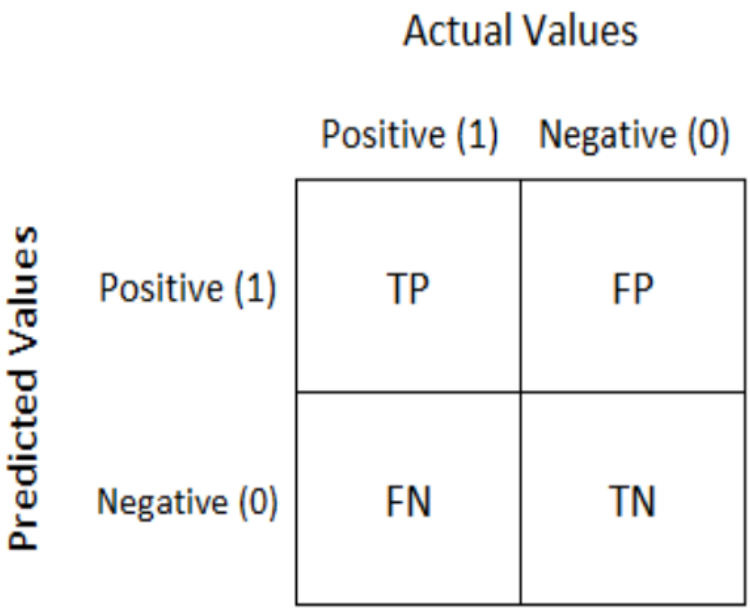

FIGURE 2.7: Confusion matrix for two classes with four metrics given in the four boxes in relation to positive/positive, positive/negative, negative/negative, and negative/positive for the actual and predicted values. Actual values correspond to the ground truth for the image classes. Predicted values are the results of prediction provided by the ML-based classification system.

of correctly classified images for the two classes as a proportion of total number of validated images is referred to as accuracy. Conversely, loss is the ratio of incorrectly classified images (i.e. sum of FP and FN) and total validated images (i.e. sum of TP, FP, FN, and TN), which is given in 2.2.

$$Accuracy = \frac{TP + TN}{TP + TN + FP + FN} \tag{2.1}$$

$$Loss = \frac{FP + FN}{TP + TN + FP + FN} \tag{2.2}$$

$$Precision = \frac{TP}{TP + FP} \tag{2.3}$$

$$Recall = \frac{TP}{TP + FN} \tag{2.4}$$

Precision and Recall are two other performance metrics that are regularly used in order to assess the performance of ML-based systems. Precision is the ratio of TP over actual positive (i.e. sum of TP and FP). Recall is the ratio of TP over predicted positives (i.e. sum of TP and FN). Recall and Precision are given in equations 2.4 and 2.3. F1-measure (also referred to as Dice Loss) is the harmonic mean of precision and recall, as highlighted in 2.5.

$$F1 - measure = 2 * \frac{Precision * Recall}{Precision + Recall} \tag{2.5}$$

$$IoU = \frac{Predicted_B \cap Actual_B}{Predicted_B \cup Actual_B} \tag{2.6}$$

$$mIoU = \frac{\sum(IoU)}{N} \tag{2.7}$$

Another metric that has been widely deployed in various ML-based systems in order to

provide a better understanding of the performance of the system is called Intersection-over-Union (IoU) and mean-IoU. IoU is the ratio of area of intersection between predicted bounding box and ground truth/ actual bounding box (referred in the equation 2.6 as $Predicted_B$ and $Actual_B$ respectively). mIoU is the sum of all IoU values calculated for all validated images divided by the total number of validated images (total number of validated images are given as N in equation 2.7). For the case of bounding-box-based annotation approach, the aforementioned calculations related to IoU and mIoU are applicable. In the context of pixel-based approaches, as in the case of semantic segmentation, the bounding box can be understood as composition of individual pixels, where each pixel has its own class label.

In order to provide contextualization for the different metrics and the manner in which performance outlined by different metrics is interpreted, there is a need to highlight a basic example to provide basic understanding to the readers of this dissertation. Table 2.4 outlines the dataset information of three hypothetical studies with their respective performance metrics. this example is specific to rebar detection and localization system with dataset information regarding number of bridges from which the data is collected and the total number of images in the dataset. Other information is related to the performance of the proposed systems in study 1, study 2 and study 3. To make things easier to understand, the calculations are traced back from the hypothetical values of TP, TN, FP and FN specified. For each dataset of the different studies, it is assumed that the class distribution of data is same (e.g. out of 1,000 image, 500

belong to positive and 500 to negative class for study 1 and 2 and out of total of 100,000 images, 50,000 for each class for study 3).

Metrics	**Study 1**	**Study 2**	**Study 3**
No. of Bridges	1	10	25
No. of Images	1,000	1,000	100,000
TP	450	400	40,000
TN	450	400	30,000
FP	50	100	10,000
FN	50	100	20,000
Accuracy	90%	80%	70%
Loss	10%	20%	30%
Precision	90%	80%	80%
Recall	90%	80%	67%
F1-measure	90%	80%	72.9%
mIoU	N/A	78%	82%

TABLE 2.4: A hypothetical example outlining three hypothetical studies with their respective dataset and performance information given

The analysis of data and its results can be challenging for a number of factors, which will be highlighted from example given in table 2.4. From a dataset perspective, the three studies disclose that they have data from 1, 10 and 25 bridges with number of images amounting to 1,000, 1,000 and 100,000 respectively. It is clearly evident that when comparing dataset alone, the diversity of data is much higher in study 3, when compared with study 1 and 2. This means that the with this amount of data available, any system developed will be able to generalize to unknown, new dataset from real bridges. In comparison, the amount of data available in study 1 and 2 is limited and any performance-related indicators used, their implications will be much lower than study 3, even if the performance of study 3 is lower in comparison to study 1 and 2. As, is the case shown in table 2.4. When comparing statistical measures

for different studies, it is important to understand that the statistics should not be directly compared, rather they should be compared with respect to their own dataset. So this means that 90% accuracy and 10% loss for study 1 has less significance as compared to 70% accuracy and 30% loss for study 3 because of the size of dataset (i.e. 100,000 images for study 3 against 1,000 for study 1). As, the number of images for both study 1 and 2 are same, it is clear that study 2 has lower accuracy, loss, and other metrics as compared to study 1. For studies not incorporating mIoU will provide partial picture of the performance of the systems. It is important to understand that mIoU as a metrics sheds light on non-statistical aspects of the results and system performance. Study 1 did not employ mIoU, so there is no way to find out about the level of overlap between ground truth and validated results. For study 2 and 3, mIoU shows that there is a greater level of overlap between ground truth and validated images for study 3.

2.6 Chapter Summary

In this chapter, a comprehensive overview of the relevant literature has been discussed, ranging from the development of different robotic platforms for bridge inspection and the taxonomy of different robot platforms used in the past to different sensors that have been leveraged for bridge inspection. Within the different sensors utilized, the distinction between single sensor and multiple sensor-based systems has been outlined. With the usage of multiple sensors, the development of different sensor

fusion techniques for bridge inspection have also been highlighted. For surface-level analysis of bridges, the extant literature pertaining to the crack detection systems has also been provided with comparison between different approaches. For sub-surface-level analysis, the focus has been towards discussing different studies developed for rebar detection and localization. In the concluding parts of the chapter, discussion regarding performance benchmarks for sub-surface-level and surface-level analysis has been provided. In order to contextualize the research in this dissertation with respect to the state-of-the-art in surface-level analysis (e.g. steel defect detection system) and sub-surface-level analysis (e.g. rebar detection and localization system) of bridges, the novel contributions of this dissertation have been discussed in the last section of this chapter.

Chapter 3

Rebar Detection and Localization for Sub-Surface Analysis of GPR Data

3.1 Study 1

3.1.1 System Methodology

The proposed technique for evaluating the effectiveness of Deep Residual Networks (ResNets) towards rebar detection has not been reported in the existing literature. It is for this reason that one of the variants of the Deep Residual Networks, namely ResNet-50 [249], has been employed in this research for the development of rebar

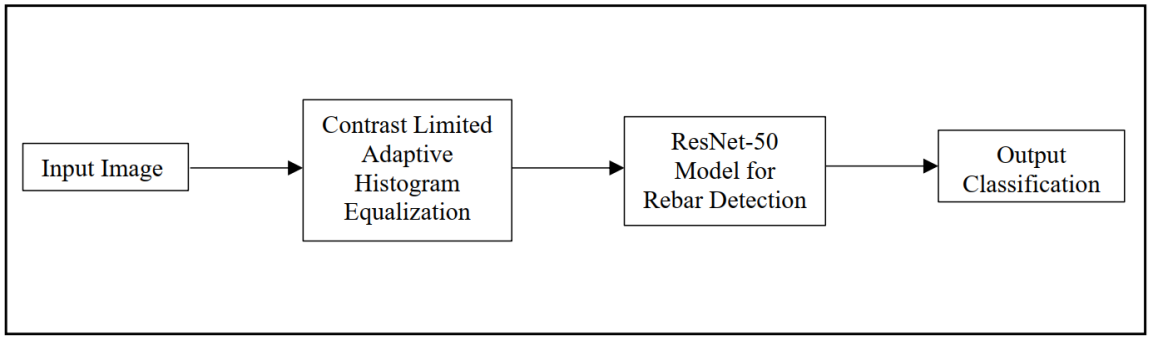

FIGURE 3.1: Proposed Method for Rebar Detection

detection system. Figure 3.1 highlights the basic model, which has been used for the development of ResNet-50. ResNet is one of the recently developed variants of CNN [249], which has gained increased acceptance and popularity in the research community in terms of its widespread application to various computer vision-based problems (e.g. object recognition, image recognition, image segmentation, image super-resolution) [249] [250] [224].

Figure 3.1 shows the model proposed in this study with Contrast Limited Adaptive Histogram Equalization (CLAHE), which was first proposed in Gibb and La [251]. Unlike Residual Networks, the traditional CNNs suffered from substantial decrease in the overall accuracy as well as increasing error rates with increasing depth of the neural networks [249]. The basic building block and structure of ResNet can clearly outline the ways in which ResNet differs from its 'plain' CNN-based counterparts, as each residual block (given in the lower part of the figure) skips a few convolutional layers, which enhances its overall optimization and resistance to degradation [199]. For the construction of ResNet-50, the block given in figure 2 is replicated multiple times to provide a network with increased depth as well as an overall improved

Network Parameters	**Dataset 1**	**Dataset 2**
Network Name	ResNet-50	ResNet-50
Bridge Name	East Helena Bridge, MT	Warren County, NJ
Number of Layers	50	50
Number of Epochs	24	8
Batch Size	4	4
Learning Rate	0.0001	0.0001
Total Number of Images	600	5,100
Train/Validation Split	520:80	3,300:1,800
Image Size	81 x 81	33 x 52

TABLE 3.1: Network Specifications and dataset information in relation to the training and validation of the proposed system

performance. The numbers given on each of the residual blocks correspond to their respective feature sizes. In this study, the system was trained on the existing dataset using learning rate of 10-5 to fine-tune the system to the most optimum performance. Depending on the type of dataset being used, the system was trained for a variable number of epochs. Table 3.1 outlines the different network parameters and dataset information for the two dataset utilized in this study. The separation between training and validation dataset is performed randomly during each training/validation phase and this process is repeated multiple times and the average values for different metrics are used.

3.1.2 Results and Discussion

In this section, the overall performance of the proposed system will be discussed, along with some insights with respect to the dataset that have been used for the training and evaluation of ResNet- 50 for rebar detection. Table 3.2 outlines some of the salient features of the different dataset and the location from which the data was collected, as it has been acquired from some of the earlier studies (e.g. dataset for Warren County, NJ from [40]), which allow validation of proposed system by comparing its performance with prior studies. Table 3.2 outlines the performance of the proposed system trained on the different available dataset using some of the widely employed performance metrics, namely accuracy rate and error rate. The proposed system was trained and evaluated using data from the two dataset individually, which allowed an assessment of different factors affecting the system accuracy. Afterwards, the data was concatenated for the system training using the two dataset.

In order to accomplish that, all of the input images were resized to ensure that the system was trained on images with the same size. It can be seen from table 3.2 that when training for a dataset with limited amount of positive and negative images, there was a need for training the system using a significant number of epochs. However, despite that, the overall error rate was very high (22%), as

the overall accuracy of the CNNs and their variants is highly dependent on the quantity of data used for system training. Conversely, when training for a dataset with a reasonable amount of data (e.g. Warren Country, NJ), the system was trained for 8

Dataset	Image Size	Epochs	Accuracy	Error
East Helena, MT	81 x 81	24	92.88%	22%
Warren County, NJ	33 x 52	8	98.11%	6%
Total	81 x 81	8	98.47%	4%

TABLE 3.2: Performance of the proposed system using the existing system

epochs to reveal promising results. It can be seen that the system trained using the collective dataset was able to provide an overall accuracy of 98.47%.

3.2 Study 2

3.2.1 System Methodology

In this section, a comprehensive evaluation of the different elements within the proposed method for rebar detection and localization will be highlighted. The present study employs one of the variants of the Deep Residual Networks Rebar Detection and Localization (i.e. ResNet-50) [249] as a critical sub-component of the overall system for rebar detection and localization. A preliminary analysis has been discussed in one of the recent works by the authors [122]. The present study is essentially a continuation and in-depth evaluation of the performance of Deep Residual Networks, along with its various pros and cons for the application towards NDE of bridges. Figure 3.2 depicts some of the salient features of the proposed system for rebar detection and localization. The first block of the proposed model is the GPR database, which leverages B-Scan data from different bridges to separate data for the two classes (i.e.

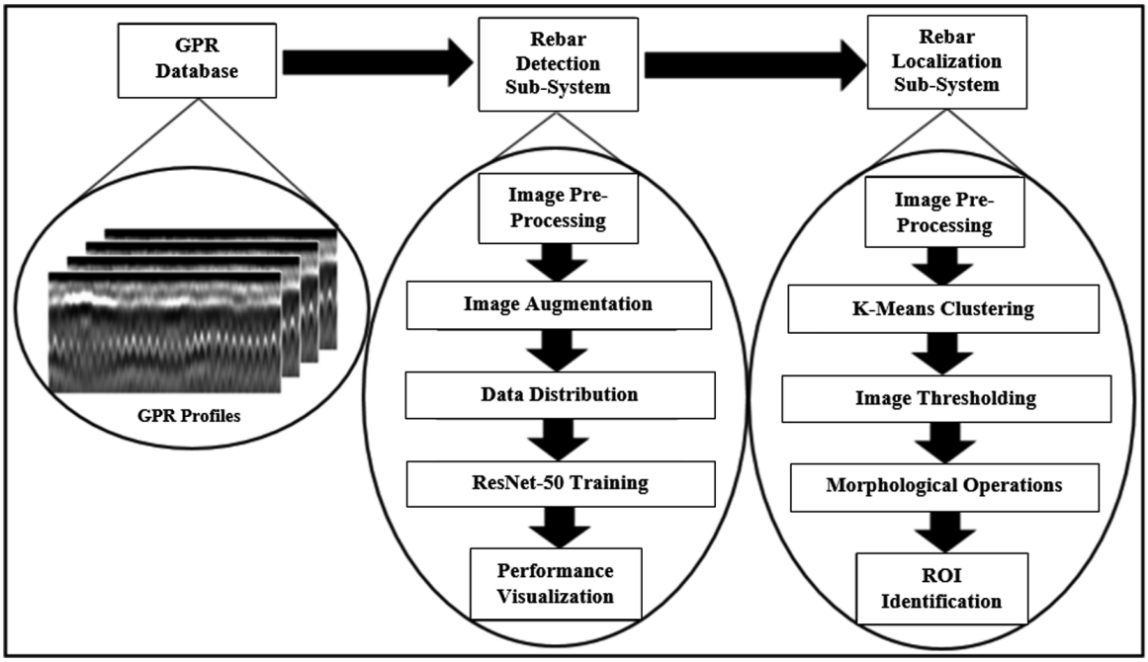

FIGURE 3.2: Proposed Model for Rebar Detection and Localization

rebar and non-rebar classes). The statistical information regarding the data and its distribution for testing and validation will be highlighted in the proceeding sections.

For system training using Deep Residual Network architecture (i.e. ResNet-50), a number of different operations have been performed, which include image pre-processing (different image operations are performed to reduce image noise and de-blurring), image augmentation (different transformation functions are applied to each image, which increases the dataset size and system performance), data distribution (random distribution of data into training and validation sets), ResNet-50 model training (use of data set for model training and validation to assess the performance of the rebar classification system) and performance evaluation and visualization (different performance measures are used to evaluate and visualize the system performance).

Network Parameters	**Dataset 1**	**Dataset 2**
Network Name	ResNet-50	ResNet-50
Bridge Name	Warren County, NJ	5 bridges
Number of Layers	50	50
Number of Epochs	5/10/20/100	5/10/20/100
Batch Size	4/8/16/32	4/8/16/32
Learning Rate	0.005	0.005
Total Number of Images	4,500	10,338
Train/Validation Split	2,243:528	9,427:2,640
Image Size	81 x 81	81 x 81

TABLE 3.3: Network Specifications and dataset information in relation to the training and validation of the proposed system

The separation between training and validation dataset is performed randomly during each training/validation phase and this process is repeated multiple times and the average values for different metrics are used. Table 3.3 outlines the system parameters, along with information regarding the dataset used in this study. The learning rate for all of the instances of system training was 0.005, which allowed for steady convergence with reduced probability of overfitting. The size of images in the dataset 1 and 2 had been fixed to 81 x 81 pixels. The system used for performing the different computations had the following specifications: Intel® i5 processor with 2.3 GHz clock speed, 4 GB RAM, and 500 GB hard disk. All other relevant details are highlighted in table 3.3.

With regard to the overall system for rebar detection and localization system, it is important to understand that there is a sequential order between the consecutive blocks. This means that before the data is available to the different processes in the rebar localization sub-system, the data undergoes processing through the different functions outlined in rebar detection sub-system, which are given in figure 3.2. Once the rebar detection subsystem is able to differentiate between the rebar and non-rebar images, the images belonging to the former category are acquired by rebar localization sub-system to establish the physical presence of rebar artefact within the available data. Similar to the rebar detection sub-system, image pre-processing functions are used in the rebar localization sub-system to sharpen the intricate details and enhance the overall boundary between the background and parabolic artefact outlining the presence of underground steel rebars. K-means clustering algorithm is used to segment the background (image pixels that do not contain rebar artefact information) and foreground (pixels that contain information related to rebar artefacts) information. In order to extract relevant information, the Image Thresholding technique has been used, which leads to the binarization of the original RGB image, along with some non-rebar artefacts. To separate noise from rebar artefacts, different morphological operations are utilized, namely morphological opening and closing operations. Finally, the Region-of-Interest (ROI) is highlighted using bounding box approach.

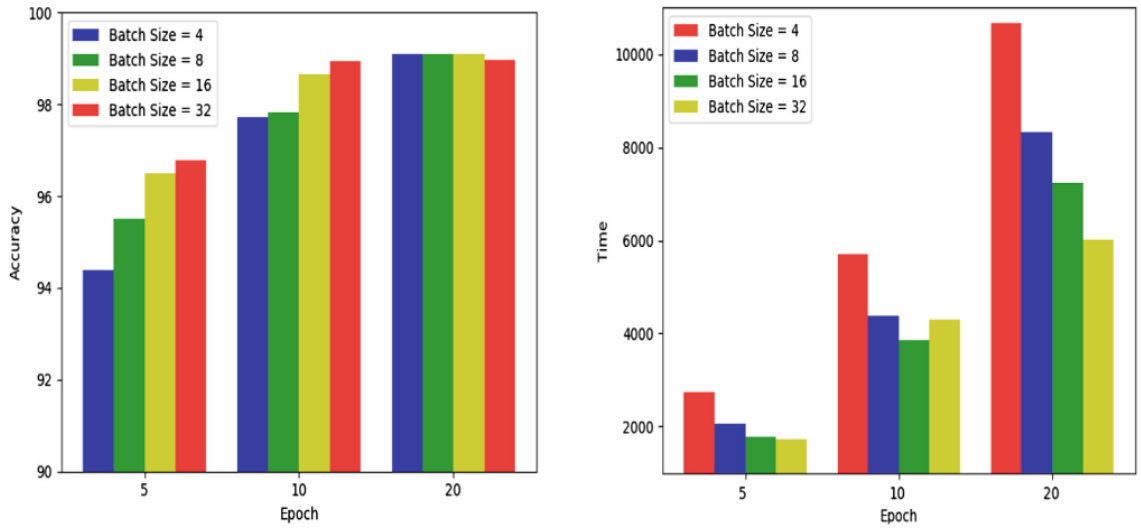

FIGURE 3.3: Barplot showing effect of different number of epochs and batch sizes on performance of the proposed model for Rebar Detection and Localization for dataset 1 (a) accuracy with number of batch size and epoch, and (b) training time with number of batch size and epoch

3.2.2 Results and Discussion

In this section, the results obtained during the training and validation of the proposed system are presented. One of the most important system characteristics is the trained system accuracy, which is shown in figures 3.3(a) and 3.4(a) for dataset 1 and 2 respectively. In these figures, it can be seen that for the case of systems trained for different batch sizes, the overall system accuracy converges when the system is trained for 20 epochs, which means that training beyond this point does not result is significant gains in system performance. When examining figure 3.3 and 3.4 collectively it is important to realize that the y-axis scales vary for both these figures. In general, systems trained for higher epochs have higher accuracy than system trained for lower epochs. Figures 3.3 (b) and 3.4 (b) demonstrate the overall trend between

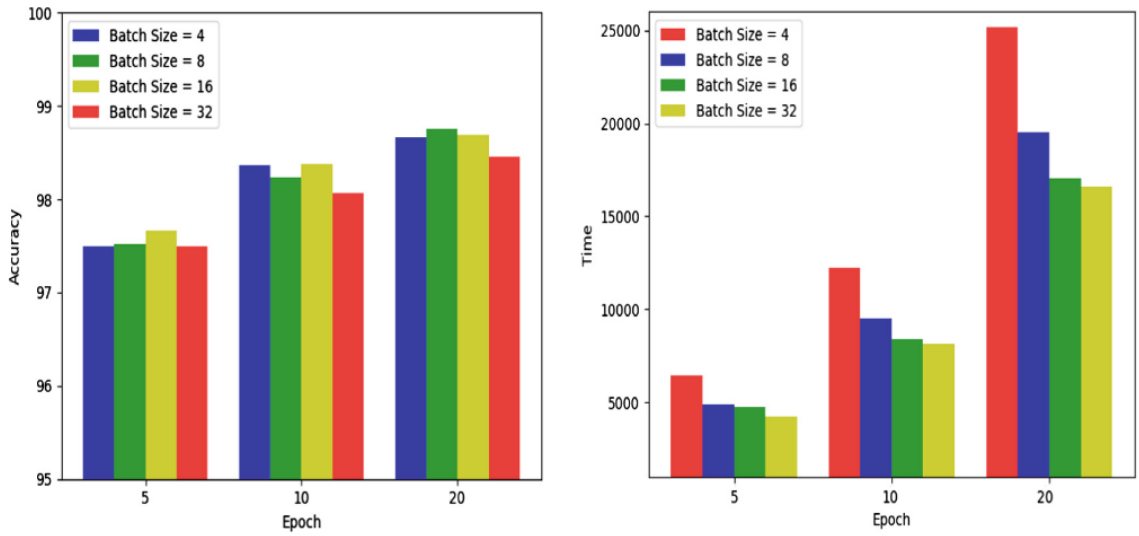

FIGURE 3.4: Barplot showing effect of different number of epochs and batch sizes on performance of the proposed model for Rebar Detection and Localization for dataset 2 (a) accuracy with number of batch size and epoch, and (b) training time with number of batch size and epoch

number of epoch and time (in seconds) for the different values specified for batch size during training of the proposed system using dataset 1 and 2 respectively. From figure 3.3 (b), it can be seen that when comparing the time taken for successful training of systems with different batch sizes, the batch size with the highest overall training time is 4. This shows that in order to optimize the training of the proposed system, a high level of batch size should be preferred. In order to fully appreciate the scale of improvement in computational performance of the proposed system, Figures 3.3 and 3.4 show that the time necessary for training with batch size of 32 and 16 epochs is comparable to the training time for batch size of 4 and 8 epochs.

In this regard, figure 3.4 (a) presents the results of system training for dataset 2 in terms of accuracy with increase in batch size and epochs for a specific range of values

chosen for different system parameters. In contrast to the results obtained for dataset 1, it can be seen that the overall improvement in accuracy with increase in number of epochs is not pronounced for dataset 2. Similarly, it can be seen in figure 3.4 (a), that increase in batch size does not necessarily result in considerably higher performance, specifically for the case of dataset 2. At the same time, there is very small variation in accuracy for the systems trained with different batch sizes. Furthermore, the results obtained for the case of batch size of 32 do not correspond to the highest performance. Due to the increased size of dataset 2, the training time is much higher in comparison to dataset 1, as highlighted in figure 3.3 (b), which shows that system trained with smaller batch sizes undergo higher increase in training time. In general, for the training of the rebar detection sub- system, the inverse relationship between batch size and training time is evident, i.e. increase in batch size reduces the overall time taken for system training. In order to fully benefit from the magnitude of available GPR data, both dataset 1 and 2 had been concatenated. It has been examined in the relevant studies that the performance of Deep Learning-based algorithms is highly dependent on the scale of dataset being used for the system training [123].

Table 3.4 outlines the overall performance of the system trained using data from different dataset. It can be seen that the system trained after concatenation of the

Dataset	**Accuracy**	**Loss**	**Training Time**
Dataset 1	99.11%	2.91%	7,229 s
Dataset 2	98.75%	3.73%	17,067 s
Total	99.42%	1.88%	21,687 s

TABLE 3.4: Summary of the results for the Rebar Detection System using different dataset

dataset 1 and 2 lead to the highest accuracy and lowest system loss metrics. However, in contrast to the training of dataset 1 and 2 separately, which were trained for 20 epochs each, the system utilizing both dataset 1 and 2 had to be trained for 100 epochs. It can be seen in table 3.4 that the training time for system trained on the total data has the highest training time. In comparison with relevant studies [251] [19] [122] [40], the results highlighted in this research provide the highest system-level performance for rebar detection system.

In the following discussion, some of the important details regarding rebar localization subsystem will be outlined. The rebar localization sub-system is the final component of the overall system proposed for rebar detection and localization in this research.

Table 3.5 outlines the overall performance of rebar localization sub-system in terms of accuracy and precision. The performance of the proposed rebar localization sub-system was evaluated on images with single and multiple rebar signatures. It can be seen from Table 3.5 that the overall accuracy for single rebar images is higher than for B-scan images containing multiple rebar signatures. For images with multiple rebar profiles, the sliding window-based approach was used to highlight different rebars

Dataset	**Single Correct**	**Single Incorrect**	**Multiple Correct**	**Multiple Incorrect**
Dataset 1	1,426	73	854	64
Dataset 2	1,299	45	869	76
Total	2,725(95.85%)	118(4.15%)	1,723(92.49%)	140(7.51%)
	Total Accuracy	94.52%	Total Precision	95.18%

TABLE 3.5: Summary of the results for the Rebar Localization System using different dataset

within B-scan images. The overall accuracy of the rebar localization sub-system is at par with the different rebar localization systems developed in the previous studies [251] [19] [122] [40]. A number of factors can affect the overall accuracy of localization of rebars in the B-scan images, such as high-level of noise artefacts in images, presence of multiple wave reflections, overlapping rebar signatures in B-scan images for multiple rebars, use of construction materials with varying properties (e.g. density, permittivity) and presence of non-rebar underground objects (e.g. pipes, utility lines, void spaces and underground metal objects) that exhibit similar hyperbolic signatures.

3.3 Study 3

3.3.1 System Methodology

In this section, a detailed examination of the proposed rebar detection and localization system will be provided. Based on Fig. 3.5, the proposed model for rebar detection and localization can be divided into three main sections, namely: (i) GPR data collection: In the previous sub-section, a considerable level of theoretical detail has been outlined for data collection using GPR sensors. In this section, some additional details regarding the practical implementations for data collection in this research will be discussed.

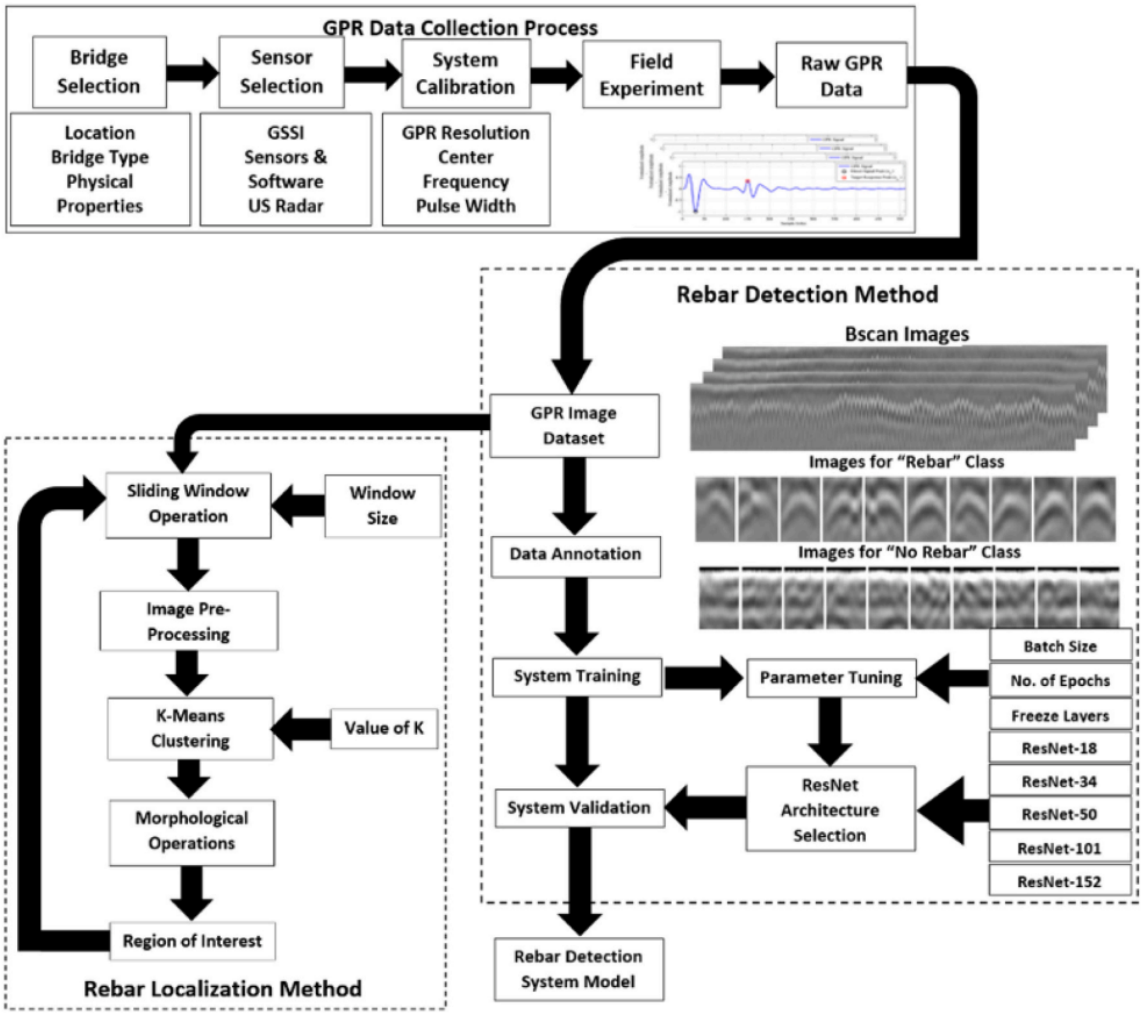

FIGURE 3.5: Proposed Model for Rebar Detection and Localization

(ii). Rebar detection system: Some of the salient features of rebar detection method will be highlighted in the following sub-section, and.

(iii). Rebar localization system: The discussion in one of the subsection will also outlined the proposed method for rebar localization.

Fig. 3.5 outlines some of the different steps undertaken from data collection using GPR sensor to getting the images output from Rebar Detection and Localization

Systems. The rebar detection system utilizes different Deep Residual Network architectures (e.g. ResNet-34, ResNet-50, ResNet-101, ResNet-152) [249] with varying network parameters (e.g. systems trained with different batch size, number of epochs and number of layers). The performance of the Deep Residual Network with the most optimal network configuration is compared with relevant DenseNet architectures (DenseNet-121, DenseNet-161) [252], which is another Deep Convolutional Network that has gained considerable attention in the recent past. The rebar localization algorithm performs the different image pre-processing functions to ensure that the smaller regions of GPR images can be used to extract the relevant rebar signatures. K-means clustering has been employed as an unsupervised form of learning algorithm, which enables the effective separation between the foreground and background regions within the GPR images. Due to the level of noise and other artefacts present in the GPR data, a number of different visual artefacts are also included in the foreground. In order to decrease the interference of noise and other artefacts, a number of different morphological operations are used, which ensure that the original image is converted into binary image with foreground regions separated from the background regions. With the use of morphological features, many of the noise and other reflective signals are separated and bounding box.

The rebar localization system is used to highlight the rebar signature within the GPR images. The details of the proposed rebar localization system have been highlighted in Fig. 3.5. The different processes for rebar localization and rebar detection systems are separate in nature, which means that they can work simultaneously towards

providing the desirable output within the larger framework of the overall system. Rebar localization system employs elements of the rebar detection system to ensure that it is able to perform different image processing functions on the parts of the larger GPR images that contain rebar signatures. Due to the large-scale size of the GPR images obtained from the raw GPR scan data, the rebar localization algorithm only works on portions of the GPR image using the sliding window-based approach. In the following section of the paper, the focus will be towards highlighting the effectiveness of the proposed rebar detection and localization method.

3.3.2 Results and Discussion

In this section, the overall performance of the proposed system will be discussed in terms of qualitative and quantitative level of analysis. Table 3.6 outlines the network parameters and dataset information from the three separate dataset used in this study. The specification for system labelled as CPU are given as follows: Ubuntu 16.04 LTS, 32 GB memory, 350 GB hard disk, Intel ® Core i7–8700 CPU with 3.2 GHz clock speed. Meanwhile, the system labelled as GPU had the following hardware and software specifications: Ubuntu 18.04 LTS, 32 GB memory, 350 GB hard disk, Intel ® Core i7–8700 CPU with 3.2 GHz clock speed and NVIDIA® GeForce® GTX 1080 TI Graphical Processing Unit (GPU). The systems information for CPU and GPU will be useful when comparing the difference in time taken for training for each network.

Network Parameters	**Dataset 1**	**Dataset 2**	**Dataset 3**
Network Name	Multiple ResNets Multiple DenseNets	Multiple ResNets Multiple DenseNets	Multiple ResNets Multiple DenseNets
Number of bridges	1 bridge	4 bridges	4 bridges
Number of Layers	18/34/50/101/152 121/161	18/34/50/101/152 121/161	18/34/50/101/152 121/161
Number of Epochs	20/40/80/100	20/40/80/100	20/40/80/100
Batch Size	4/8/16/32	4/8/16/32	4/8/16/32
Learning Rate	0.005	0.005	0.005
Total Number of Images	10,338	4,500	18,421
Train/Validation Split	8,070:2,268	3,600:900	16,421:2,000
Image Size	81 x 81	81 x 81	81 x 81

TABLE 3.6: Network Specifications and dataset information in relation to the training and validation of the proposed system

3.3.2.1 Rebar Detection System

The details of the performance of the different ResNet architecture networks have been given in Fig. 3.6, 3.7 and 3.8. Figs. 3.6 and 3.7 show bar-plot with average, maximum and minimum values for the different Deep Residual networks. It can be seen from Fig. 3.6(a) and 3.7(b) that the average accuracy of ResNet frameworks increases with number of epochs and batch sizes. The increase is steady and varies from one network architecture to another. Similar results are revealed for findings in Fig. 3.6(a) and Fig. 3.7(b). Overall, the increase in the number of epochs lead to increase in the accuracy of the rebar detection systems. It can be concluded from Figs. 3.6 and 3.7 that there is a positive correlation between number of layers and performance of rebar detection method, which is measured here using accuracy and loss metrics.

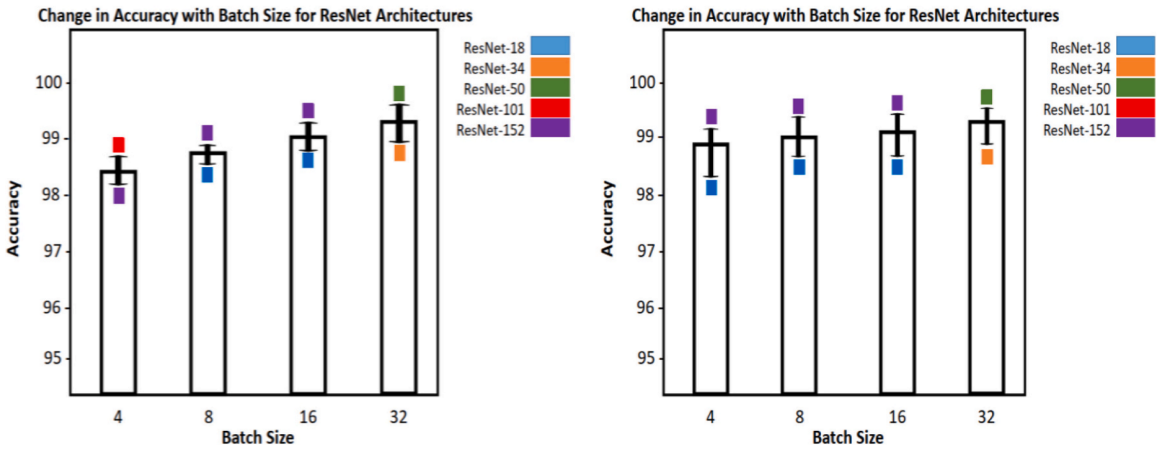

FIGURE 3.6: Result from dataset 3 providing information regarding change in accuracy with constant batch sizes and (a). number of epoch = 20, and (b) number of epoch = 100

The separation between training and validation dataset is performed randomly during each training/validation phase and this process is repeated multiple times and the average values for different metrics are used. It can be seen from Fig. 3.8(a) that increasing number of layers by a small fraction leads to greater increase in training for the different ResNet frameworks,

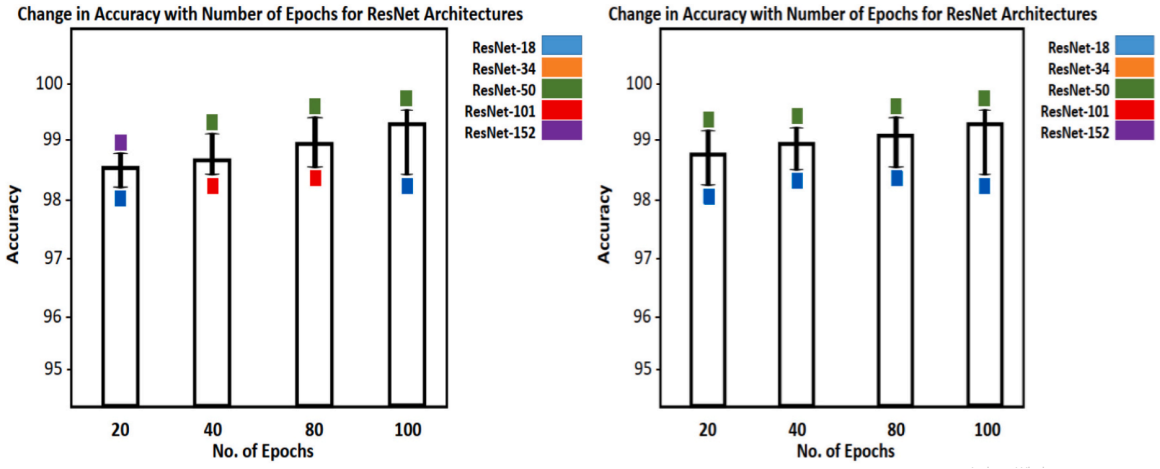

FIGURE 3.7: Result from dataset 3 providing information regarding change in accuracy with constant batch sizes and (a). batch size = 4, and (b) batch size = 32

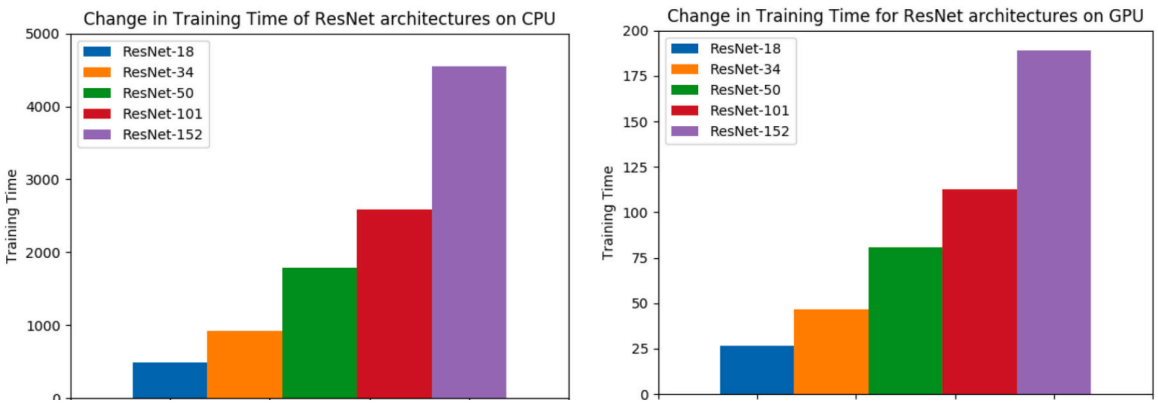

FIGURE 3.8: The results for dataset 3 provide information regarding training time with respect to the number of layers for which the system is being trained for the case of CPU, and GPU.

especially when training using CPU alone. The training time increases from less than 1000 min for ResNet-18 to approximately 5000 min for ResNet-152 architecture, which is roughly five times increase in the training time with eight times increase in network size (in terms of number of layers).

In comparison with these results, it can be seen that the system trained on GPU take significantly reduced time for training and there is a marginal increase in the training time with corresponding increase in the number of layers of the networked architecture. There is a wide difference in training time between CPU and GPU for the different layered architectures, which is evident from cross-examination of Fig. 3.8(a) and 3.8(b).

Table 3.7 outlines the final results for the rebar detection system, which shows the system training using the most promising system training configuration, based on the results obtained in the previous sections. Consequently, each of the system is trained with batch size of 32 and number of epochs equal to 100. In the final evaluation of the

Network	Train Accuracy	Train Loss	Validation Accuracy	Validation Loss	Train Time
ResNet-18	99.23%	2.15%	80.60%	10.2%	25
ResNet-34	99.31%	2.03%	84.70%	8.51%	47
ResNet-50	99.37%	1.66%	93.20%	7.44%	75
ResNet-101	99.37%	1.69%	94.30%	7.05%	118
ResNet-152	99.23%	2.00%	96.67%	18.9%	273
DenseNet-121	99.42%	1.51%	97.20%	5.32%	190
DenseNet-161	99.30%	1.89%	97.19%	11.2%	622

TABLE 3.7: Summary of the results for the Rebar Detection System using different Deep Convolutional Neural Network Architecture

rebar detection system, the total dataset containing data from nine bridges is divided into six bridges for testing and three bridges for validation of the system training. The overall performance is examined using training accuracy, training loss, validation accuracy, validation loss and training time. It can be seen in Table 3.7 that increase in the number of layers of network architecture improves the overall capabilities of the system to accurately detect rebar images from bridges that have not been previously been encountered by the rebar detection system.

Comparison of ResNet and DenseNet architectures and their performance given in Table 3.7 reveal that ResNet-152 contains an increased number of parameters, but provides better performance than Densenet-161 in terms of training time, validation accuracy, training accuracy, validation loss and training loss. These results are comparable to the state-of-the-art in the rebar detection systems [122] [123] [124] [19] [40].

3.3.2.2 Rebar Localization System

In this section, the performance of the rebar localization system will be discussed.The discussion of the results for rebar localization will be divided into two sections, namely the qualitative and quantitative analyses. In the qualitative analysis section, the focus will be towards examining the qualitative aspects of the results, which pertain to the visual evaluation of the way in which the rebar localization process has taken place. For the quantitative analysis of the results, there will be a need to examine the performance of the proposed rebar localization using different statistical measures. The qualitative analysis for rebar localization system deals with the examination of the results obtained using the human visual system in terms of accuracy and the overall quality of rebar localization.

3.3.2.3 Qualitative Analysis

Fig. 3.9 outlines results for rebar localization from different dataset using green bounding boxes within GPR images. The GPR scan images in Fig. 3.9 are small portions of the overall GPR scan. data obtained from different bridges. It can be seen that each of the dataset from the different bridges contain varying levels of noise, reflection signals and other non-rebar artefacts. For the case of Fig. 3.9(a), which contains GPR image from dataset 1 (i.e. Warren County, NJ bridge) with limited amount of noise leading to effective rebar detection and localization. Similar findings

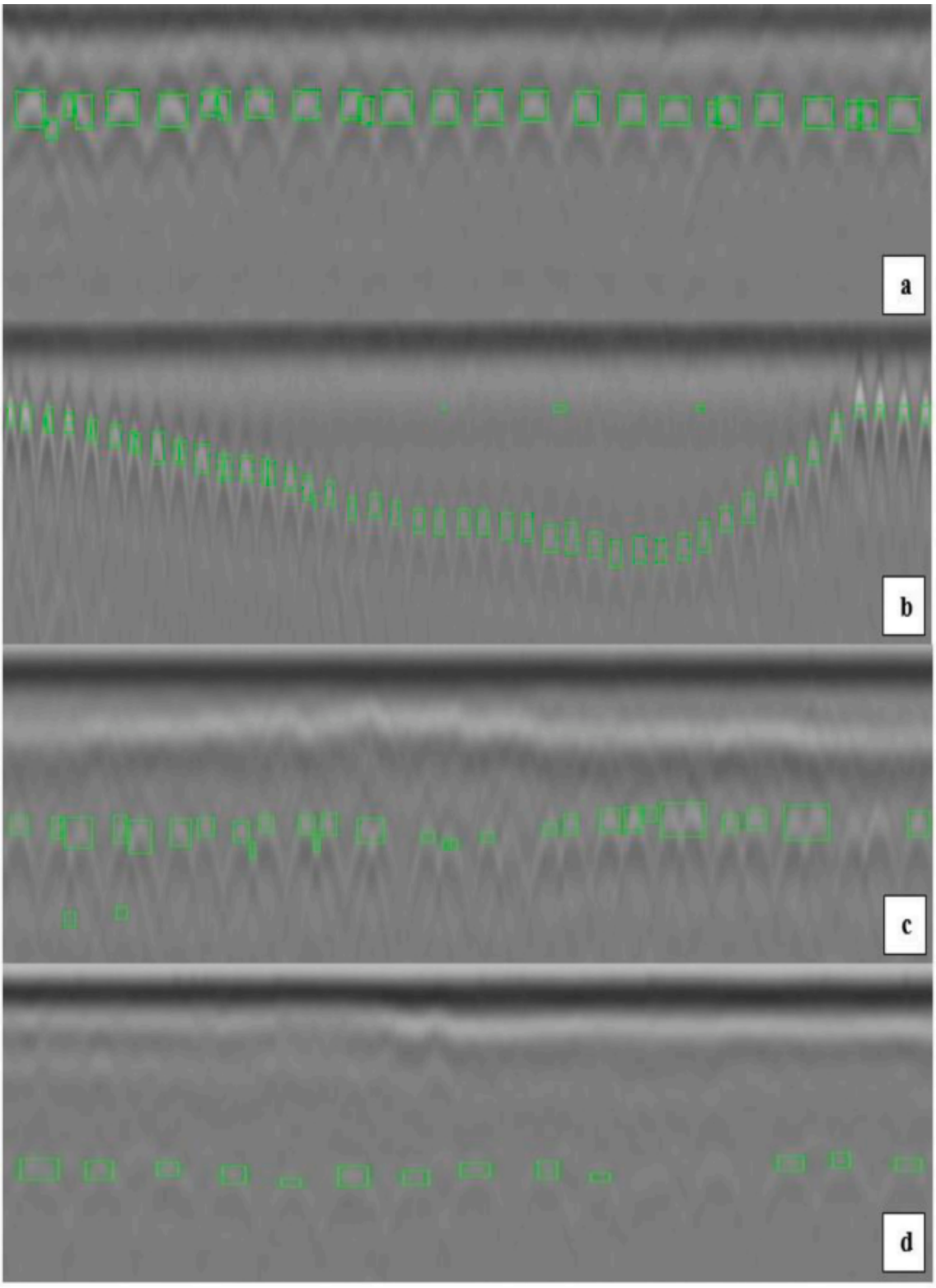

FIGURE 3.9: Rebar Localization Data Output with Bounding Boxes highlighting the different rebar signatures for the varying bridge data used in this study

are revealed for Fig. 3.9(b) containing GPR image from dataset 2 leading to accurate localization of rebar signatures.

Conversely, for the case of bridge dataset from Dove Creek bridge and Fordway bridge, which are given in Fig. 3.9(c) and 3.9(d) respectively, there is a considerable level of noise and reflection artefacts, which prevented the successful recognition and localization of different rebar signatures. At the same time, there is some misclassification of reflective signals and artefacts as correct rebar signatures. There are reflective signals in the shape of parabolic shapes that are depicted above and below the actual rebar profiles, which has led to the false classification of some of these reflective signals as actual rebar signatures. Due to the noise-related artefacts in the GPR data, there are some instances of false negative (the actual rebar profiles that are not accurately detected) and false positive (noise and other artefacts that are wrongly classified as rebar profile) within the dataset 3. In contrast to the dataset 1 and 2, the GPR data for bridges in dataset 3 contain considerable level of noise, and reflective artefacts, which leads to difficulties in the accurate localization of the rebar signals. These types of anomalous artefacts are not present in GPR data from dataset 1 and 2.

3.3.2.4 Quantitative Analysis

The quantitative analysis deals with the statistical aspect of the performance related to the rebar localization system developed in this study. A number of different performance evaluation metrics are used in the relevant literature for the effective

Study	Accuracy	Error	Precision	Recall	F1-score	Time
Dou [125]	N/A	N/A	70.07%	70.80%	70.20%	730 ms
Kaur [40]	91.98%	N/A	N/A	N/A	N/A	N/A
Gibb [39]	95.05%	N/A	N/A	N/A	N/A	N/A
Dinh [19]	99.60%	N/A	N/A	N/A	N/A	N/A
Ahmed [124]	94.52%	N/A	%	N/A	N/A	N/A
Harkat [236]	88.99%	N/A	N/A	N/A	N/A	N/A
This Study [234]	91.91%	8.14%	96.89%	94.41%	90.20%	372 ms

TABLE 3.8: Summary of the results for the Rebar Localization System with Comparison of the different metrics used in the state-of-the-art

examination of system performance. For the calculation of the different statistical properties related to performance evaluation, a number of different mathematical formulas have been used. Table 3.8 outlines the comparison between the performance of the proposed method in this research with state-of-the-art for rebar localization methods in relation to the different performance evaluation metrics [125] [40] [251] [19] [123] [236]. The performance of the rebar localization system is comparable or superior to the different algorithms discussed in the state-of-the-art.

3.4 Study 4

3.4.1 System Methodology

In this section, the particular details of the proposed method will be discussed. The building blocks for the proposed system for rebar detection and localization has been outlined in figure 1. The original raw data is in the form of one-dimensional A-scan

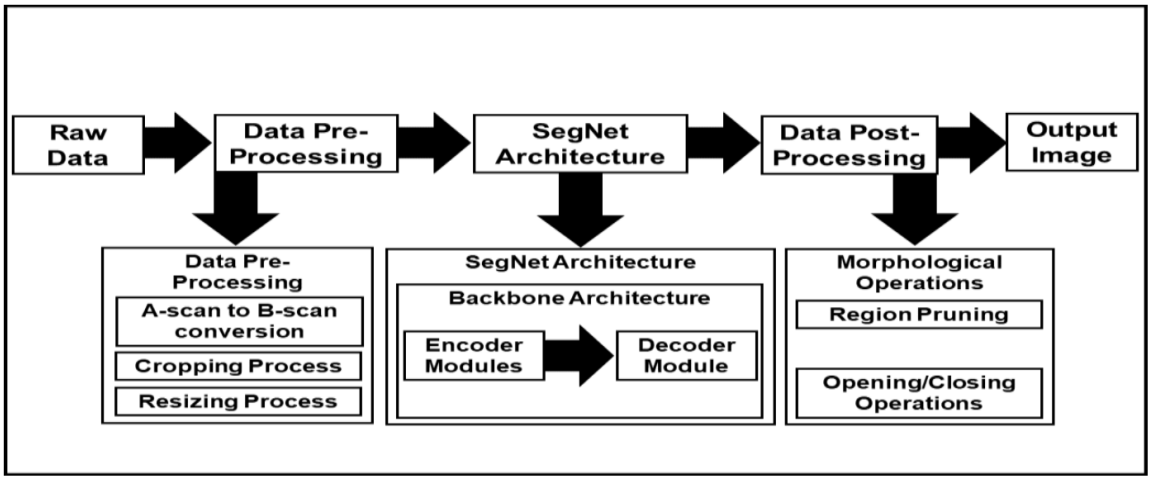

FIGURE 3.10: Proposed Method for Rebar Detection and Localization

signals, which is converted to GPR B-scan images with varying dimensions. Before SegNet is able to train on the GPR image data, different pre-processing techniques (e.g. editing, cropping and resizing) are used to convert the raw GPR B-scan image data from different bridges each of varying dimensions to image data with fixed dimensions. In contrast to most of the existing studies in this research area [125] [40] [251] [19] [123] [236], which utilize the bounding box approach of annotation, this study employs the pixel-level annotation technique. This allows the system to train the different model parameters to enable the pixel-level classification of input data into either belonging to foreground (e.g. rebar signatures) or background (e.g. non-rebar regions, noise, signal reflection).

With the different encoder modules, the decoder module used is this study employs the original native SegNet decoder that has been used in the original seminal study [253], which includes 13 consecutive decoding and up-sampling layers from the original VGG16 network. The GPR B-scan images, after undergoing different pre-processing

functions are given as input to the SegNet for training with seven bridge data and the performance is validated using data from the other remaining bridge. This ensures that the training and validation are performed on completely different data. There are different encoder modules (e.g. Vanilla-CNN, VGG16, VGG19, ResNet50, and ResNet-Xception modules) that have been used within the framework of SegNet. After the B-scan images are segmented using SegNet, a number of different post-processing operations (e.g. region pruning, removal of erroneous segmented artefact and noise) are performed to remove noise, reflection and other artefacts from the segmented image.

Table 3.9 outlines the network specifications and dataset information for the dataset from eight bridges used in this research. It is important to note that, due to the large size of the images, the overall number of images appear to be limited. However, this

Network Parameters	**Dataset 1**
Network Name	SegNet with multiple Encoder modules and default Decoder module
Number of bridges	8 bridges
Number of Layers	16/19/50/71
Number of Epochs	100
Batch Size	8
Learning Rate	0.001
Total Number of Images	920
Train/Validation Split	7:1
Image Size	768 x 768

TABLE 3.9: Network Specifications and dataset information in relation to the training and validation of the proposed system

number of sufficient to develop system that is able to provide reliable performance for data from different bridges. The detailed specifications of the computer system used for the training and validation of the proposed rebar detection and localization system are given as follows: Ubuntu 18.04 LTS, 32 GB memory, 350 GB hard disk, Intel ® Core i7–8700 CPU with 3.2 GHz clock speed and NVIDIA® GeForce® GTX 1080 TI Graphical Processing Unit (GPU). For the purpose of training and validation of the proposed system for rebar detection and localization, Tensorflow and Keras libraries have been used within Python programming language framework. The data is divided between training and validation sets based on "leave-one-out" approach, such that out of the total data from eight bridges, training of SegNet [253] is conducted on seven bridges and validation is performed on data from one bridge. This process is used to perform validation on all of the bridges to assess the performance of the proposed system for rebar detection and localization.

3.4.2 Results and Discussion

3.4.2.1 Quantitative Results

For the quantitative aspect of performance, the performance will be examined in terms of mean intersection-over-union (mIOU), which highlights the level of difference between the masks obtained for the ground-truth and output from trained SegNet. Table 3.10 outlines the performance of the different Architecture-Encoder pairs from a

Model	**Encoder**		**mIoU(%)**	**Train Time(s)**
SegNet	Vanilla CNN	Min.	62.1	12,600
”	”	Max.	71.8	12,700
”	”	Avg.	66.9	12,600
”	VGG-16	Min.	51.8	24,300
”	”	Max.	72.0	47,100
”	”	Avg.	63.6	35,800
”	VGG-19	Min.	52.8	27,400
”	”	Max.	71.9	27,500
”	”	Avg.	62.6	27,500
”	ResNet-50	Min.	53.7	38,100
”	”	Max.	71.3	38,200
”	”	Avg.	65.1	38,100
”	Xception	Min.	62.4	39,400
”	”	Max.	73.9	77,600
”	”	Avg.	67.3	60,200
”		Overall Average	72.2	40,620

TABLE 3.10: Summary of the results for the Rebar Detection and Localization System with maximum, average and minimum values given for each encoder module for the two quantitative metrics used in this study

quantitative aspect. Different encoder modules have been used for the training of SegNet for rebar detection and localization. For each encoder module (e.g. VanillaCNN, VGG16, VGG19, ResNet-50, and ResNet-Xception modules), the results obtained for the validation for different bridges have been classified in terms of the minimum, maximum and average values. Training time is another quantitative metric used in table 3.10.

Figure 3.11 outlines the average, minimum and maximum values for the training time for the different Architecture-Encoder pairs. Out of the different encoder modules, SegNet framework utilizing ResNet-Xception module is able to provide the highest performance in terms of mIoU. However, the slight increase in the maximum value for mIOU is followed with an exponential increase in the overall average training time.

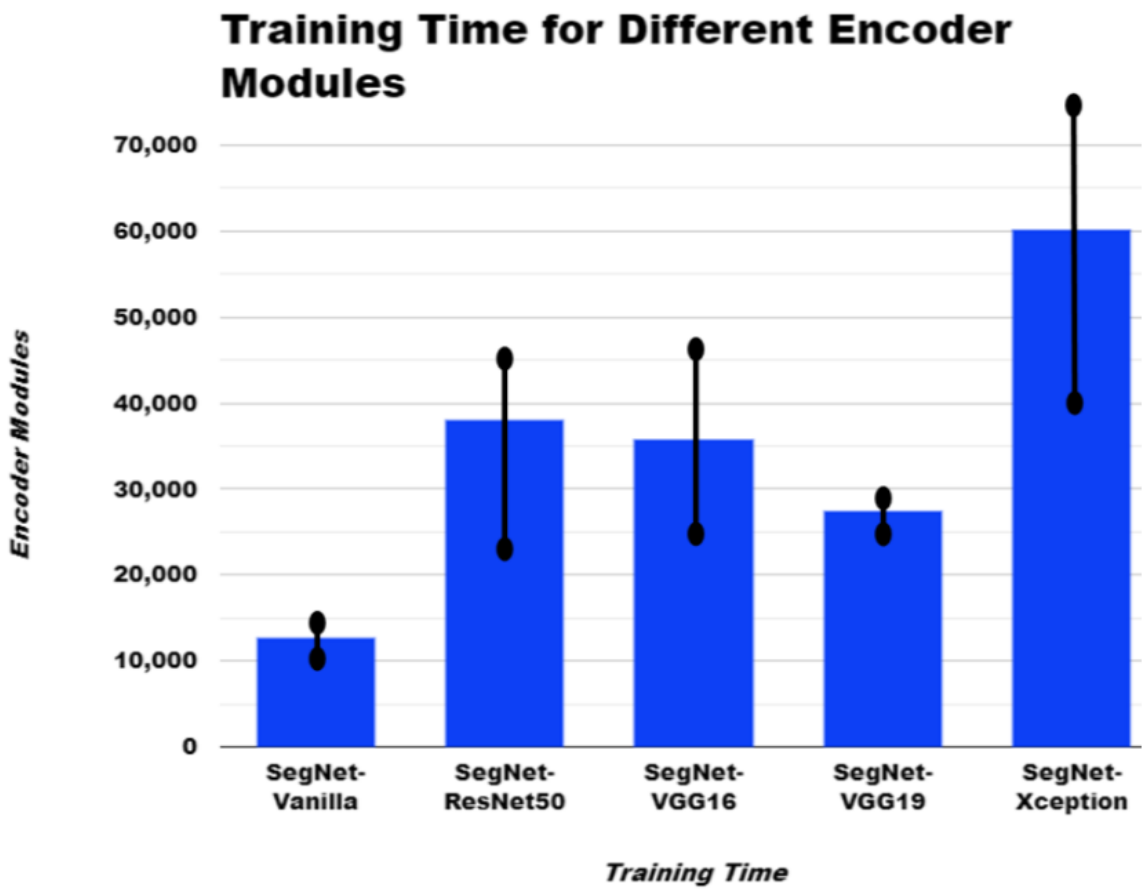

FIGURE 3.11: Comparison between the training time for the different Encoder Modules

Apart from that, there is varying difference in the maximum and minimum values of mIOU for the different encoder modules. For majority cases, the lower values of the mIOU remain between 60%-70%. The values of mIOU greater than 50% are considered as reliable results. There are also various issues in the dataset, which have been adequately discussed in [234]. These issues provide challenges towards effective detection and localization of rebar profiles by increasing the number of false positives and addition of noise artefact.

The comparison between the training time of the different encoder modules can be

better appreciated in figure 3 3.11. It can be seen in figure 3 that the SegNet with Vanilla CNN provides the lowest amount of training time as compared to other encoder modules with average training time slightly above 12,000 s. The highest training time has been obtained by Xception encoder module with an average training time around 60,000 s.

3.4.2.2 Qualitative Results

For the qualitative performance of the proposed system, the quality of the rebar signatures obtained from system validation will be discussed. Figure 3.12 outlines a comparison between bridge 4 and 5 with results from different Encoder modules within the SegNet architecture. It can be seen in figure 3.12 that out of the different results obtained using different encoder modules within the SegNet framework, ResNet-Xception module has shown the most promising results. The data from bridges 4 is challenging, as the distance between individual rebar profiles is small, which can lead to merger between adjacent rebar profiles. Figure 3.12 shows that in comparison with bridge 4, the data from bridge 5 contains separated rebar signatures. Out of the different encoder modules, Vanilla-CNN, VGG-16 and VGG-19 modules demonstrate considerable degradations. The results obtained from ResNet-50 and ResNet-Xception have a higher quality of rebar profiles obtained from noisy and challenging dataset.

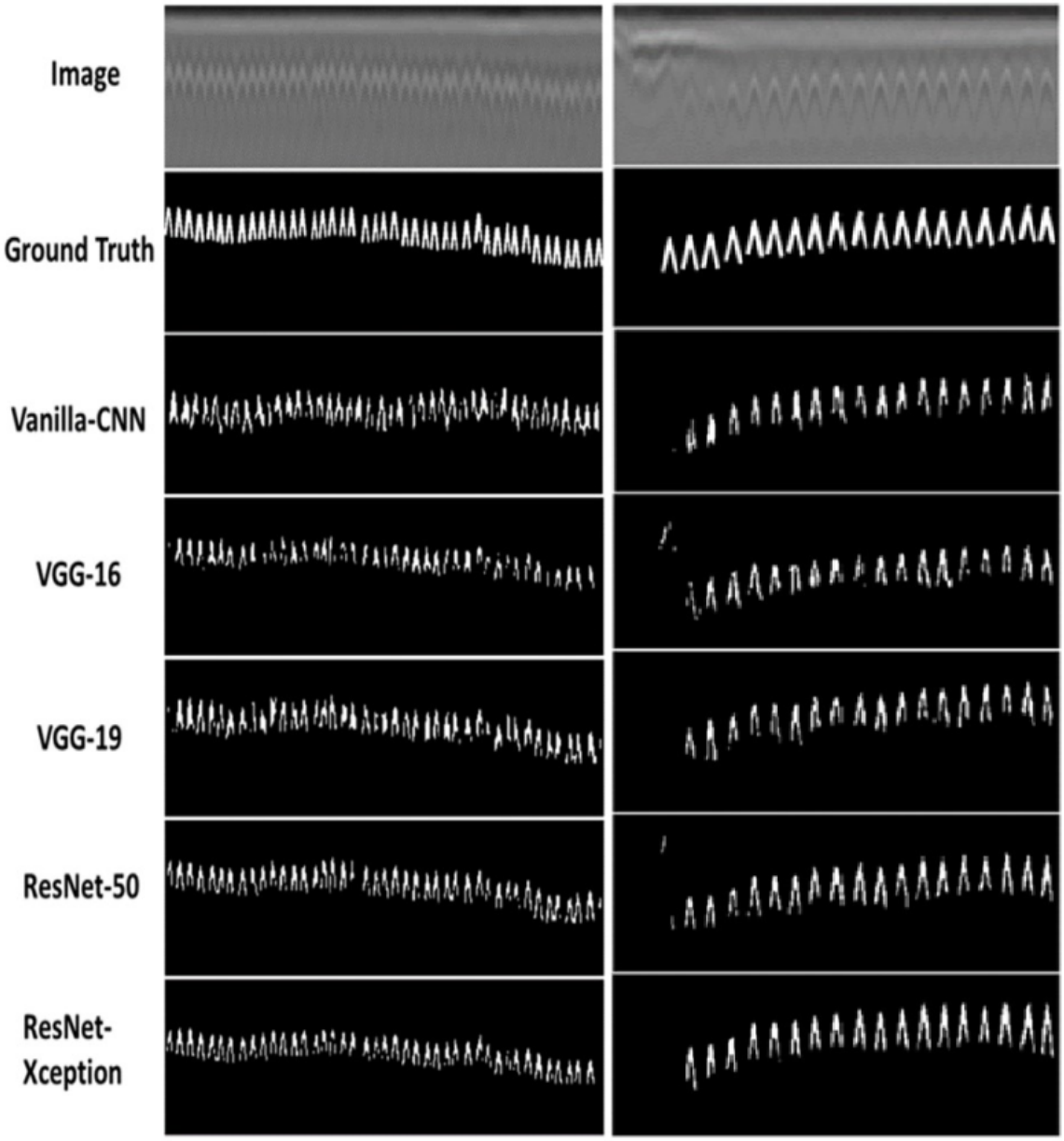

FIGURE 3.12: Comparison between the results for the different Encoder Modules for data from bridges 4 and 5

3.5 Study 5

3.5.1 System Methodology

The proposed model of the Deep Encoder-Decoder Network has been inspired by studies related to Deep Encoder-Decoder Networks developed in the recent past (some of which have been covered in the prior section). Before highlighting the individual elements of the proposed model in sufficient detail, it is imperative to examine some of the underlying assumptions that have not been explicitly given in figure 3.13. The different pre-processing functions that have been used require manual operations by the researcher. Some of these functions include cropping, resizing, and modification of image brightness, contrast, and color balance to ensure that the rebar signatures can be effectively highlighted within the diverse bridge data in a uniform manner irrespective of the bridge data being analyzed. Another assumption in this section that needs to be emphasized is that the terms 'block' and 'modules' will be used interchangeably in order to refer to the essential building elements that have been highlighted in figure 3.13.

Figure 3.13 highlights the basic overview of the proposed model. The proposed network has two main parts, namely the Rebar Layer Identification Framework (RLIF) and the Rebar Signature Localization Framework (RSLF). These two stages have been explicitly defined, as they highlight the novelty of the proposed approach in comparison with recent studies [39, 40, 123, 124, 234]. The details regarding each

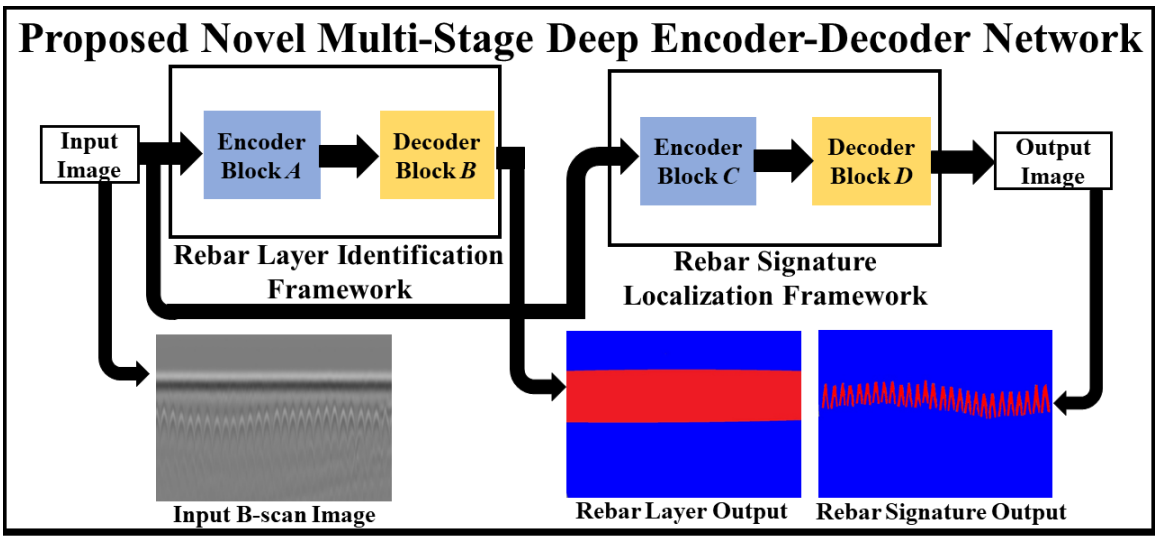

FIGURE 3.13: Overview of the Proposed Model of the Novel Multi-Stage Deep Encoder-Decoder Network for Rebar Detection and Localization. The input image of the B-scan after undergoing pre-processing operations is put through the First and Second Stages of the Deep Encoder Decoder Network

part of the proposed network will be discussed in sufficient detail in the proceeding sub-section.

3.5.1.1 Rebar Layer Identification Framework

As the name suggests, the Rebar Layer Identification Framework (RLIF) primarily deals with the visual differentiation between pixels belonging to image regions containing the rebar signatures and background pixels. These regions or collections of pixels can also be termed the 'rebar layer.' The Encoder Block A and B constitute the RLIF. Similarly, the Encoder Blocks C and D constitute the RSLF, which will be discussed in the following sub-section. Although images can contain reflection signals similar to parabolic rebar signatures, most B-scan images contain a single rebar layer to specify the underground depth at which the rebar is visually present within the

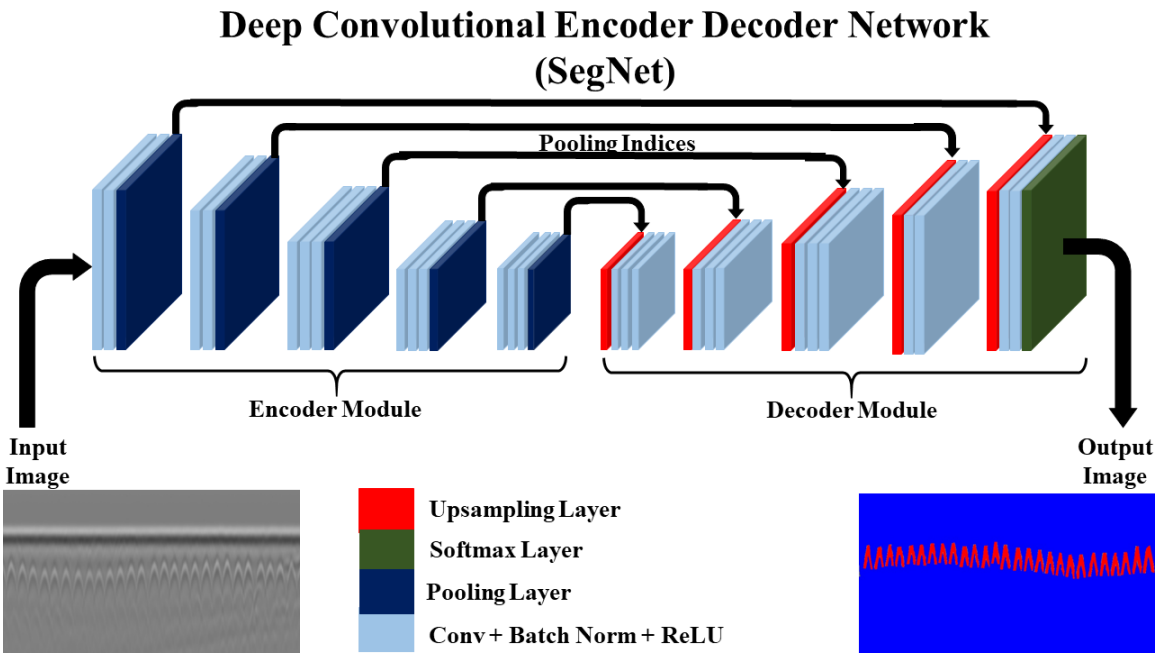

FIGURE 3.14: Architectural Framework for SegNet [11] with one Encoder and one Decoder module, which has gained considerable attention in the recent past. The RLIF will make use of different widely-deployed Deep Encoder Decoder Networks, which are similar in construction to the SegNet [11]

B-scan images. For this reason, the RLIF focuses on highlighting a single layer, where most of the rebar parabolic signatures are present. This will be possible by providing a pixel-level annotation of the pre-processed GPR image data into either rebar layer or background pixels, making it a binary classification problem. The architecture of the proposed RLIF will be similar to SegNet, which is shown in figure 3.14, such that the Encoder-Decoder model used in RLIF will consist of a single Encoder and Decoder modules. Several different architectures (e.g., UNet [13] and PSPNet [254], and MobileNet [12] encoder used as part of the overall SegNet architecture) will be tested and evaluated for the construction of RLIF. The details regarding the results will be discussed in the next section.

3.5.1.2 Rebar Signature Localization Framework

The Encoder Block C and the Decoder Block D, which are given in figure 3.13, constitute the Rebar Signature Localization framework (RSLF). The architecture of the proposed RSLF is also similar to SegNet, which is shown in figure 3.14, such that the Encoder-Decoder model used in RSLF will consist of a single Encoder and Decoder modules. However, the type of Encoder-Decoder architectures used in RSLF and RLIF are different in terms of their internal network-level characteristics. At the same time, the type of pixel-level annotation performed for the two framework is also different. As, the first stage of the proposed framework (i.e. RLIF) seeks to highlight the rebar layer and the second stage (i.e. RSLF) attempts to identify the individual rebar parabolic signatures, preferably present within the rebar layer. It can be seen in figure 3.14 that the initial stages of the SegNet architecture constitute the Encoder block and the final stages belong to the Decoder block. Two main types of blocks have been used in this study, including the Deep Encoder block with different network layers connected and pooling layers. The Deep Decoder block is similar in construction to the Deep Encoder block. The only difference is that instead of the pooling layers, the up-sampling layers are used to ensure that the output from the encoder can be resized to the actual image size provided at the input of the proposed model.

3.5.2 Results and Discussion

This section will discuss the salient features of the proposed network and its performance, along with their various implications for future research. The proposed method has two main parts, namely the Rebar Layer Identification framework (RLIF) and Rebar Signature Localization Framework (RSLF). For the first stage of the proposed network (i.e., RLIF), three major Deep Encoder-Decoder Networks have been used, namely the UNet [13], PSPNet [254] with two variants (e.g. PSP-50 and PSP-101), and SegNet with MobileNet encoder module [12]. For the case of the second stage of the proposed network (i.e., RSLF), three main Encoder-Decoder networks (e.g., UNet [13], PSPNet [254], and SegNet [11]) have been used, along with variations in the Encoder modules to find the most suitable Architecture-Encoder pair in terms of different qualitative and quantitative performance metrics. Some of the different Encoder modules leveraged within the context of the different Architectures include VGG-16, VGG-19, ResNet-50, and ResNet-Xception.

The detailed specifications of the computer system used for the training and validation of the proposed rebar detection and localization system are given as follows: Ubuntu 18.04 LTS, 32 GB memory, 350 GB hard disk, Intel ® Core i7–8700 CPU with 3.2 GHz clock speed and NVIDIA® GeForce® GTX 1080 TI Graphical Processing Unit (GPU). For the purpose of training and validation of the proposed system for rebar detection and localization, Tensorflow, PyTorch and Keras libraries have been used within Python programming language framework. Table 3.11 highlights the network

Network Parameters	**Dataset 1**
Network Name	SegNet/PSPNet/UNet with multiple Encoder modules and default Decoder module
Number of bridges	8 bridges
Number of Encoder Layers	16/19/50/71
Number of Epochs	100
Batch Size	8
Learning Rate	0.001
Total Number of Images	920
Train/Validation Split	7:1
Image Size	768 x 768

TABLE 3.11: Network Specifications and dataset information in relation to the training and validation of the proposed system

parameter specifications as well as dataset information. The data is divided between training and validation sets based on "leave-one-out" approach, such that out of the total data from eight bridges, training of SegNet [253] is conducted on seven bridges and validation is performed on data from one bridge. This process is used to perform validation on all of the bridges to assess the performance of the proposed system for rebar detection and localization. Using this approach allows the researchers to assess the ability of the proposed system to provide reliable performance on unseen data.

3.5.2.1 Quantitative Analysis

In this section, the primary emphasis will be on examining the statistical evaluation of the different aspects of the proposed method for rebar detection and localization. Table 3.12 highlights the overall quantitative performance of the different Architectures and Encoder modules for the two stages of the proposed system for rebar detection and localization. Several different performance evaluation metrics have been used for assessing the performance of the Deep Encoder-Decoder networks in the different applications in the recent past [11–13, 254]. The different metrics used in this study include Dice Loss, mean-Intersection-over-Union (mIoU), Precision, and Recall. The lower values for Dice Loss are more suitable as they correspond to the level of loss incurred for the different combinations of network frameworks used in the proposed system for rebar detection and localization. For all the other performance metrics (e.g. mIoU, Precision, and Recall), the higher values correspond to improved performance of the proposed rebar detection and localization system.

For the case of stage 1 of the proposed framework, four different types of base networks have been used, namely UNet, PSPNet-50, PSPNet-101, and SegNet framework. Out of the different Deep Encoder-Decoder networks utilized in the first stage, the most promising results have been outlined by the SegNet with MobileNet Encoder. Many of the original Deep Encoder-Decoder architectures (e.g. UNet, PSPNet-50 and PSPNet-101) used in stage 1 utilize default encoder modules in order to limit the level of complexity and variables being used in this study. The MobileNet framework

S1 Model	**S1 Encoder**	**S2 Model**	**S2 Encoder**	**Dice Loss**	**mIoU**	**Precision**	**Recall**
UNet	Default	SegNet	VGG16	25.15	85.73	88.43	82.26
”	”	”	VGG19	22.19	87.24	88.55	86.72
”	”	”	ResNet	16.68	90.65	90.53	90.06
”	”	”	Xception	**15.45**	**92.48**	**93.06**	**92.50**
”	”	UNet	VGG16	20.14	89.50	85.29	86.63
”	”	”	VGG19	19.24	90.57	88.33	88,21
”	”	”	ResNet	18.91	91.74	89.66	88.37
”	”	PSP	N/A	32.17	86.63	85.75	84.28
PSP-50	”	SegNet	VGG16	23.53	84.58	81.77	80.08
”	”	”	VGG19	20.06	86.64	84.17	82.21
”	”	”	ResNet	19.21	89.83	84.45	86.33
”	”	”	Xception	**18.75**	**90.48**	**91.06**	**90.50**
”	”	UNet	VGG16	23.16	83.25	81.76	81.24
”	”	”	VGG19	21.77	85.36	83.62	80.14
”	”	”	ResNet	19.15	87.51	82.50	80.19
”	”	PSP	N/A	32,27	82.25	80.37	79.92
PSP-101	”	SegNet	VGG16	29.38	81.55	76.23	77.56
”	”	”	VGG19	26.15	85.40	82.61	82.57
”	”	”	ResNet	20.26	88.72	82.63	83.45
”	”	”	Xception	**18.41**	**90.55**	**91.26**	**90.59**
”	”	UNet	VGG16	21.88	85.65	83.32	85.22
”	”	”	VGG19	24.42	88.58	80.26	80.17
”	”	”	ResNet	20.69	90.75	84.13	83.38
”	”	PSP	N/A	30.16	82.69	82.15	78.86
SegNet	MNet	SegNet	VGG16	21.46	91.12	92.50	93.36
”	”	”	VGG19	22.18	91.50	90.07	91.23
”	”	”	ResNet	17.37	92.21	95.24	94.45
”	”	”	Xception	**12.20**	**93.57**	**97.43**	**96.62**
”	”	UNet	VGG16	20.15	90.11	89.83	86.58
”	”	”	VGG19	14.31	92.42	90.50	92.21
”	”	PSP	N/A	27.25	87.55	82.94	80.88

TABLE 3.12: Results are shown for the dataset from three different bridges with different base architectures and encoder pairs. The best results are given in bold fonts. S1 is Stage-1. S2 is Stage-2. ResNet is ResNet-50. Xception is ResNet-Xception. PSP-50 is PSPNet-50. PSP-101 is PSPNet-101. MNet is MobileNet-v2

utilized as an encoder within the SegNet framework provides a lightweight Deep Encoder-Decoder network from the different models utilized in stage 1 of the proposed rebar detection and localization system. For the different encoder modules

and base architectures used in the second stage of the proposed network, the highest performance has been highlighted by combining the SegNet framework with the ResNet-Xception encoder module. When comparing the performance of PSPNet with 50 and 101 layers in the first stage of the proposed system, increasing the complexity and number of layers has an overall negative effect on the performance of the rebar detection and localization system. Compared to these two frameworks, the complexity and number of layers for UNet and MobilNet are limited. However, as it can be seen in table 3.12 these two networks (e.g., MobileNet and UNet) can provide a higher level of performance with the different combinations of Architecture-Encoder pairs leveraged at the second layer of the proposed framework for rebar detection and localization system.

A different combination of base architecture and encoder modules was used for stage 2 of the proposed rebar detection and localization system. It is important to understand that PSPNet with different number of layers does not support the usage of different encoder modules. The different base architectures used in the second stage of the proposed system include SegNet, UNet, and PSPNet. The different encoder modules utilized include VGG-16, VGG-19, ResNet-50, and ResNet-Xception. In terms of the number of layers, the different encoder modules can be ranked from the lowest to the highest number of layers can be ranked as follows: VGG-16, VGG-19, ResNet-Xception, and ResNet-50. In terms of improved performance, the most crucial combination of Architecture-Encoder pairs at the second stage of the proposed

framework is SegNet-ResNet-Xception (where SegNet is the base architectural framework and ResNet-Xception is the encoder module). Of the different encoder modules used, the most effective one can be classified as ResNet-Xception, which has shown improved performance when leveraged within different base architectural frameworks. ResNet-Xception encoder module with the SegNet framework at the second stage and SegNet framework with MobileNet encoder module at the first stage have the highest values for the different metrics (e.g., Dice Loss, mIoU, Precision, and Recall) are 12.20 %, 93.57 %, 97.43 %, and 96.62 %. All other values for the different frameworks at the first and second stage have comparatively lower values of mIoU, Precision, and Recall, as well as higher values for Dice Loss, as can be seen in table 3.12.

The performance of the proposed system cannot be directly compared with the majority of the existing studies in the field of rebar detection and localization conducted with an emphasis on bridge inspection in particular. The primary reason for this fact is that earlier studies utilize block-based techniques, which make use of different metrics, such as accuracy and loss [122–124, 234]. These metrics cannot be used for the current study since it leverages pixel-based methods for classification, such as individual pixels are classified as either belonging to rebar or non-rebar classes. The performance evaluated using these metrics (e.g., mIoU, Dice Loss, Precision, and Recall) can be considered a more reliable and accurate reflection of the actual performance of the proposed rebar detection and localization system.

3.5.2.2 Qualitative Analysis: Rebar Layer Identification Framework

In this sub-section, the discussion will deal with the visual results obtained for the first stage of the proposed framework for rebar detection and localization, namely the Rebar Layer Identification Framework (RLIF). In figure 3.15, a number of different results have been highlighted from stage 1 of the proposed framework for rebar detection and localization. The top two images are actual GPR images and ground truth annotated images respectively. The annotation classified between the foreground (i.e. rebar layer) and background (i.e. anything in the image that is not part of the rebar layer). This part highlights a different perspective as compared to quantitative analyses, as there are different visual elements of the results that cannot be adequately be discussed in statistical terms.

Out of the different Encoder-Decoder architectures leveraged for the development of the RLIF, some of the Architectures include SegNet, UNet, smaller-version of UNet (i.e., UNet-mini), and PSPNet. The reason UNet-mini results are not highlighted in table 3.12 is because they do not provide adequate performance in terms of the different statistical measures (e.g. mIoU, Dice Loss, Precision and Recall). The qualitative results for UNet-mini are shown in figure 3.15 in order to gain a better understanding of the reason for reduced performance. For the case of SegNet architecture in stage 1, MobileNet-v2 was used as the encoder module in order to attempt to reduce the overall size of the two stage framework. The individual encoder-decoder architectures

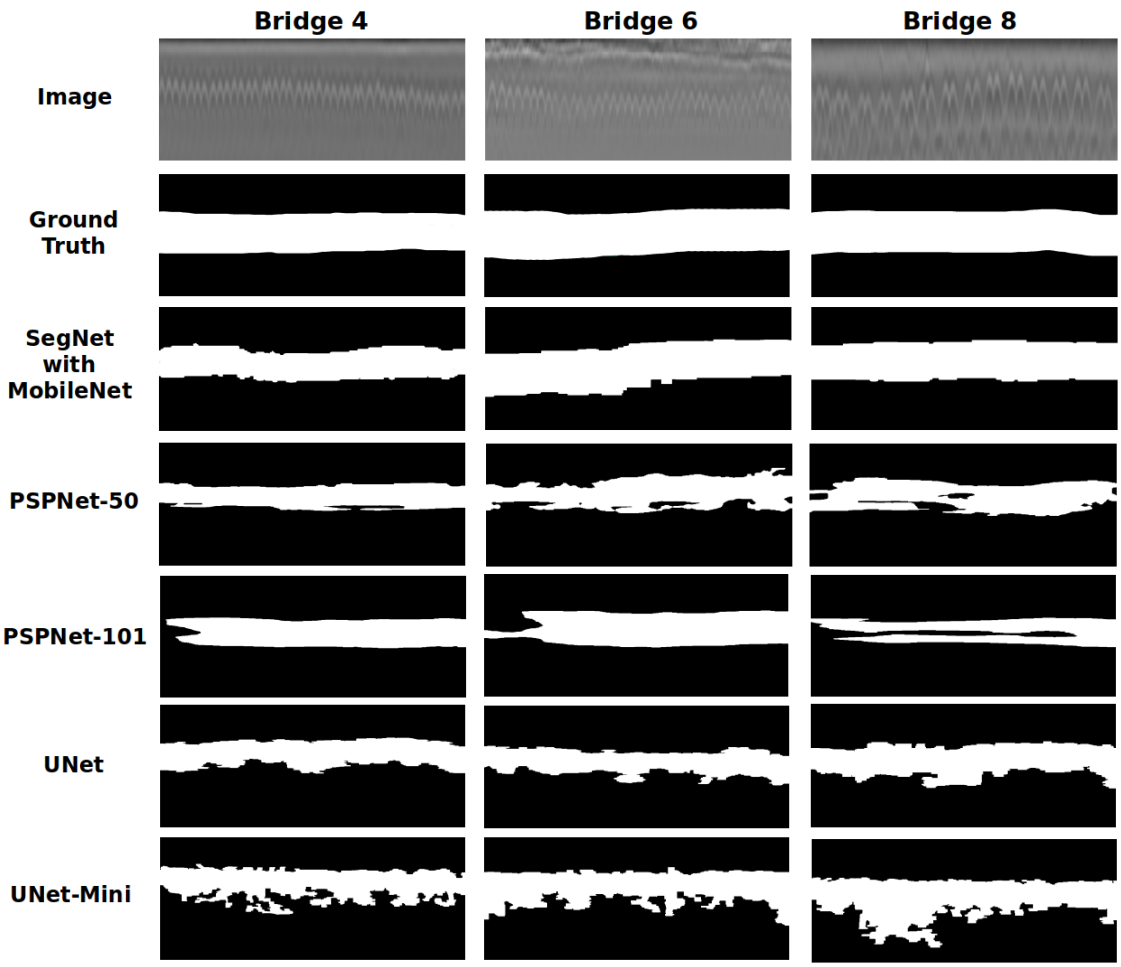

FIGURE 3.15: Results shown for the dataset from three different bridges. The results are shown for different set of base architectures and encoder pairs used in the first stage of the proposed framework

(e.g. SegNet, PSPNet, UNet) are deep networks with considerable complexities and computational overheads.

In order to reduce these overheads, the goal was to introduce a smaller version of Encoder-Decoder network at the first stage for rebar layer identification with the second stage for the rebar signature localization. Another benefit of using a smaller framework for the first stage was that the original version of MobileNet-v2 could not

process the image data with dimensions 768 x 768 x 3. In order to work with SegNet architecture with MobileNet-v2 encoder module at the first stage of the framework, the data has to be resized to 256 x 256 x 3, which improves the computational cost of using multiple stages of Deep Encoder-Decoder networks. At the same time, it also increases the performance of the first stage framework leveraging MobileNet-v2 to compare with other Deeper frameworks, (e.g., SegNet, PSPNet and UNet). After passing through the first stage, the results obtained are re-sized back to their original size, so that the results from different Architectures in the first stages can be effectively compared, as shown in figure 3.15. It can be seen in figure 3.15 that SegNet framework with MobileNet-v2 Encoder module is able to provide the most promising results at the stage 1 of the proposed framework. For data from all three bridges, it can be seen that the results are closer to the ground truth in comparison with other frameworks developed for stage 1. Furthermore, the results from SegNet-MobileNet shows the effects of resizing on the output in the form of block-based effects visible at the lower and upper edges of the layer results that were magnified after resizing the images from 256 x 256 x 3 to 768 x 768 x 3 (i.e. the noise and other artefacts that were smaller in the original result images were magnified many times after the images were resized).

For the case of PSPNet-50 and PSPNet-101, the results are more smooth in terms of visual texture. However, there are some issues in terms of patches missing from the different data results shown in figure 3.15. For example, the results from PSPNet-101 bridge 8 data shows some missing portion in the middle of the rebar layer region.

Similarly, for PSPNet-101, some minor regions of the rebar layer are missing for the results given for bridge 4 and 6. For the case of PSPNet-50, the results from bridge 4, there are some slight defects at the bottom of the rebar layer region. Similarly, the results from bridge 6 show some minor issues from the top and bottom of the identified rebar layer region. For the results obtained from PSPNet-50, there are some minor missing regions from the middle of the rebar layer region, along with minor issues at the top and bottom of the identified rebar region. The results from PSPNet-101 are more smooth in comparison with PSPNet-50. This shows that the increase in number of layers of the Deep Networks might have some positive impact towards effectively highlighting the rebar layer. At the same time, there is a need to better understand how the first layer networks can better distinguish between features for the foreground (i.e. features belonging to the rebar layer) and background (i.e. features belonging to all other regions of the B-scan images) regions.

For the case of UNet, visually, the output results are much less smooth in comparison to results from the two PSPNet frameworks highlighted. For UNet, the results show some false positive regions, when the output results are compared with the ground truth. The effect of noise and other artefacts are also more pronounced for the case of UNet frameworks. For the case of UNet-mini, which is a smaller, more compact version of the original framework, it can be seen that the output results are much more sensitive towards inaccurately classifying noise and other reflective artefacts as part of the rebar layer region. This phenomenon is much more visible for the case of UNet-mini with data from bridge 8. However, since rebar profiles belong to the

upper portion of the rebar layer, which is covered for the majority of the output images from UNet and UNet-mini, the regions of the rebar layer containing the rebar profile signatures are still covered within the output regions.

The overall qualitative analyses of the results from the first stage of the proposed framework for rebar detection and localization has been provided in this sub-section. The main issue highlighted is concerning the false positive regions and the addition of noise and other reflective artefacts below the rebar layer that can be incorrectly classified as actual rebar signatures in the further stages of the framework. This particular issue is not present in results from many frameworks (e.g. SegNet with MobileNet framework, PSPNet-50, PSPNet-101 and UNet). However, one of the examined frameworks (e.g. UNet-mini) has this particular issue much more pronounced in some of the results. This particular issue will be left for future research to further examine these issues and try to work towards ensuring that the first stage of the framework for rebar detection and localization is able to provide better performance in terms of accurately highlighting the rebar layer region. Since, this particular type of exploration and approach has not been previously used in any of the relevant literature, it is difficult to ascertain the different factors that can affect the accurate detection of rebar layer region. Furthermore, there will also be a need to examine the different network-level characteristics (e.g. number of network layers, type of network layers (pooling, convolution and concatenation layers) and their combination, and network layer dimensions for each layer in the network) that can prevent the inaccurate classification of rebar layer region.

3.5.2.3 Qualitative Analysis: Rebar Signature Localization Framework

In this sub-section, the discussion will deal with the visual results obtained for the second stage of the proposed framework for rebar detection and localization, namely the Rebar Signature Localization Framework (RSLF). Figure 3.16 highlights the overall qualitative performance of the different Architectures and Encoder modules for the two stages of the proposed system for rebar detection and localization. The results highlight the qualitative aspects of rebar detection and localization. The information provided on the left-hand side of the images is based on the corresponding architecture's base architecture and encoder modules for the second stage of the rebar detection and localization system.

In figure 3.16, several promising results for the Architecture-Encoder pair have been highlighted, along with some examples of average and low performance results for the other networks leveraged in the second stage of the proposed framework for rebar detection and localization. The primary framework used for the second stage of the proposed framework include UNet [13], PSPNet [254], and SegNet [11]. With these base networks, the different encoders were used to examine the effect of different encoders on the overall performance of the rebar detection and localization system. When comparing results for SegNet and UNet, it can be seen that the overall thickness of the rebar signatures is smaller for SegNet results. The results from the UNet framework are closer to the actual ground truth results. ResNet-50, ResNet-Xception, and Inception encoders are not shown here since the increasing number of

layers in the encoder does not significantly improve the quality of rebar signatures segmented from the original B-scan images. For the case of Architecture-Encoder pairs with SegNet, the most promising results are revealed for the SegNet framework with ResNet-50 and ResNet-Xception encoder modules. For the case of the UNet framework, both VGG-16 and VGG-19 encoder results are similar in terms of qualitative aspects. However, it is interesting to note that both results are unable to accurately segment some of the rebar signatures for data from bridge 6. However, rebar signatures' overall thickness and quality are closer to the ground truth. For the case of PSPNet [254], only the results for PSPNet-101 layers have been shown as a reference of relatively inaccurate results with the segmentation of rebar signatures appearing not as parabolic signatures. Instead, the rebars appear as regional blobs with pixel regions for individual rebars intersecting neighboring rebars. Although, this network (i.e. PSPNet-101) can be used for the localization of the rebars. However, the primary issue relates to the instances when the localization results for two neighboring rebars appears as a single region. This particular issue becomes problematic when the distance between two neighboring rebar signatures is reduced, as it can be seen for the output results from bridge 8 for PSPNet-101. Due to the inherent limitation of the PSPNet architecture, it cannot provide flexibility in utilizing multiple different encoder pairs, as is the case with other Deep Encoder-Decoder pairs, e.g., SegNet and UNet. The results for PSPNet with 50 layers architecture were not included, as the results were not very accurate, and it was not accessible to qualitatively separate individual rebar parabolic signatures. Another set of sub-optimal results is given for

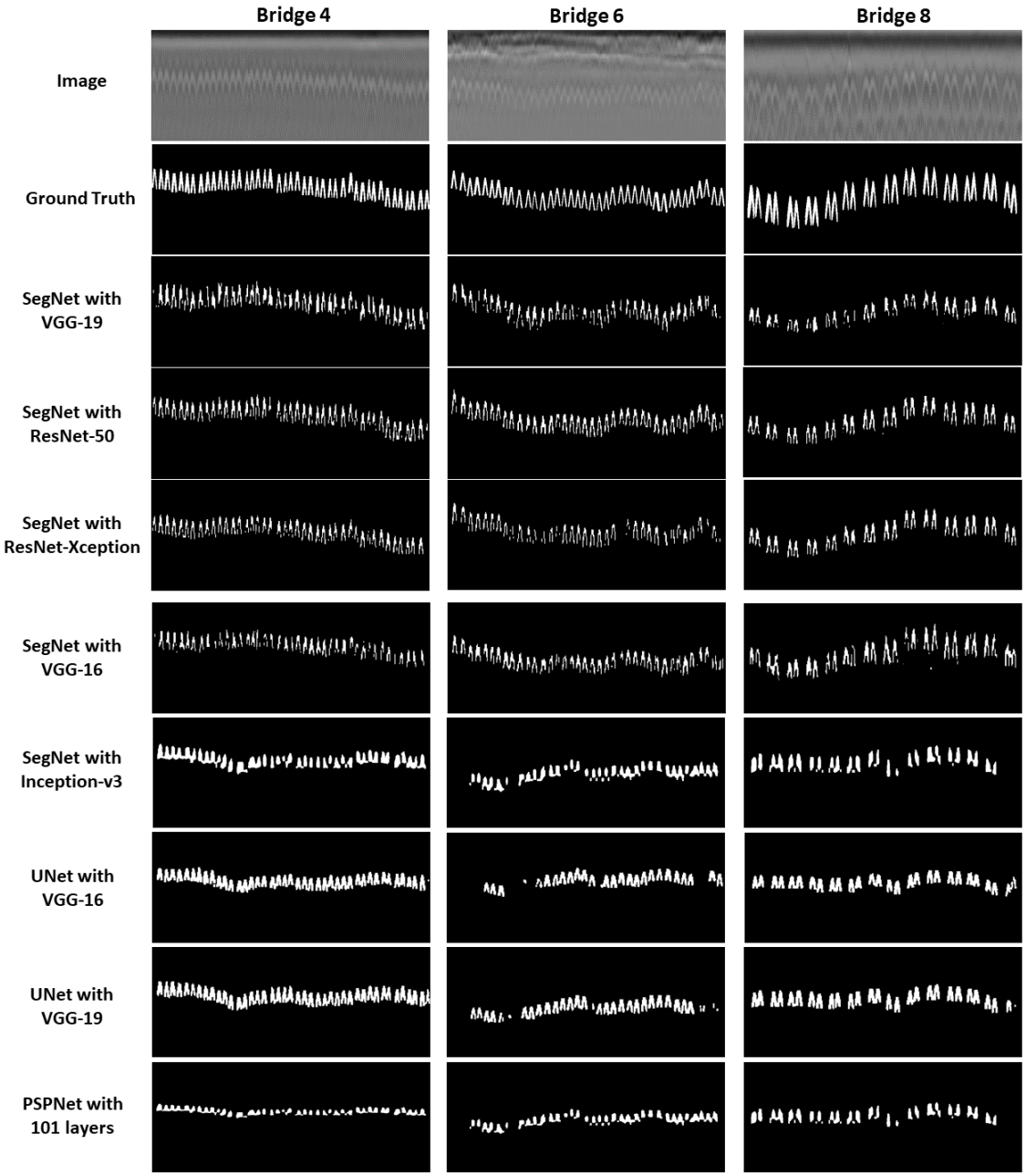

FIGURE 3.16: Results shown for the dataset from three different bridges. The results are shown for different set of base architectures and encoder pairs for the second stage of the proposed framework. The first stage framework is assumed to be MobileNet [12]

the case of SegNet architecture with the Inception-v3 encoder module—both these results are given in fig. 3.16 suffer from the same issue, such that the final results are unable to separate the results for individual rebar profiles from the neighboring rebar signatures. In conclusion, it can be seen in figure 3.16 that the most promising results in terms of qualitative aspects include MobileNet-v2 for the first stage of the framework. SegNet with ResNet-50 encoder module or UNet with VGG-16 encoder module gives the best result for the second stage of the proposed framework for rebar detection and localization.

There are a few primary issues that have been highlighted from the qualitative analyses of the results from the second stage of the proposed framework for rebar detection and localization. The first issue is related to the reduced thickness of the output rebar signatures for some output results (e.g. SegNet-ResNet-Xception, SegNet-VGG19 and SegNet-VGG16 Architecture-Encoder pairs). This can be beneficial in cases where the distance between the neighboring rebar signatures is very less. However, it can be a cause for concern, especially in the presence of noise in the images, i.e. if the intensity of noise increases in the image, it can potentially affect the ability of the proposed framework to accurately localize individual rebar signatures. This particular issue needs to be further investigated in future studies in the relevant research area. The second issue is the merger of neighboring rebar signatures for some output result highlighted (e.g. PSPNet-101). This potential issue can seriously affect the output for bridge data with minimal distance between neighboring rebar signatures.

This issue needs to be further explored in future works to fully examine the optimal network characteristics that can cater to the diverse types of data with different physical bridge characteristics (e.g. depth of rebar layer, number of rebars used in construction of the bridge, distance between neighboring rebars, type of material used within bridge deck). The third issue highlighted in this section is the disappearance of individual rebar signatures or failure to accurately classify individual rebar signature by some of the Architecture-Encoder pairs (e.g.UNet-VGG16 and UNet-VGG19) used in the second stage of the proposed framework for rebar detection and localization. Future research should try to explore ways to prevent this issue from affecting the performance of the rebar detection and localization frameworks.

3.6 Conclusion

This chapter discusses the timely progression and development of different solutions for rebar detection and localization. A total of four studies have already been published in different renowned conferences and journals. There is another publications that has been submitted, which has been added as the fifth study in this chapter. In the first study [123], a novel rebar detection method has been presented with data from two bridges to provide a proof-of-concept that was later expanded in other studies that followed. In the second study, the proposed system in first study was expanded to propose a novel rebar detection and localization system [124]. In the third

study, a novel framework for rebar detection and localization was developed leveraging supervised (e.g. multiple Deep Residual Networks were analyzed and compared) and unsupervised (e.g. K-means clustering algorithm with sliding-window-based approach) [234]. All of the prior studies [123, 124, 234] were developed with block-based annotation approach for data labelling. In order to improve the quality of the developed systems for rebar detection and localization in terms of the final output, a pixel-based annotation approach with Deep Encoder-Decoder networks was discussed in the next studies [240, 241].

Chapter 4

Defect Detection System for Steel Bridge Inspection using Multi-Directional Bicycle Robot

4.1 Defining "Defect" in the context of Steel Defect Detection System for Bridges

Bridges are large-scale, complex structures composed of multiple parts made up of different materials. In this for this reason, there is a need to specify the scope and context in which the proposed systems for defect detection system will operate in. The terms "damage" and "defect" in the context of steel parts of bridges has diverse

meanings given in different technical and professional civil inspection reports by the different global and regional authorities around the world. According to New Zealand Instructional Manual [255], defects in steel are primarily a by-product of environmental wear-and-tear and construction-related errors and issues, which can be classified into protective coating failure, corrosion, loose or defective fastening, cracks, impact damage, deformation, distortion, manufacturing defects, and detailing faults. Conversely, main types of defects provide by another report from European Union [256], the major types of defects can be classified into contamination, deformation, deterioration, discontinuity, displacement and loss of material. Another study [257] reported the steel defect classification into strains, curvature, nicks, gouges, and cracks.

Due to diverging classification of cracks, it is challenging to include all types of defects mentioned or include some type and exclude others. Since, the research on defect detection system developed and discussed in this dissertation is still in its early stages, a basic and simple definition of defect will be utilized in this dissertation. The terms "damage", "corrosion", "rust" and other terminologies that are related to steel defects will not be used. In the context of steel defect detection system, the term "defect" will only be used to relate to surface-level corrosion and rust appearing on the steel regions of the bridge infrastructure. In order to include all types of steel defects that have been mentioned in the different official documentations [255–257], there is a need to collect data from this perspective and develop a multi-class classification system that is able to not only highlight defects, but also provide further details regarding the type of defect that has been detected. This will be included as one of the next

steps in the evolution of the proposed approaches for steel defect detection in bridges. Consequently, emphasis on development of steel defect classification system will be put on future studies to extend the state-of-the-art in this regard.

4.2 Climbing Robots for Steel Defect Detection used in Study 1 and 2

Going into the brief details of the proposed mechanical design of the proposed novel multi-directional bicycle robot, the following requirements should be addressed and fulfilled by the proposed mechanical design of the bicycle robot: (1) The robot can climb surfaces with a wide range of outer diameters (greater than or equal to 150mm), which are normally encountered on circular tubes or cylindrical surfaces; (2) The robot can pass convex, or concave obstacles at structural transition joints on truss structures; (3) The robot can travel on steel structures with complex arrangements of obstacles such as bolts, nuts, and gaps; and (4) The locomotion system can maneuver through narrow areas (greater than or equal to 100mm wide) and can move sideways with considerable flexibility.

The high mobility of the two steering actuators allow the robot to operate in two different modes. Mode 1 figure 4.1 (a-e) that supports only one steering unit and the robot works like a bicycle, which facilitate the robot to travel on structures with limited contacting areas figure 4.1 (a) and ability to change direction simultaneously

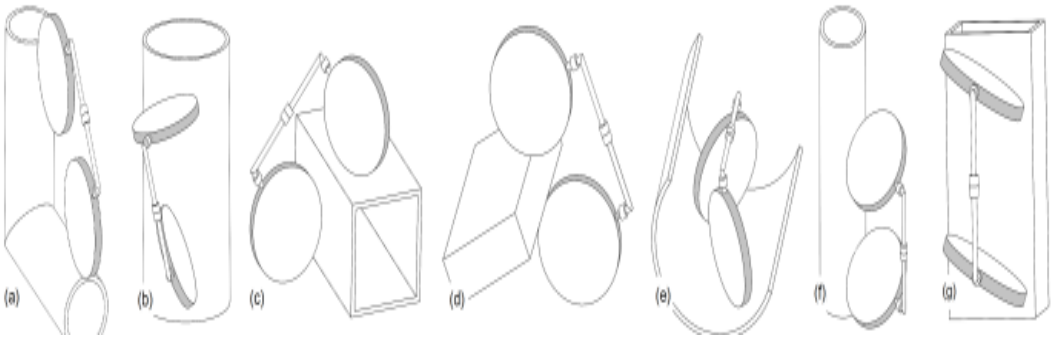

FIGURE 4.1: (a) Mode 1 (bicycle-like): The robot can handle cylindrical structures with limited contacting areas. (b) Mode 1: The robot changes the direction by first stopping the back wheel. Then, the front steering servo turns 90 degrees, and finally the front wheel moves to help the robot change direction. (c) Mode 1: With a free joint, the robot can travel on two intersecting surfaces. (d) Mode 1: The robot can traverse on edges that are thicker than the space between its two wheels (4cm). (e) Mode 1: The robot is flexible enough travel on the internal surface of a tube. (f) Mode 2: Two steering servos turn the wheels at the same angle. The robot moves spirally around a circular tube. In this mode, the robot can also perform well on tube shapes such as rectangles or hexagons. (g) Mode 2: The robot can rotate around its body center or move sideways (left, right) at steering angles that are close to 90 degrees.

figure 4.1 (b). The free joint in the middle allows the robot to traverse two intersecting surfaces figure 4.1 (c). Robot can also pass edges thicker than space between its two wheels figure 4.1 (d) and traverse the internal surface of hollow cylindrical tube-like structures (figure 4.1 (e). Mode 2 figure 4.1 (f-g) allows both steering units to remain active with independent and parallel control, facilitating the robot to move spirally (around a cylinder), sideways (left or right) or rotate around its center.

Fig. 4.2 shows the overall mechanical design of the bicycle robot. The robot's weight is 1 kg (without sensors), while it can carry 600g of load (sensors, on-board PC, etc.). To ensure that the frame is light-weight in nature, plastic is used as the primary material. The robot is powered by a 3000mAh LiPo battery that allows 1 hour of

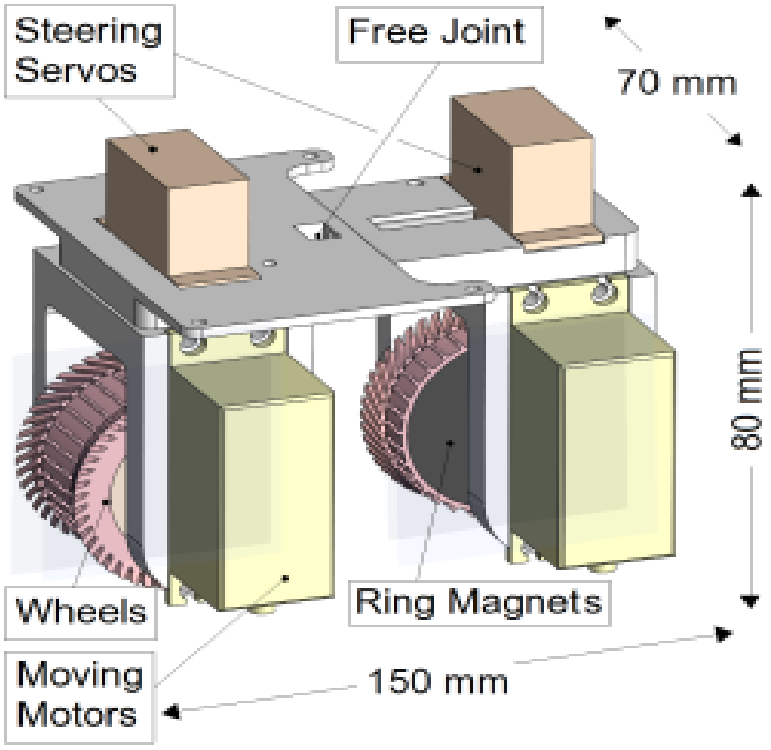

FIGURE 4.2: The 3D mechanical design of our proposed robot

operation. The robot's physical dimensions are 150mm × 80mm × 70mm. The ring magnets are placed at the cores of the wheels, which are covered by silicone tires. The wheels are driven by two high-torque gear DC motors (100kg·cm torque each), and the steering actuators are controlled by two servo motors (32kg·cm torque each). The front and back of the frame are linked by a bearing acting as a free joint. The design concept of our robot is inspired by a bicycle, which involve the use of two revolute joints equipping the robot with two independent steering actuators, which increases its mobility considerably. An additional free joint in the middle of the robot's body allows its two wheels to make full contact with surfaces of different shapes and sizes. The moving wheels are designed with permanent ring-shaped magnets to generate large adhesive forces.

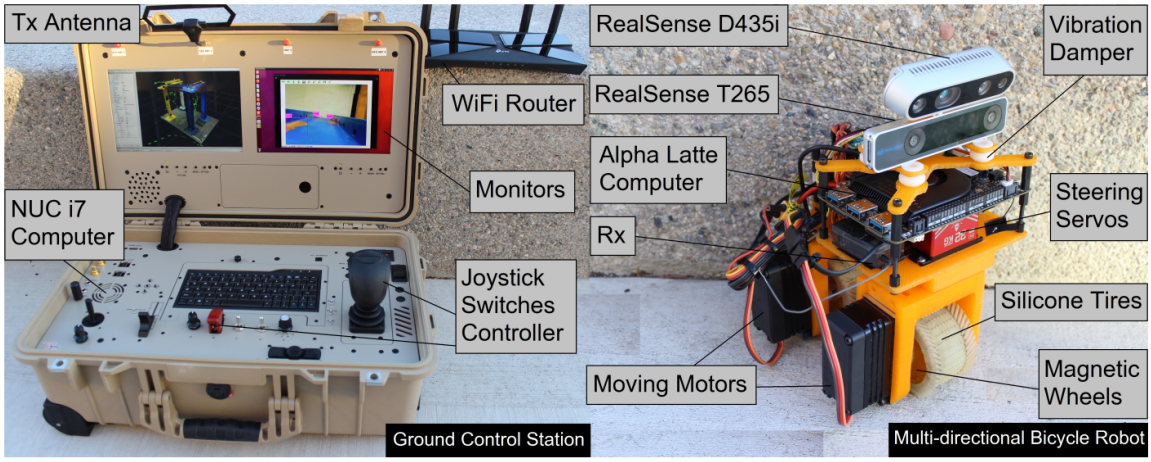

FIGURE 4.3: Multi-directional Bicycle Robot is controlled remotely from a Ground Control Station (GCS) using a joystick via a radio channel. The robot carries a depth camera D435i and a pose tracking camera T265 (both from Intel RealSense). An Alpha Latte computer onboard saves raw data from the sensors and continuously transfers the data back to GCS via a WiFi router. The GCS performs localization, object detection, and visualizes the received data online on its two screens. We use an Intel NUC i7 as the computer for the GCS.

The whole system is depicted in Fig. 4.3. On the robot side, we utilize an Intel RealSense D435i camera, which provides both color and depth images. However, for the development of Steel Defect Detection System, only the RGB color image data was used in this study. A LattePanda Alpha 864 is selected as an on-board computer, which connects the ground control station (GCS) computer (Intel NUC i7) via a WiFi router to the robot for enabling manual steering operation of the robot using the GCS. The two computers form a Robot Operating System (ROS) network, in which the GCS acts as the master. This novel multi-directional robot was used in study 1 and 2 to collect validation data from real bridge to test the proposed steel defect detection systems discussed in study 1 and 2. The details regarding proposed methods for steel defect detection systems are given below:

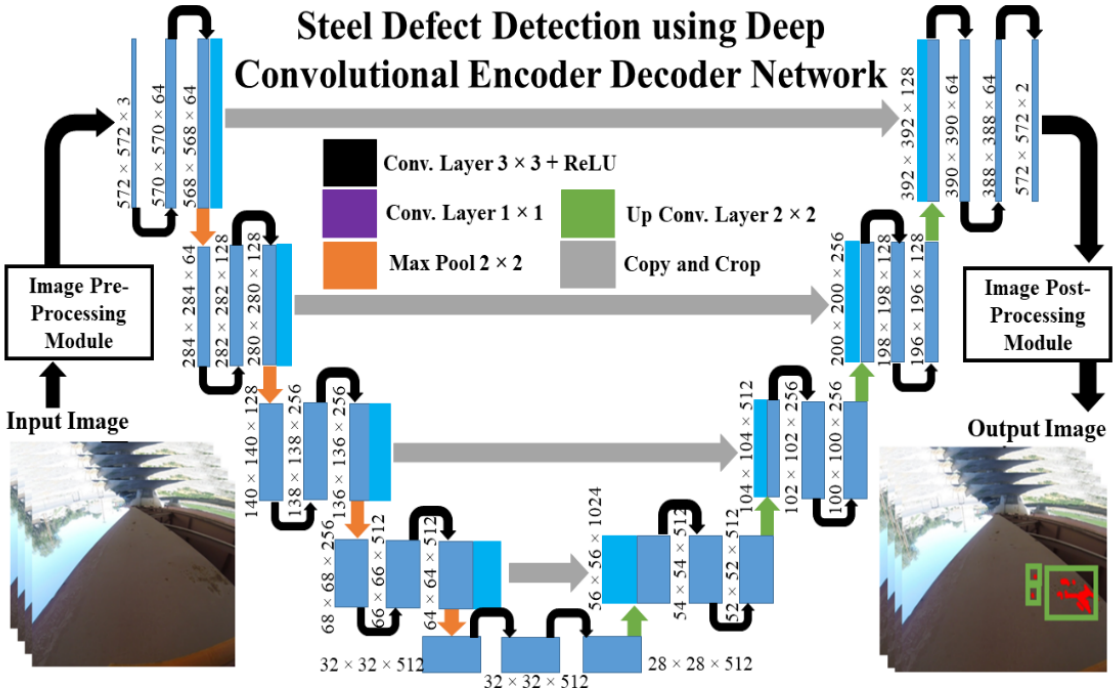

FIGURE 4.4: The proposed model being utilized in this study for the steel defect detection system with UNet [13] Deep Encoder-Decoder framework as the primary central learning-based module to train and validate bridge images with steel regions containing varying levels of defects

4.3 Study 1

4.3.1 System Methodology

The complete block diagram of the proposed system for steel defect detection has been given in figure 4.4. As it can be seen in figure 4.4, there are five steps of the proposed system. Starting from the input video frames, which are individually pre-processed using a number of steps, e.g. the Region-of-Interest (ROI) selection. The original size of the high-resolution image frame is very large, due to which, a selected region is separated out. This ensures that the background regions are separated and majority

of the steel region close to the robot can be cropped, resized and saved separately. The image ROI is resized to $572 \times 572 \times 3$, which is the input size permitted for the validation of the input video frames using Deep Encoder Decoder Networks. These networks are pre-trained on Vietnam bridge dataset.

A state-of-the-art Deep Encoder-Decoder Network architecture has been used in this study, namely U-Net [13], which has found considerable application in the field of medical imaging and other research fields in the recent past. A number of different Encoders modules are leveraged to examine and compare the performance of the different Architecture-Encoder pairs. Some of the Encoders used in this study include the ResNet-18 [249], ResNet-34 [249], EfficientNet-B0 [258], EfficientNet-B2 [258], and RegNet-X2 [259]. The output image from this stage in the video processing pipeline contains pixel-level masks highlighting steel defect locations. This output is modified to ensure that the predicted defect locations are highlighted using red pixels and green color bounding box surrounding each of these pixel regions.

System Specifications	**System 1**	**System 2**
Processor	Intel® NUC10i7FNH1 Core i1 with 1.1 GHz clock speed	Intel® Core i7-8700 CPU with 3.2 GHz clock speed
RAM	16 BG SDRAM	32 GB SDRAM
ROM	256 GB SSD	N/A
Hard Disk	1 TB HDD	250 GB HDD
Operating System	Ubuntu 20.04	Ubuntu 18.04
GPU	Intel® Integrated UHD Graphics	NVIDIA® GeForce® GTX 1080 TI

TABLE 4.1: The proposed system outlined in prior figure is trained and the results are validated on two different types of systems with varying computational capabilities

Two different types of systems were used to examine the performance of the proposed model for Steel Defect Detection. The training process was conducted offline on System 2, which is equipped with on-board GPU with details given in table 4.1. The different Deep Learning models trained for varying Architecture-Encoder pairs were saved and the validation process was performed on two separate systems to examine whether the validation process could be performed in real-time for the two different PCs with varying system configurations.

Table 4.1 highlights the different aspects of the two different types of PCs that have been used to examine the performance of pre-trained models in terms of providing real-time steel defect detection. It can be seen from table 4.1 that system 1 has Intel ® Integrated UHD Graphics Card, which is not supported by Nvidia ® CUDA ® libraries leading to slower validation time. In comparison, the onboard GPU within system 2 had full support from the Nvidia ® CUDA ® libraries, which allowed a faster training and validation processing time, which will be elaborated in the next section. For the purpose of training and validation of the proposed system for rebar detection and localization, Tensorflow, PyTorch and Keras libraries have been used within Python programming language framework. Table 4.2 highlights the network parameter specifications as well as dataset information.

Network Parameters	**Dataset 1**
Network Name	UNet with multiple Encoder modules
Number of bridges	Multiple bridges from Vietnam and USA
Number of Encoder Layers	18-342
Number of Epochs	100
Batch Size	16
Learning Rate	0.001
Total Number of Images	6,500
Train/Validation Split	5,000:1,500
Image Size	572 x 572

TABLE 4.2: Network Specifications and dataset information in relation to the training and validation of the proposed system

4.3.2 Results and Discussion

Table 4.3 outline statistical evaluation for the different Architecture-Encoder pairs in terms of the different metrics, such as Dice Loss, mIoU, Precision, and Recall. For the metrics such as mIoU, Precision and Recall, higher values reflect better performance. Each metric and encoder module has the highest, lowest and average values specified, as it allows the exploration of level of variance as well as upper and lower bounds on the different metrics. For Dice Loss, the opposite rule has to be applied; the smaller values reflect better performance of the system. The bold values in tables 4.3 specify the highest value for a particular Architecture. The bold values with an underline specify the highest value in comparison to all the different Architecture-Encoder pairs. For performance regarding UNet [13] Architecture, EfficientNet-B0 [258] outperforms other Encoder modules with best performance for two out of four

Model	**Encoder**		**Dice Loss**	**mIoU**	**Precision**	**Recall**
UNet	ResNet-18	Max.	31.80	91.86	99.92	91.59
”	”	Min.	4.37	54.87	99.54	54.86
”	”	Avg.	12.59	80.88	99.73	81.02
”	ResNet-34	Max.	28.11	96.40	99.83	96.57
”	”	Min.	1.96	59.40	99.56	59.43
”	”	Avg.	11.11	83.47	99.72	82.13
”	RegNet-X2	Max.	18.81	97.13	99.78	99.35
”	”	Min.	1.59	71.56	99.55	71.71
”	”	Avg.	7.26	88.01	99.65	87.06
”	EfficientNet-b0	Max.	32.17	97.33	99.80	97.53
”	”	Min.	1.41	55.85	99.53	55.92
”	”	Avg.	11.44	83.26	99.61	83.46
”	EfficientNet-b2	Max.	47.25	96.06	99.75	96.36
”	”	Min.	2.16	43.56	99.56	96.36
”	”	Avg.	14.39	69.84	99.65	81.87

TABLE 4.3: Performance analysis of the UNet framework with different encoder modules. The best results for each metric has been highlighted in bold font. All values are given in percentages

metrics, namely Dice Loss (a.k.a. F1-score) and mIoU. For the case of Precision, the best results are highlighted by ResNet-18 encoder module [249] with UNet architecture. Whereas, the encoder module RegNet-X2 [259] is able provide the highest performance in terms of Recall. Since, most of the studies pertaining to the deployment of Deep Encoder-Decoder networks for different applications leverage F1-score and mIoU as the most reliable metrics, the most optimal performance can be obtained by using UNet architecture with EfficientNet-B0 encoder module.

There are some relevant studies, which have presented their own approach towards steel corrosion detection. For example, study by [208] make use of roughness analysis and color comparison on image patches to separate corrosion patches for steel images. The recall and precision levels computed by the study range between 5% and 100%

and 25% and 30% respectively, which is much lower than results obtained in this study. Another study [209] made use of texture analysis with variables such as contrast, correlation and energy. Since, these variables do not correlate with the metrics used in this study, no comparison can be possible. Study by [210] is used for crack and corrosion detection, which made use of a supervised classification method with code-word dictionary consisting of stacked RGB histograms for image patches symmetric gray-level co-occurrence matrix for each patch. The metrics used by this study [210] are also different from our study. The study [210] reports that the false positive rate ranges from 1 pixel (0.2 percent of image patches), 25% (0.1 percent of image patches) and 100% (very low percent) When comparing the results in the other studies [208–210] in terms of depth of evaluation and the metrics used within this study, the performance of the proposed system far surpasses other study highlighted with demonstrable high-performance using quantitative and qualitative analysis.

Figure 4.5 highlights a side-by-side comparison between the validation time between System 1 and System 2 with values for each Architecture-Encoder Pair highlighted on top of each bar plot. For system 1, lowest value for validation time is outlined by UNet architecture [13] with RegNet-X2 encoder module [259]. For system 2, the lowest values for validation time have been reported by UNet [13] architecture with ResNet-18 encoder module [249]. The EfficientNet-B0 encoder module [258], which provided the optimal performance has significantly higher validation time in comparison to other encoder modules selected. It can be seen here that there is always a trade-off between the best validation time and best performance, as improving one variable

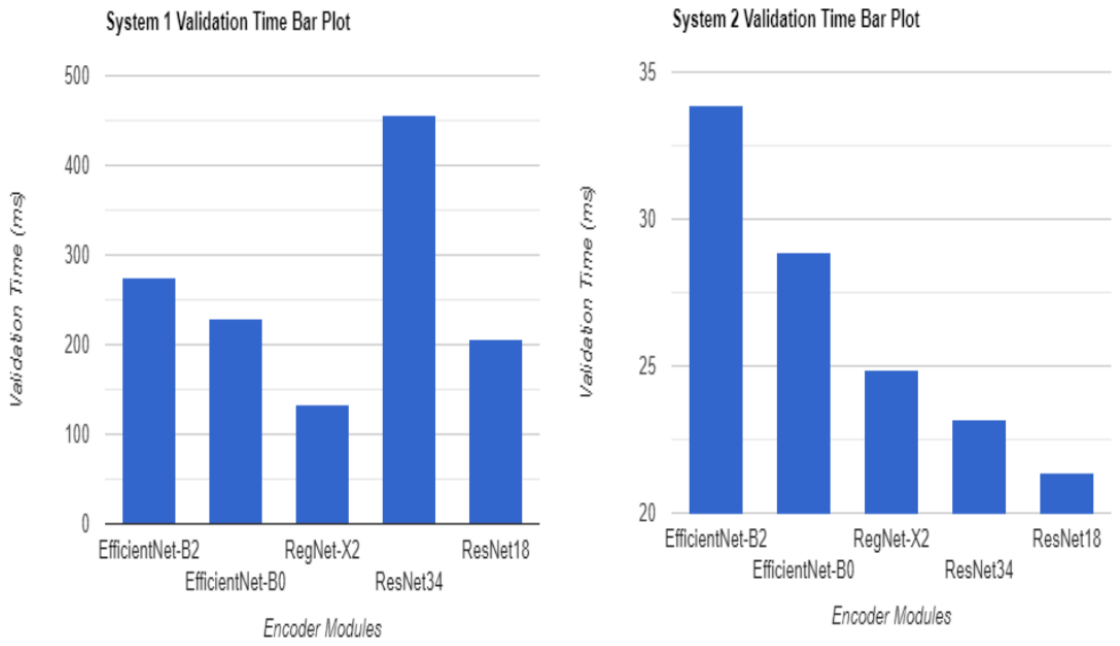

FIGURE 4.5: Comparison of time taken for validating the UNet architecture with different encoder modules on the two different systems.

leads to decrease in another and vice versa. For obvious reasons, the validation time values for GPU are considerably lower than their counterparts leveraging CPU computational capabilities alone. The difference in validation time between system 1 and 2 is significant, where the system 2 is able to provide real-time performance if it is implemented on an actual robot with GPU resources to compute defect detection algorithm for bridge inspection.

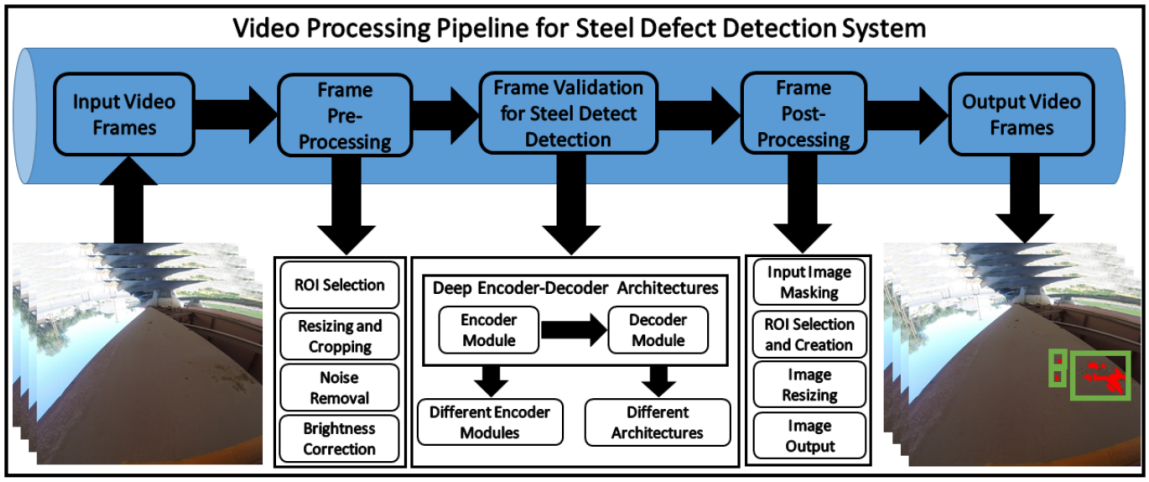

FIGURE 4.6: Details regarding the Video Processing Pipeline for Steel Defect Detection System starting from Input Video Frames, which are put through a number of image pre-processing steps. As, the system is based on offline training and validation processes, some of the pre-and post-processing steps involve manual intervention from human researcher. Only a portion of high-resolution input frame is selected to be validated in later stages of the video processing pipeline. The different pre-processing steps ensure that the quality of the input video frames is enhanced. The output image frame from the Deep Encoder-Decoder Network is put through different post-processing operations. Finally, the output of the system is highlighted using red colored pixel-level defects on the steel surface, along with green colored bounding boxes.

4.4 Study 2

4.4.1 System Methodology

In this section, a detailed evaluation of the video processing pipeline for Steel Defect Detection System will be discussed. The complete block diagram of the video processing pipeline has been given in figure 4.6. As it can be seen in figure 4.6, there are five steps of the video processing pipeline. Starting from the input video frames, which are individually pre-processed using a number of steps, e.g. the Region-of-Interest (ROI) selection. The original size of the high-resolution image frame is very

large, due to which, a selected region is separated out. This ensures that the background regions are separated and majority of the steel region close to the robot can be cropped, resized and saved separately. The image ROI is resized to 512 × 512 × 3, which is the input size permitted for the validation of the input video frames using Deep Encoder Decoder Networks.

These networks are pre-trained on Vietnam bridge dataset. A variety of state-of-the-art Deep Encoder-Decoder Networks architectures have been used in this study, namely the U-Net [13], LinkNet [260] and DeepLab [250]. For each of these architectures, a number of different Encoders modules are leveraged to examine and compare the performance of the different Architecture-Encoder pairs. Some of the Encoders used in this study include the ResNet-18 [249], ResNet-34 [249], EfficientNet-b0 [258], EfficientNet-b2 [258], and RegNet-X2 [259]. One of the prime focus was towards selecting Encoder modules that are not very large in terms of number of layers and parameters. The output image from this stage in the video processing pipeline contains pixel-level masks highlighting steel defect locations. This output is modified to ensure that the predicted defect locations are highlighted using red pixels and green color bounding box surrounding each of these pixel regions.

Two different types of systems were used to examine the performance of the proposed model for Steel Defect Detection. The training process was conducted offline on System 2, which is equipped with on-board GPU with details given in table 4.4. The different Deep Learning models trained for varying Architecture-Encoder pairs were

System Specifications	**System 1**	**System 2**
Processor	Intel® NUC10i7FNH1 Core i7 with 1.1 GHz clock speed	Intel® Core i7-8700 CPU with 3.2 GHz clock speed
RAM	16 GB SDRAM	32 GB SDRAM
ROM	256 GB SSD	N/A
Hard Disk	1 TB HDD	250 GB HDD
Operating System	Ubuntu 20.04	Ubuntu 18.04
GPU	Intel® Integrated UHD Graphics	NVIDIA® GeForce® GTX 1080 TI

TABLE 4.4: The proposed system outlined in prior figure is trained and the results are validated on two different types of systems with varying computational capabilities

saved and the validation process was performed on two separate systems to examine whether the validation process could be performed in real-time for the two different PCs with varying system configurations. Table 4.4 highlights the different aspects of the two different types of PCs that have been used to examine the performance of pre-trained models in terms of providing real-time steel defect detection. It can be seen from table 4.4 that system 1 has Intel ® Integrated UHD Graphics Card, which is not supported by Nvidia ® CUDA ® libraries leading to slower validation time. In comparison, the onboard GPU within system 2 had full support from the Nvidia ® CUDA ® libraries, which allowed a faster training and validation processing time, which will be elaborated in the next section. For the purpose of training and validation of the proposed system for rebar detection and localization, Tensorflow, PyTorch and Keras libraries have been used within Python programming language framework. Table 4.5 highlights the network parameter specifications as well as dataset information.

Network Parameters	**Dataset 1**
Network Name	Multiple Deep Encoder Decoder frameworks with multiple Encoder modules
Number of bridges	Multiple bridges from Vietnam and USA
Number of Encoder Layers	18-342
Number of Epochs	100
Batch Size	16
Learning Rate	0.001
Total Number of Images	6,500
Train/Validation Split	5,000:1,500
Image Size	512 x 512

TABLE 4.5: Network Specifications and dataset information in relation to the training and validation of the proposed system

4.4.2 Results and Discussion

In this section, the overall performance of the different Architecture-Encoder pairs will be outlined. The different Architecture-Encoder pairs were trained on Vietnam dataset. After offline training of the different Architecture-Encoder pairs, the validation was performed on six separate video frame data (1,500 images) obtained using Bicycle Robot taken from the actual bridge on Highway-80 located in Lovelock, NV, USA. There are variations in the level of defect and lightning conditions on the different parts of the bridge, which reflect on the performance of the different Architecture-Encoder pairs. In order to capture this variation in performance, three separate rows for each Architecture-Encoder pair outline the minimum, maximum and average values have been given in tables 4.6 and 4.7. Table 4.6 outline statistical

evaluation for the different Architecture-Encoder pairs in terms of the different metrics, such as Dice Loss, mIoU, Precision, and Recall. For the metrics such as mIoU, Precision and Recall, higher values reflect better performance. For Dice Loss, the opposite rule has to be applied; the smaller values reflect better performance of the system.

The bold values in tables 4.6 and 4.7 specify the highest value for a particular Architecture. The bold values with an underline specify the highest value in comparison to all the different Architecture-Encoder pairs. It can be seen in table 4.6 that for LinkNet [260] Deep Encoder-Decoder architecture, the most optimal performance has been shown by the RegNet-X2 [259] Encoder module for four out of total of five performance metrics. For performance regarding UNet [13] Architecture, EfficientNet-B0 [258] outperforms other Encoder modules with best performance for two out of four metrics. For table 4.7 with details regarding DeepLab Architecture [250], RegNet-X2 [259] encoder performs the most optimal for three out of four performance metrics. There are some relevant studies, which have presented their own approach towards steel corrosion detection. For example, study by [208] make use of roughness analysis and color comparison on image patches to separate corrosion patches UNet [13] Architecture for steel images. The recall and precision levels computed by the study range between 5% and 100% and 25% and 30% respectively, which is much lower than results obtained in this study. Another study [261] made use of texture analysis with variables such as contrast, correlation correlation and energy. Since, these variables do not correlate with the metrics used in this study, no comparison can be possible.

Model	Encoder		Dice Loss	mIoU	Precision	Recall
UNet	ResNet-18	Max.	31.80	91.86	99.92	91.59
”	”	Min.	4.37	54.87	99.54	54.86
”	”	Avg.	12.59	80.88	99.73	81.02
”	ResNet-34	Max.	28.11	96.40	99.83	96.57
”	”	Min.	1.96	59.40	99.56	59.43
”	”	Avg.	11.11	83.47	99.72	82.13
”	RegNet-X2	Max.	18.81	97.13	99.78	99.35
”	”	Min.	1.59	71.56	99.55	71.71
”	”	Avg.	7.26	88.01	99.65	87.06
”	EfficientNet-b0	Max.	32.17	97.33	99.80	97.53
”	”	Min.	1.41	55.85	99.53	55.92
”	”	Avg.	11.44	83.26	99.61	83.46
”	EfficientNet-b2	Max.	47.25	96.06	99.75	96.36
”	”	Min.	2.16	43.56	99.56	96.36
”	”	Avg.	14.39	69.84	99.65	81.87
LinkNet	ResNet-18	Max.	16.80	97.33	99.74	97.68
”	”	Min.	1.41	73.65	99.56	73.69
”	”	Avg.	6.11	89.89	99.65	90.07
”	ResNet-34	Max.	32.96	94.55	99.93	94.91
”	”	Min.	4.23	53.44	99.56	53.14
”	”	Avg.	12.20	82.25	99.75	82.31
”	RegNet-X2	Max.	19.91	98.52	99.77	99.80
”	”	Min.	0.08	69.32	99.56	69.47
”	”	Avg.	6.81	89.11	99.67	90.37
”	EfficientNet-b0	Max.	31.20	94.17	99.78	94.45
”	”	Min.	3.28	57,56	99.53	57.39
”	”	Avg.	11.51	82.89	99.66	82.99
”	EfficientNet-b2	Max.	16.83	99.36	99.73	99.78
”	”	Min.	0.32	73.30	99.58	73.44
”	”	Avg.	4.93	91.95	99.64	92.24

TABLE 4.6: Table Outlining the Performance of Different Architecture-Encoder Pairs in Terms of Different Quantitative Metrics for the LinkNet and UNet Architectures. All values are given in percentages

Study by [262] is used for crack and corrosion detection, which made use of a supervised classification method with code-word dictionary consisting of stacked RGB histograms for image patches symmetric gray-level co-occurrence matrix for each patch. The metrics used by this study [262] are also different from our study. The study [262]

Model	Encoder		Dice Loss	mIoU	Precision	Recall
DeepLab	ResNet-18	Max.	31.80	91.86	99.92	91.59
”	”	Min.	4.37	54.87	99.54	54.86
”	”	Avg.	12.59	80.88	99.73	81.02
”	ResNet-34	Max.	28.11	96.40	99.83	96.57
”	”	Min.	1.96	59.40	99.56	59.43
”	”	Avg.	11.11	83.47	99.72	82.13
”	RegNet-X2	Max.	18.81	97.13	99.78	99.35
”	”	Min.	1.59	71.56	99.55	71.71
”	”	Avg.	7.26	88.01	99.65	87.06
”	EfficientNet-b0	Max.	32.17	97.33	99.80	97.53
”	”	Min.	1.41	55.85	99.53	55.92
”	”	Avg.	11.44	83.26	99.61	83.46
”	EfficientNet-b2	Max.	47.25	96.06	99.75	96.36
”	”	Min.	2.18	43.56	99.56	43.60
”	”	Avg.	14.39	69.84	99.65	81.87

TABLE 4.7: Table Outlining the Performance of Different Architecture-Encoder Pairs in Terms of Different Quantitative Metrics for the DeepLab Architectures. All values are given in percentages

reports that the false positive rate ranges from 1 pixel (0.2 percent of image patches), 25% (0.1 percent of image patches) and 100% (very low percent) When comparing the results in the other studies [208] [261] [262] in terms of depth of evaluation and the metrics used within this study, the performance of the proposed system far surpasses other study highlighted with demonstrable high-performance using quantitative and qualitative analysis.

Figure 4.7 highlights a side-by-side comparison between the validation time between System 1 and System 2. The values for each Architecture-Encoder Pair have been highlighted on top of each bar plot in figure 4.7. For system 1, lowest values for validation are outlined by LinkNet architecture [260]. For system 2, the lowest values for validation time have been reported by UNet [13] architecture and associated Encoder

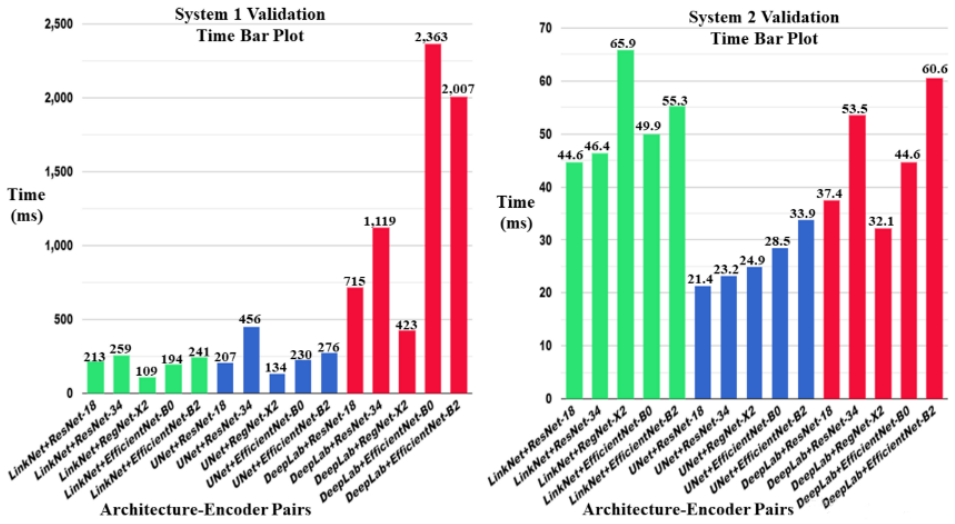

FIGURE 4.7: A side-by-side comparison between the validation time for System 1 and System 2. There are wide variations between the validation times for each image frame as the maximum value for System 1 is 2,007 ms and the maximum value for System 2 is 65.95 ms, which clearly highlights the benefits of GPU for real-time steel defect detection. When comparing the different Architectures for System 1, the variations are more pronounced across architectures. For the case of System 2, the variations are much less pronounced, with the highest values ranging between 20 ms and 70 ms.

modules. One of the architecture, namely LinkNet [260] has demonstrated lowest validation time results for system 1. However, for system 2, it has the highest values out of all the other Architectures, which is an interesting contrast in the validation time results. There are actual results obtained from the validation of the data obtained from bridge located in Highway-80, Lovelock, NV, USA.

4.5 Conclusion

This chapter highlighted the progression of the dissertation into examining and highlighting ways towards using existing Deep Learning algorithms for Steel Defect Detection system with the potential to be deployed on real-time robotic systems. In the context of bridge inspection, the research pertaining to steel defect detection has not received attention in the past. Many steel defect studies exist, but for detecting defects in steel sheets during manufacturing processes. However, these studies are not relevant, as there are considerable variations between the manufacturing and bridge inspection contexts. There are two recent studies that have been discussed in this chapter. The first study [246] utilized UNet with multiple encoder modules to provide steel defect detection with data obtained from steel bridges in Vietnam. The proposed approach in [246] highlighted the promise of this approach. In order to extend this work utilizing a real robot, the next study [245] provided a novel real-time video processing pipeline for multi-directional bicycle robot. The system training was performed on dataset from bridges in Vietnam and validation was performed from data obtained from vision sensor mounted on the multi-directional robot [245]. The performance evaluation of the proposed approach in [245] highlighted that the steel defect detection system is able to provide real-time evaluation.

Chapter 5

Conclusion and Future Works

This is the final chapter of this dissertation, which will effectively concluded the dissertation with some final concluding remarks and guidance for future researchers to extend the presented work in the near-future. Since, this dissertation has been covering two primary aspects of bridge inspection in relation to surface-level and sub-surface-level analyses, the following two sub-sections will conclude the major aspects of the studies implemented. In the final section of this chapter, some recommendations will be discussed as guidance for future researchers in the relevant research area towards extending this work in the near future. These recommendations will be important insights gathered after examining the state-of-the-art and implementing relevant studies in this field, facing challenges and limitations and potential solutions that can aid in mitigating the specific issues.

5.1 Rebar Detection and Localization for Bridge Deck Inspection

This part of the dissertation discussed the timely progression and development of different solutions for rebar detection and localization. A total of four studies have already been published in different renowned conferences and journals. There is another publications that has been submitted, which has been added as the fifth study in this chapter. In the first study [123], a novel rebar detection method has been presented with data from two bridges to provide a proof-of-concept that was later expanded in other studies that followed. In the second study, the proposed system in first study was expanded to propose a novel rebar detection and localization system [124]. In the third study, a novel framework for rebar detection and localization was developed leveraging supervised (e.g. multiple Deep Residual Networks were analyzed and compared) and unsupervised (e.g. K-means clustering algorithm with sliding-window-based approach) [234]. All of the prior studies [123, 124, 234] were developed with block-based annotation approach for data labelling. In order to improve the quality of the developed systems for rebar detection and localization in terms of the final output, a pixel-based annotation approach with Deep Encoder-Decoder networks was discussed in the next studies [240, 241].

5.2 Defect Detection System for Steel Bridge Inspection

This part of the dissertation examined and highlighted ways towards using existing Deep Learning algorithms for Steel Defect Detection system with the potential to be deployed on real-time robotic systems. In the context of bridge inspection, the research pertaining to steel defect detection has not received attention in the past. Many steel defect studies exist, but for detecting defects in steel sheets during manufacturing processes. However, these studies are not relevant, as there are considerable variations between the manufacturing and bridge inspection contexts. There are two recent studies that have been discussed in this chapter. The first study [246] utilized UNet with multiple encoder modules to provide steel defect detection with data obtained from steel bridges in Vietnam. The proposed approach in [246] highlighted the promise of this approach. In order to extend this work utilizing a real robot, the next study [245] provided a novel real-time video processing pipeline for multi-directional bicycle robot. The system training was performed on dataset from bridges in Vietnam and validation was performed from data obtained from vision sensor mounted on the multi-directional robot [245]. The performance evaluation of the proposed approach in [245] highlighted that the steel defect detection system is able to provide real-time evaluation.

5.3 Future Works

There are number of ways in which the current state-of-the-art can be further explored in the near-future. Survey of the state-of-the-art in bridge inspection [122] has revealed that most existing automated systems for bridge inspection rely on single robot utilizing single type of sensors. However, to provide a comprehensive examination of bridge inspection, future studies should rely on data acquired from multiple sensors (e.g. GPR, multiple RGB cameras, thermal cameras, acoustic sensors, ER sensors), which can be leveraged by civil experts to provide reliable assessment of structural deficiencies of bridges. At the same time, the use of multiple, diverse robot platforms will allow bridge inspection teams to easily and effectively acquire data from dangerous and inaccessible regions of the bridges without putting themselves in harms way. For example, using Unmanned Aerial Vehicles (UAVs) can allow the bridge inspectors the versatility and mobility to provide a surface-level inspection of the bridge surfaces in an efficient and timely manner. At the same time, relying on multiple robots rather than single robots can enable the bridge inspection systems to provide a wide range and coverage of different areas and parts of bridges. For example, UGV can provide coverage of different surface and sub-surface-level analyses of bridge decks, and multiple UAVs can cover the underside of bridge deck and upper steel parts of the bridge.

In this regard, the future works can leverage the data from multitude of sensors on different robotic platforms (e.g. ground robots, aerial robots). Data from each

sensor can be analysed using suitable data analyses techniques to individually and collectively examine the data in multi-sensor, multi-robot systems. In relation to the utilization of learning-based approaches for surface-level and sub-surface-level analysis of bridges, the future researchers can attempt to explore the utility of lightweight Encoder-Decoder frameworks, which may provide a promising approach towards efficient on-board implementations. To provide a deeper evaluation of the inspection of the bridges in the future, different 3D reconstruction techniques can be leveraged to provide a 3D model of the bridge being inspection in an application, along with individual sensor systems and robots enabling the identification of different defects on the different surfaces of the bridge infrastructure. These types of future implementations on multiple real robot platforms equipped with multiple sensory modalities will have practical implications for actual bridge inspection teams and Transportation Departments in the different states in the US and across the world.

5.4 Research Contributions from this Dissertation

Throughout the duration of the doctoral research, as discussed in the prior chapters, the effort has been towards extending the state-of-the-art with novel contributions that can be published in peer-reviewed, credible avenues of international conferences and journals relevant to the field of bridge inspection and automation of different inspection methods. The list of different publications that have been either submitted, accepted or published in different conferences and journals are given below:

[1]. H. Ahmed, H. M. La, and N. Gucunski. Review of Non-Destructive Civil Infrastructure Evaluation for Bridges: State-of-the-art Robotic Platforms, Sensors, and Algorithms. Sensors, 20, 3954, pages 1-38. http://dx.doi.org/10.3390/s20143954, July 2020. Impact Factor: 3.275.

[2]. H. Ahmed, H. M. La and K. Tran. Rebar Detection and Localization for Bridge Deck Inspection and Evaluation using Deep Residual Network. Journal of Automation in Construction, Elsevier publisher, Vol. 120, December 2020. Impact Factor: 5.669.

[3]. H. Ahmed, H. M. La, and N. Gucunski. Rebar Detection using Ground Penetrating Radar with State-of-the-art Convolutional Neural Networks. In proceedings of the 9th International Conference on Structural Health Monitoring of Intelligent Infrastructure (SHMII-9), August 4-7, 2019. St. Louis, Missouri, USA.

[4]. H. Ahmed, H. M. La and G. Pekcan. Rebar Detection and Localization for Non-Destructive Infrastructure Evaluation using Deep Residual Networks, the 14th International Symposium on Visual Computing (ISVC), Oct. 7-9, 2019, Lake Tahoe, NV, USA.

[5]. H. Ahmed, A. Tavakolli and H. M. La. Use of Deep Encoder-Decoder Network for Sub-Surface Inspection and Evaluation of Bridge Decks. In: Proceedings of the 13th International Workshop on Structural Health Monitoring 2021, Stanford, CA, USA. pp. 832-841.

[6]. H. Ahmed, C. P. Le and H. M. La. Pixel-Level Classification for Bridge Deck Rebar Detection and Localization using Multi-Stage Deep Encoder-Decoder Network. [**Submitted to Automation in Construction**].

[7]. H. Ahmed, and H. M. La. Steel Defect Detection in Bridges Using Deep Encoder-Decoder Networks. In: Proceedings of 13th International Workshop on Structural Health Monitoring (IWSHM), pp. 842-849. Stanford, CA, USA. 2021.

[8]. H. Ahmed, S. T. Nguyen, D. La, C. P. Le, and H. M. La, (2022). Multi-directional Bicycle Robot for Bridge Inspection with Steel Defect Detection System. Accepted to the 2022 IEEE International Conference on Intelligent Robots and Systems (IROS). **Best Application Paper Finalist**.

[9]. H. Ahmed, and H. M. La. Education-Robotics Symbiosis: An Evaluation of Challenges and Proposed Recommendations. In Proceedings of the 9th IEEE Integrated STEM Education Conference (ISEC), March 16, 2019, Princeton University, New Jersey, USA.

[10]. H. Ahmed, and H. M. La. Evaluating the Co-Dependence and Co-Existence between Religion and Robots: Past, Present and Insights on the Future. International Journal of Social Robotics, Springer Publisher, 2021. Impact Factor: 2.296.

Bibliography

[1] C. Cheng and Z. Shen. Time-series based thermography on concrete block void detection. *arXiv*, arXiv:preprint/1802.04869, 2018.

[2] N. Busse. Using an infrared camera to inspect a bridge deck. *Available online: https: //mntransportationresearch.org/2013/08/29/using-an-infrared-camera-to-inspect-a-bridge-deck/*, 2013.

[3] A.P. Annan. Neural detection of pipe signatures in ground penetrating radar images. *IEEE Trans. Geosci. Remote Sens.*, 38:790–797, 2000.

[4] A.P. Annan. Electromagnetic principles of ground penetrating radar. in ground penetrating radar theory and applications. *Elsevier*, Amsterdam, The Netherlands:pp. 1–40, 2009.

[5] A. Ellenberg, A. Kontsos, F. Moon, and I. Bartoli. Bridge deck delamination identification from unmanned aerial vehicle infrared imagery. *Autom. Constr.*, 72:155–165, 2016.

[6] J. Seo, L. Duque, and J. Wacker. Drone-enabled bridge inspection methodology and application. *Autom. Constr.*, page 112–126, 2018.

[7] M. Sakuma, Y. Kobayashi, T. Emaru, and A.A. Ravankar. Mapping of pier substructure using uav. *In Proceedings of the IEEE International Symposium on System Integration*, 13–15 December(Sapporo, Japan):pp. 361–366, 2016.

[8] K. Asa, Y. Funabora, S. Doki, and K Doki. Measuring position determination for accurate and efficient visual inspection using uav. *In Proceedings of the IEEE the International Symposium on System Integration*, Taipei, Taiwan (11–14 December):pp. 188–193., 2017.

[9] S. Abiko, T. Harada, T. Hasegawa, S. Yuta, and N. Shimaji. Semi-autonomous collision avoidance flight using two dimensional laser range finder with mirrors for bridge inspection. *In Proceedings of the 2018 IEEE International Conference on Robotics and Biomimetics (ROBIO)*, Kuala Lumpur, Malaysia(12–15 December):pp. 2268–2272, 2018.

[10] R. Ladig and K. Shimonomura. High precision marker based localization and movement on the ceiling employing an aerial robot with top mounted omni wheel drive system. *In Proceedings of the 2016 IEEE/RSJ International Conference on Intelligent Robots and Systems (IROS)*, Daejeon, South Korea(9–14 October):pp. 3081–3086, 2016.

[11] V. Badrinarayanan, A. Kendall, and R. Cipolla. Segnet: A deep convolutional encoder-decoder architecture for image segmentation. *IEEE Transactions on*

Pattern Recognition and Machine Intelligence, pages 2481–2496, 2017. doi: https://doi.org/10.1109/TPAMI.2016.2644615[Accessedon02June2022].

[12] A. G. Howard, M. Zhu, B. Chen, D. Kalenichenko, W. Wang, T. Weyand, M. Andreetto, and H. Adam. Mobilenets: Efficient convolutional neural networks for mobile vision applications. *ArXiv*, pages 1–9, 2017. doi: https://doi.org/10.48550/arXiv.1704.04861[Accessedon22June2022].

[13] Olaf Ronneberger, Phillip Fischer, and Thomas Brox. U-net: Convolutional neural networks for biomedical image segmentation. In *arXiv preprint: 1505.04597*, pages 1–8. arXiv, 2015.

[14] A Penn. The deadliest bridge collapses in the us in the last 50 years. *CNN*, 15 March 2018.

[15] R S Kirk and W J Mallett. Highway bridge conditions: Issues for congress. *CNN*, Us Congressional Research Service(Washington, DC), 2013.

[16] J.-L. Briaud, L. Brandimarte, J. Wang, and P D'Odorico. Probability of scour depth exceedance owing to hydrologic uncertainty. *Georisk*, 1(2):77–88, 2014.

[17] L. Wright, P. Chinowsky, and K. et al. Strzepek. Estimated effect of climate change on flood vulnerability of us bridges. *Mitigation and Adaptation Strategies for Global Change*, 17(8):939–955, 2012.

[18] Z. W. Wang, M. Zhou, G.G. Slabaugh, J. Zhai, and T. Fang. Automatic detection of bridge deck condition from ground penetrating radar images. *IEEE Transactions of Automation Science and Engineering*, 8(3):633–640, 2011.

[19] K. Dinh, N. N. Gucunski, and T.H. Doung. Automatic detection of bridge deck condition from ground penetrating radar images. *Automation in Construction*, 89(0):292–298, 2018.

[20] I. Tolstoy and E. Usdin. Dispersive properties of stratified elastic and liquid media: A ray theory. *Geophysics*, 18:844–870, 1953.

[21] R. M. Morey and A. Kovacs. Detection of moisture in construction materials. *Cold Region Research and Engineering Laboratory*, Hannover, NH, USA, 1977.

[22] J.R. Moore and J.D Erhard. Radar detection of voids under concrete highways. *Georgia Institute of Technology*, Atlanta, GA, USA, 1978.

[23] Detection of delamination in bridge decks with infrared thermography. Clemena, g.g. and mckeel, w.t. *Tranportation Research Records*, 664(0):180–182, 1978.

[24] A.E. Cawkell and T.N.W. Akroyd. The investigation of the quality of thick concrete by ultrasonic pulse porpagation. *Magazine on Concrete Research*, 10: 143, 1958.

[25] G.B. Wilson. Some aspects on data fusion. *Harris, C.J., Ed.*, P. Peregrinus: London, UK(In Advances in Command, Control and Communication Systems): pp. 321–338, 1987.

[26] A.K. Jain, M.P. Dubuisson, and M.S. Madhukar. Multi-sensor fusion for non-destructive inspection of fiber reinforced composite materials. *In Proceedings of the 6th Technical Conference of the American Society of Composite*, Albany, NY, USA:941–950, 1991.

[27] 2021 report card for america's infrastructure. `https://infrastructurereportcard.org/wp-content/uploads/2020/12/National_IRC_2021-report.pdf`, 2022. Accessed: 2022-08-08.

[28] Federal highway administration. bridge condition by highway system 2022. `https://www.fhwa.dot.gov/bridge/nbi/no10/condition22.cfm`, 2022. Accessed: 2022-08-08.

[29] J. Neumann, J. Price, and P. Chinowsky. Climate change risks to us infrastructure: impacts on roads, bridges, coastal development and urban drainage. *Climate Change*, 131(1):97–109, 2014.

[30] H. M. La, N. Gucunski, S-H. Kee, J. Yi, T. Senlet, and L. Nguyen. Autonomous robotic system for bridge deck data collection and analysis. In *IEEE Intern. Conf. on Intelligent Robots and Systems (IROS)*, pages 1950–1955, Sept 2014.

[31] I. Lee, S.-H. Kwon, J. Park, and T. Oh. The effective near-surface defect identification by dynamic behavior associated with both impact-echo and flexural modes for concrete structures. *KSCE J. Civ. Eng.*, 22:747–754., 2017.

[32] M. Flint, O. Fringer, S.L. Billington, D. Freyberg, and N.S. Diffenbaugh. Historical analysis of hydraulic bridge collapses in the continental united states. *J. Infrastruct. Syst.*, 23:pp. 1–10, 2017.

[33] A. Khelifa, L. A. Garrow, M. J. Higgins, and M. D. Meyer. Impact of climate change on scour-vulnerable bridges: assessment based on hyrisk. *Journal of Infrastructure System*, 19(2):138–146, 2013.

[34] Bureau of transportation statistics. `https://www.bts.gov/content/condition-us-highway-bridges`, 2022. Accessed: 2022-08-08.

[35] N. Gucunski, S-H. Kee, H.M. La, B. Basily, and A. Maher. Delamination and concrete quality assessment of concrete bridge decks using a fully autonomous rabit platform. *International Journal of Structural Monitoring and Maintenance*, 2(1):19–34, 2015.

[36] W. Cook, P.J. Barr, and M.W. Haling. Bridge failure rate. *Journal of Performance Construction Facilities*, 29(3):1–8, 2015.

[37] N. Gucunski, S-H. Kee, H. M. La, B. Basily, A. Maher, and H. Ghasemi. Implementation of a fully autonomous platform for assessment of concrete bridge decks rabit. In *Structures Congress*, pages 367–378, Apr 2015.

[38] H. M. La, N. Gucunski, K. Dana, and S.-H. Kee. Development of an autonomous bridge deck inspection robotic system. *Journal of Field Robotics*, 34(8):1489–1504, 2017.

[39] S. Gibb, H.M. La, T. Le, L. Nguyen, R. Schmid, and N. Pham. Non-destructive evaluation sensor fusion with autonomous robotic system for civil infrastructure inspection. *J. Field Robot*, 35:988–1004, 2018.

[40] P. Kaur, K.J. Dana, F.A. Romero, and N. Gucunski. Automated gpr rebar analysis for robotic bridge deck evaluation. *IEEE Trans. Cybern.*, 46:2265–2276, 2015.

[41] Nhan H Pham and Hung M La. Design and implementation of an autonomous robot for steel bridge inspection. In *2016 54th Annual Allerton Conference on Communication, Control, and Computing (Allerton)*, pages 556–562. IEEE, 2016.

[42] Aaron Sirken, Gedaliah Knizhnik, Jessica McWilliams, and Sarah Bergbreiter. Bridge risk investigation diagnostic grouped exploratory (bridge) bot. In *2017 IEEE/RSJ International Conference on Intelligent Robots and Systems (IROS)*, pages 6526–6532. IEEE, 2017.

[43] P. Prasanna, K. J. Dana, N. Gucunski, B. B. Basily, H. M. La, R. S., and H. Parvardeh. Automated crack detection on concrete bridges. *IEEE Transactions on Automation Science and Engineering*, 13(2):591–599, 2014.

[44] T. Le, S. Gibb, N. Pham, H.M. La, L. Falk, and T. Berendsen. Autonomous robotic system using non-destructive evaluation methods for bridge deck inspection. *In Proceedings of the 2017 IEEE International Conference on Robotics and Automation (ICRA)*, Singapore, 29 May–3 June:pp. 3672–3677, 2017.

[45] R. S Lim, H. M. La, Z. Shan, and W. Sheng. Developing a crack inspection robot for bridge maintenance. In *Robotics and Automation (ICRA), 2011 IEEE Intern. Conf. on*, pages 6288–6293, May 2011.

[46] S. T. Nguyen and H. M. La. Roller chain-like robot for steel bridge inspection. In *9th International Conference on Structural Health Monitoring of Intelligent Infrastructure (SHMII-9)*, pages 1–6. SHMII-9, 2019.

[47] Z. Zheng, S. Hu, and N. Ding. Biologically inspired cable climbing robot: Ccrobot-design and implementation. *In Proceedings of the 2018 IEEE International Conference on Robotics and Biomimetics (ROBIO)*, Kuala Lumpur, Malaysia(12–15 December):pp. 2354–2359, 2018.

[48] M. Zheng, M. Yang, X. Yuan, and N. Ding. A light-weight wheel-based cable inspection climbing robot: From simulation to reality. *In Proceedings of the 2018 IEEE International Conference on Robotics and Biomimetics (ROBIO)*, Kuala Lumpur, Malaysia(12–15 December):pp. 1365–1370, 2018.

[49] R.T. Pack, J.L. Christopher, and K. Kawamura. A rubbertuator-based structure-climbing inspection robot. *In Proceedings of the International Conference on Robotics and Automation (ICRA)*, Washington, DC, USA(11–15 May): pp. 1869–1874., 2002.

[50] Z. Liu, D.S. Forsyth, J.P. Komorowski, K. Hanasaki, and T. Kirubarajan. Survey: State of the art in nde data fusion techniques. *IEEE Trans. Instrum. Meas.*, 56:2435–2451, 2007.

[51] X. Li, C. Gao, Y. Guo, F. He, and Y. Shao. Cable surface damage detection in cable-stayed bridges using optical techniques and image mosaicking. *Opt. Laser Technol.*, 110:pp. 36–43., 2019.

[52] K.H. Cho, Y.H. Jin, H.M. Kim, and H.R. Choi. Development of novel multi-functional robotic crawler for inspection of hanger cables in suspension bridges. *In Proceedings of the 2014 IEEE International Conference on Robotics and Automation (ICRA)*, Hong Kong, China(31 May–5 June):pp. 2673–2678, 2014.

[53] A. Leibbrandt, G. Caprari, U. Angst, R.Y. Siegwart, R.J. Flatt, and B. Elsener. Climbing robot for corrosion monitoring of reinforced concrete structures. *In Proceedings of the 2012 2nd International Conference on Applied Robotics for the Power Industry (CARPI)*, Zurich, Switzerland(11–13 September):pp. 10–15, 2012.

[54] Son T Nguyen, Anh Q Pham, Cadence Motley, and Hung M La. A practical climbing robot for steel bridge inspection. In *2020 IEEE International Conference on Robotics and Automation (ICRA)*, pages 9322–9328. IEEE, 2020.

[55] A. Q. Pham, H. M. La, K. T. La, and M. T. Nguyen. A magnetic wheeled robot for steel bridge inspection. In *International Conference on Engineering Research and Applications*, pages 11–17, 2019.

[56] H. D. Bui, S. T. Nguyen, U. H. Billah, C Le, A. Tavakkoli, and H. M. La. Control framework for a hybrid-steel bridge inspection robot. In *In Proceedings of the*

2020 IEEE/RSJ International Conference on Intelligent Robots and Systems (IROS), pages 2585–2591. IEEE, 2020.

[57] Z. Zheng and N. Ding. Design and implementation of ccrobot-ii: A palm-based cable climbing robot for cable-stayed bridge inspection. *In Proceedings of the 2019 International Conference on Robotics and Automation (ICRA)*, Montreal, QC, Canada(20–24 May):pp. 9747–9753, 2019.

[58] K.H. Cho, Y.H. Jin, H.M. Kim, H. Moon, J.C. Koo, and H.R. Choi. Caterpillar-based cable climbing robot for inspection of suspension bridge hanger rope. *In Proceedings of the 2013 IEEE International Conference on Automation Science and Engineering (CASE)*, Madison, WI, USA(17–21 August):pp. 1059–1062, 2013.

[59] P. Kriengkomol, K. Kamiyama, M. Kojima, M. Horade, Y. Mae, and T. Arai. New tripod walking method for legged inspection robot. *In Proceedings of the 2016 IEEE International Conference on Mechatronics and Automation*, Harbin, China(7–10 August):pp. 1078–1083, 2016.

[60] K.H. Cho, H.M. Kim, Y.H. Jin, F. Liu, H. Moon, J.C. Koo, and H. R. Choi. Inspection robot for hanger cable of suspension bridge: Mechanism design and analysis. *Mechatronics, IEEE/ASME Transactions on*, 18(6):1665–1674, Dec 2013.

[61] Z. Zheng, X. Yuan, H. Huang, X. Yu, and N. Ding. Mechanical design of a cable climbing robot for inspection on a cable-stayed bridge. *In Proceedings of*

the World Congress on Intelligent Control and Automation, Changsha, China (4–8 July 2018):pp. 1680–1684., 2018.

[62] G. Andrikopoulos, A. Papadimitriou, A. Brusell, and G. Nikolakopoulos. On model-based adhesion control of a vortex climbing robot. *In Proceedings of the 2019 IEEE/RSJ International Conference on Intelligent Robots and Systems (IROS)*, Macau, China(4–8 November):pp. 1460–1465, 2019.

[63] T. Ikeda, S. Yasui, M. Fujihara, K. Ohara, S. Ashizawa, A. Ichikawa, A. Okino, T. Oomichi, and T Fukuda. Wall contact by octo-rotor uav with one dof manipulator for bridge inspection. *In Proceedings of the 2017 IEEE/RSJ International Conference on Intelligent Robots and Systems (IROS)*, Vancouver, BC, Canada (24–28 September):pp. 5122–5127, 2017.

[64] H. M. La, R. S. , B. B. Basily, N. Gucunski, J. Yi, A. Maher, F. A. Romero, and H. Parvardeh. Mechatronic systems design for an autonomous robotic system for high-efficiency bridge deck inspection and evaluation. *IEEE/ASME Transactions on Mechatronics*, 18(6):1655–1664, 2013.

[65] N. Morozovsky and T. Bewley. A low dof, dynamic high wire robot. *In Proceedings of the 2013 IEEE/RSJ International Conference on Intelligent Robots and Systems (IROS)*, Tokyo, Japan(3–7 November):pp. 2339–2344, 2013.

[66] R. Xie, J. Yao, K. Liu, X. Lu, Y. Liu, M. Xia, and Q. Zeng. Automatic multi-image stitching for concrete bridge inspection by combining point and line features. *Autom. Constr.*, 90:265–280, 2018.

[67] B.W. Jiang, C.H. Kuo, K.J. Peng, K.C. Peng, S.H. Hsiung, and C.M. Kuo. Thrust vectoring control for infrastructure inspection multirotor vehicle. *In Proceedings of the 2019 IEEE 6th International Conference on Industrial Engineering and Applications (ICIEA)*, Tokyo, Japan(26–29 April):pp. 209–213, 2019.

[68] N. Gucunski, B. Basily, J. Kim, J. Yi, T. Duong, K. Dinh, S.-H. Kee, and A. Maher. Rabit: Implementation, performance validation and integration with other robotic platforms for improved management of bridge decks. *Int. J. Intell. Robot. Appl.*, 1:271–286, 2017.

[69] R.R. Murphy, E. Steimle, M. Hall, M. Lindemuth, D. Trejo, S. Hurlebaus, Z. Medina-Cetina, and D Slocum. Robot-assisted bridge inspection. *Journal of Intelligent Robotics Systems*, 64:77–95, 2011.

[70] J. DeVault. Robotic system for underwater inspection of bridge piers. *IEEE Instrum. Meas. Mag.*, 3:pp. 32–37, 2000.

[71] P. Ratsamee, P. Kriengkomol, T. Arai, K. Kamiyama, Y. Mae, K. Kiyokawa, T. Mashita, Y. Uranishi, and H. Takemura. A hybrid flying and walking robot for steel bridge inspection. *In Proceedings of the IEEE International Symposium on Safety, Security and Rescue Robotics (SSRR)*, page 62–67, 2016.

[72] A. Jimenez-Cano, J. Braga, G. Heredia, and A. Ollero. Aerial manipulator for structure inspection by contact from the underside. *In Proceedings of the*

2015 IEEE/RSJ International Conference on Intelligent Robots and Systems (IROS), Hamburg, Germany(28 September–3 October):pp. 1879–1884, 2015.

[73] W. Myeong and J. Koo. Development of a wall-climbing drone capable of vertical soft landing using a tilt-rotor mechanism. *IEEE Access*, 7:pp. 4868–4879, 2018.

[74] P.J. Sanchez-Cuevas, G. Heredia, and A. Ollero. Multirotor uas for bridge inspection by contact using the ceiling effect. *In Proceedings of the 2017 International Conference on Unmanned Aircraft Systems (ICUAS)*, Maimi, FL, USA(13–16 June):pp. 767–774, 2017.

[75] A. Ichikawa, Y. Abe, T. Ikeda, K. Ohara, J. Kishikawa, S. Ashizawa, T. Oomichi, A. Okino, and T. Fukuda. Uav with manipulator for bridge inspection: Hammering system for mounting to uav. *In Proceedings of the IEEE International Symposium on System Integration*, Taipei, Taiwan(11–14 December):pp. 775–780, 2017.

[76] Y. Guan, H. Zhu, W. Wu, X. Zhou, L. Jiang, C. Cai, L. Zhang, and H. Zhang. A modular biped wall-climbing robot with high mobility and manipulating function. *IEEE/ASME Trans. Mechatron.*, 18:1787–1798, 2012.

[77] H.M. La, R.S. Lim, B. Basily, N. Gucunski, J. Yi, A. Maher, F.A. Romero, H. Parvardeh, and A. Maher. Autonomous robotic system for high-efficiency non-destructive bridge deck inspection and evaluation. *In Proceedings of the*

2013 IEEE International Conference on Automation Science and Engineering (CASE), Madison, WI, USA(17–21 August):pp. 1053–1058, 2013.

[78] Son Thanh Nguyen and Hung Manh La. Development of a steel bridge climbing robot. In *2019 IEEE/RSJ International Conference on Intelligent Robots and Systems (IROS)*, pages 1912–1917. IEEE, 2019.

[79] M. Minor, H. Dulimarta, G. Danghi, R. Mukherjee, R.L. Tummala, and D. Aslam. Design, implementation, and evaluation of an under-actuated miniature biped climbing robot. *In Proceedings of the 2000 IEEE/RSJ International Conference on Intelligent Robots and Systems (IROS 2000)*, Takamatsu, Japan (31 October–5 November):pp. 1999–2005, 2002.

[80] R. S. Lim, H. M. La, and W. Sheng. A robotic crack inspection and mapping system for bridge deck maintenance. In *IEEE Transactions on Automation Science and Engineering*, pages 367–378. IEEE, 2014.

[81] H. M. La, N. Gucunski, Seong-Hoon Kee, J. Yi, T. Senlet, and Luan Nguyen. Autonomous robotic system for bridge deck data collection and analysis. In *2014 IEEE/RSJ Intern. Conf. on Intelligent Robots and Systems*, pages 1950–1955, 2014.

[82] N. Gucunski, S.H. Kee, H.M. La, J. Kim, R. Lim, and H. Parvardeh. Bridge deck surveys on eight illinois tollways bridges using robotics assisted bridge inspection tool. *Applied Research Associates*, Urbana-Champaign, IL, USA, 2014.

[83] L. Van Nguyen, S. Gibb, H.X. Pham, and H.M. La. A mobile robot for automated civil infrastructure inspection and evaluation. *In Proceedings of the IEEE Symposium on Safety, Security and Rescue Robotics (SSRR)*, Philadelphia, PA, USA(6–8 August):pp. 1–6, 2018.

[84] Q. Liu and Y. Liu. An approach for auto bridge inspection based on climbing robot. *In Proceedings of the 2013 IEEE International Conference on Robotics and Biomimetics (ROBIO)*, Shenzhen, China(12–14 December):pp. 2581–2586, 2013.

[85] S. Hirose, A. Najakubo, and R. Toyama. Machine that can walk and climb on floors, walls and ceilings. *In Proceedings of the Fifth International Conference on Advanced Robotics and Robots in Unstructured Environments*, Pisa, Italy, 19–22 June(1):pp. 753–758, 1991.

[86] B.L. Luk, D.S. Cooke, S. Galt, A.A. Collie, and S. Chen. Intelligent legged climbing service robot for remote maintenance applications in hazardous environments. *Robot. Auton. Syst.*, 53:pp. 142–152, 2005.

[87] C. Balaguer, A. Gimenez-Fernandez, C. Abderrahim, and M. Abderrahim. A climbing autonomous robot for inspection applications in 3d complex environments. *Robotica*, 18:287–297, 2000.

[88] D. Longo and G. Muscato. The alicia climbing robot. *IEEE Robot. Autom. Lett.*, 13:pp. 42–50, 2006.

[89] Y. Liu, Q. Dai, and Q. Liu. Adhesion-adaptive control of a novel bridge-climbing robot. *In Proceedings of the 2013 IEEE International Conference on Cyber Technology in Automation, Control and Intelligent Systems*, Nanjing, China (26–29 May):pp. 102–107, 2013.

[90] S. Jung, S. Song, S. Kim, J. Park, J. Her, K. Roh, and H. Myung. Toward autonomous bridge inspection: A framework and experimental results. *In Proceedings of the 2019 16th International Conference on Ubiquitous Robots (UR)*, Jeju, South Korea(24–27 June):pp. 208–211, 2019.

[91] C.A. Mueller, T. Fromm, H. Buelow, A. Birk, M. Garsch, and N. Gebbeken. Robotic bridge inspection within strategic flood evacuation planning. *In Proceedings of the OCEANS 2017*, page 1–6, 2017.

[92] N. Diamanti and D. Redman. Field observations and numerical models of gpr response from vertical pavement cracks. *J. Appl. Geophys.*, 81:106–116, 2012.

[93] B.A. Mazzeo, J. Larsen, J. McElderry, and W.S. Guthrie. Rapid multichannel impact-echo scanning of concrete bridge decks from a continuously moving platform. *In Proceedings of the 43rd Annual Review of Progress in Quantitative Nondestructive Evaluation*, Atlanta, GA, USA(1806):17–22 July, 2017.

[94] J. Zhu and J.S. Popovics. Non-contact ndt of concrete structures using air coupled sensors. *University of Illinois at Urbana-Champaign*, Urbana, IL, USA: pp. 1–6, 2008.

[95] J.C. Ashlock, B. Phares, and J. Lu. Imaging concrete structures using air-coupled impact-echo. *J. Eng. Mech.*, 133:628–640, 2007.

[96] S. Lin and J.C. Ashlock. Comparison of masw and msor for surfave wave testing of pavements. *J. Env. Eng. Geophys.*, 20:277–285, 2015.

[97] H. Sun, J. Zhu, and S. Ham. Acoustic evaluation of concrete delaminations using ball-chain impact excitation. *J. Acoust. Soc. Am.*, 141:EL477–EL481, 2017.

[98] M. Malhotra and C. Nicholas. Crc handbook on nondestructive testing of concrete. *CRC Press Inc.*, Boca Raton, FL, USA, 2004.

[99] Y. Dong and F. Ansari. Non-destructive testing and evaluation (ndt/nde) of civil structures rehabilitated using fiber reinforced polymer (frp) composites. *In Service Life Estimation and Extension of Civil Engineering Structures*, Elsevier (Amsterdam, The Netherlands):pp. 193–222, 2011.

[100] Y. Zhang and H.Z. Xie. Ensemble empirical mode decompisition in the impact-echo test. *NDT and E Int.*, 51:74–84, 2012.

[101] G. Li, S. He, Y. Ju, and K. Du. Long-distance precision inspection method for bridge cracks with image processing. *Autom. Constr.*, 41:83–95, 2014.

[102] O. Abraham and J.S. Popovics. Non-destructive evaluation of reinforced concrete structures. *Non-Destructive Testing Methods*, Elsevier Inc.(London, UK), 2010.

[103] T. Sakagami. Remote nondestructive evaluation technique using infrared thermography for fatigue cracks in steel bridges. *Fatigue and Fractures in Engineering Materials and Structures*, 38:755–779, 2015.

[104] D. Meng and H. Azari. Reducing thermal reflections for infrared thermography applications on tunnel liners with reflective finishes. *Transp. Res. Rec. J. Transp. Res. Board*, 2672:145–155, 2018.

[105] K. Kobayashi and N. Banthia. Corrosion detection in reinforced concrete using induction heating and infrared thermography. *J. Civ. Struct. Health Monit.*, 1: pp. 25–35, 2012.

[106] T. Omar and M.L. Nehdi. Application of passive infrared thermography for the detection of defects in concrete bridge elements. *In Proceedings of the International Conference of the Transportation Association of Canada*, Toronto, ON, Canada(22–28 September):pp. 1–12, 2016.

[107] G. Washer, J. Dawson, P. Ruiz-Fabian, A. Sultan, and M. Trial. Field testing of hand-held infrared thermography. *Phase II TPF-5(247) Final Report*, Missouri Department of Transportation(Jefferson, MO, USA), 2016.

[108] T. Sakagami, Y. Izumi, D. Shiozawa, T. Fujimoto, Y. Mizokami, and T. Hanai. Nondestructive evaluation of fatigue cracks in steel bridges based on thermoelastic stress measurement. *Procedia Struct. Integr.*, 2:pp. 2132–2139, 2016.

[109] B. Zou, Z. Luo, J. Wang, G. Wang, and L. Hu. Infrared thermography analysis of tunnel surrounding rock damage under blasting. *J. Eng. Blasting*, 4:pp. 1–6, 2016.

[110] G. Barla, F. Antolini, and G. Gigli. 3d laser scanner and thermography for tunnel discontinuity mapping. *Geomech. Tunn.*, 9:pp. 29–36, 2016.

[111] X. Feng. Rockburst: Mechanism, monitoring, warning and mitigation. *Butterworth-Heinemann*, Waltham, MA, USA,, 2017.

[112] S. Rana and R. Fanguiero. Advanced composite materials for aerospace engineering: Processing, properties and applications. *Woodhead Publishing*, Cambridge, UK, 2016.

[113] F. Ciampa, P. Mahmoodi, F. Pinto, and M. Meo. Recent advances in active infrared thermography for non-destructive testing of aerospace components. *Sensors*, 18(609), 2018.

[114] J.S. Popovics. Nde techniques for concrete and masonry structures. *Prog. Struct. Eng. Mater.*, 5:49–59, 2003.

[115] S. Yehia, O. Abudayyeh, S. Nabulsi, and I. Abdelqader. Detection of common defects in concrete bridge decks using nondestructive evaluation techniques. *J. Bridg. Eng.*, 12:215–225, 2007.

[116] C.-C. Cheng, T.-M. Cheng, and C.-H. Chiang. Defect detection of concrete structures using both infrared thermography and elastic waves. *Autom. Constr.*, 18:87–92, 2008.

[117] S.-H. Kee, T.K. Oh, J.S. Popovics, R.W. Arndt, and J. Zhu. Nondestructive bridge deck testing with air-coupled impact-echo and infrared thermography. *J. Bridg. Eng.*, 17:928–939, 2012.

[118] T.K. Oh, S.-H. Kee, R.W. Arndt, J.S. Popovics, and J. Zhu. Comparison of ndt methods for assessment of a concrete bridge deck. *J. Eng. Mech.*, 139:305–314, 2013.

[119] N. Gucunski, S.H. Kee, H.M. La, R. Lim, and H. Parvardeh. Bridge deck surveys on four new jersey tollway bridges using robotics assisted bridge inspection tool. *Parsons Brinckerhoff Inc.*, Lawrenceville, NJ, USA, 2014.

[120] G. Washer, R. Fenwick, N. Bolleni, and J. Harper. Effects of environmental variables on infrared imaging of subsurface features of concrete bridges. *Transp. Res. Rec. J. Transp. Res. Board*, 2108:107–114, 2009.

[121] K. Vaghefi, T.M. Ahlborn, D. Harris, and C.N. Brooks. Combined imaging technologies for concrete bridge deck condition assessment. *J. Perform. Constr. Facil.*, 29, 2015.

[122] H. Ahmed, H. M. La, and N. Gucunski. Review of non-destructive civil infrastructure evaluation for bridges: State-of-the-art robotic platforms, sensors and algorithms. In *Sensors*, pages 1–35. MDPI, 2020.

[123] H. Ahmed, H.M. La, and N. Gucunski. Rebar detection using ground penetrating radar with state-of-the-art convolutional neural networks. *In Proceedings of the 9th International Conference on Structural Health Monitoring of Intelligent infrastructure*, St. Louis, MI, USA(4–7 August):pp. 1–6, 2019.

[124] H. Ahmed, H.M. La, and G. Pekcan. Rebar detection and localization for non-destructive infrastructure evaluation of bridges using deep residual networks. *In Proceedings of the 14th International Symposium on Visual Computing*, Lake Tahoe, NV, USA(7–9 October):pp. 1–6, 2019.

[125] Q. Dou, L. Wei, D.R. Magee, and A. Cohn. A real-time hyperbola recognition and fitting in gpr data. *IEEE Trans. Geosci. Remote Sens.*, 55:51–62, 2016.

[126] P.A. Torrione, K.D. Morton, R. Sakaguchi, and L.M. Collins. Histogram of oriented gradient for landmine detection in ground penetrating radar data. *IEEE Trans. Geosci. Remote Sens.*, 52:1539–1550, 2014.

[127] P. Torrione and L.M. Collins. Texture features for antitank landmine detection using ground penetrating radar. *IEEE Trans. Geosci. Remote Sens.*, 45: 2374–2382, 2007.

[128] J. Hugenschmidt. Concrete bridge inspection with a mobile gpr system. *Constr. Build. Mater.*, 16:147–154, 2002.

[129] S. Shihab and W. Al-Nuaimy. Radius estimation for cylindrical objects detection by ground penetrating radar. *Int. J. Sens. Imaging*, 6:151–166, 2005.

[130] X. Feng, Y. Yu, C. Liu, and M. Fehler. Subsurface polarimetric migration imaging for full polarimetric ground-penetrating radar. *Geophys. J. Int.*, 202: 1324–1338, 2015.

[131] E. Pasolli, F. Melgani, and M. Donelli. Automatic analysis of gpr images: A pattern-recognition approach. *IEEE Trans. Geosci. Remote Sens.*, 47: 2206–2217, 2009.

[132] L. Mertens, R. Persico, L. Matera, and S. Lambot. Automated detection of reflection hyperbolas in complex gpr images in no a priori knolwedge on the medium. *IEEE Trans. Geosci. Remote Sens*, 54:580–596, 2016.

[133] W. Al-Nuaimy, Y. Huang, M. Nakhkash, M. Fang, V. Nguyen, and A. Eriksen. Automatic detection of buried utilities and solid objects with gpr using neural networks and pattern recognition. *J. Appl. Geophys.*, 43:157–165, 2000.

[134] D. Li, A. Cong, and S. Guo. Sewer damage detection from imbalanced cctv inspection data using deep convolutional neural networks with hierarchical classification. *Autom. Constr.*, 101:199–208, 2019.

[135] Y. Ren, J. Huang, Z. Hong, W. Lu, J. Yin, L. Zou, and X. Shen. Image-based concrete crack detection in tunnels using deep fully convolutional networks. *Constr. Build. Mater.*, 234, 2020.

[136] E. Menendez, J. Victores, R. Montero, S. Martínez, and C. Balaguer. Tunnel structural inspection and assessment using an autonomous robotic system. *Autom. Constr.*, 87:117–126, 2018.

[137] L. Wang, K. Kawaguchi, and P. Wang. Damaged ceiling detection and localization in large-span structures using convolutional neural networks. *Autom. Constr.*, 116, 2020.

[138] H. Maeda, Y. Sekimoto, T. Seto, T. Kashiyama, and H. Omata. Road damage detection and classification using deep neural networks with smartphone images. *Comput. Civ. Infrastruct. Eng.*, 33:1127–1141, 2018.

[139] Z. Tong, J. Gao, A. Sha, L. Hu, and S. Li. Convolutional neural network for asphalt pavement surface texture analysis. *Comput. Civ. Infrastruct. Eng.*, 33: 1056–1072, 2018.

[140] S. Zhou and W. Song. Deep learning-based roadway crack classification using laser-scanned range images: A comparative study on hyperparameter selection. *Autom. Constr.*, 114:1–17, 2020.

[141] B. Dai, C. Gu, E. Zhao, K. Zhu, W. Cao, and X. Qin. Improved online sequential extreme learning machine for identifying crack behavior in concrete dam. *Adv. Struct. Eng.*, 22:402–412, 2018.

[142] K. Zhang, H. Cheng, and B. Zhang. Unified approach to pavement crack and sealed crack detection using preclassification based on transfer learning. *J. Comput. Civ. Eng.*, 22, 2018.

[143] M. Song and D. Civco. Road extraction using svm and image segmentation. *Photogramm. Eng. Remote Sens.*, 70:1365–1371, 2004.

[144] L. Ying and E. Salari. Beamlet transform-based technique for pavement crack detection and classifcation. *Comput. Aided Civ. Infrastructural Eng.*, 25:572–580, 2010.

[145] E. Zalama, J. Gómez-García-Bermejo, R. Medina, and J. Llamas. Road crack detection using visual features extracted by gabor filters. *Comput. Civ. Infrastruct. Eng.*, 29:342–358, 2013.

[146] T.H. Dinh, Q.P. Ha, and H.M. La. Computer vision-based method for concrete crack detection. *In Proceedings of the 2016 14th International Conference on Control, Automation, Robotics and Vision (ICARCV)*, Phuket, Thailand(13–15 November):1–6, 2016.

[147] S.E. Park, S.-H. Eem, and H. Jeon. Concrete crack detection and quantification using deep learning and structured light. *Constr. Build. Mater*, 252, 2020.

[148] J.P. Rivera, G. Josipovic, E. Lejeune, B.N. Luna, and A.S. Whittaker. Automated detection and measurement of cracks in reinforced concrete components. *ACI Struct. J.*, 112:397–407, 2015.

[149] T. Merazi-Meksen, M. Boudraa, and B. Boudraa. Mathematical morphology for tofd image analysis and automatic crack detection. *Ultrasonics*, 54:1642–1648, 2014.

[150] H. M. La, T. H. Dinh, N. H. Pham, Q. P. Ha, and A. Q. Pham. Automated robotic monitoring and inspection of steel structures and bridges. *Robotica*, pages 1 – 21, 2018. doi: 10.1017/S0263574717000601.

[151] N. H. Pham, H. M. La, Q. P. Ha, S. N. Dang, A. H. Vo, and Q. H. Dinh. Visual and 3d mapping for steel bridge inspection using a cbing robot. In *The 33rd Intern. Symposium on Automation and Robotics in Construction and Mining (ISARC)*, pages 1–8, July 2016.

[152] C. Maierhofer, G. Zacher, C. Kohl, and J. Wöstmann. Evaluation of radar and complementary echo methods for ndt of concrete elements. *J. Nondestruct. Eval.*, 27:47–57, 2008.

[153] M.-A. Ploix, V. Garnier, D. Breysse, and J. Moysan. Nde data fusion to improve the evaluation of concrete structures. *NDT and E Int.*, 44:442–448, 2011.

[154] H. Masoom, R.S. Adve, and R.S. Cobbold. Target detection in diagnostic ultrasound: Evaluation of a method based on the clean algorithm. *Ultrasonics*, 53:335–344, 2013.

[155] D.C. Wright, A. Miltreyger, A. Bron, and S. Rabinovich. 1000 gates-a novel approach and method for ultrasonic inspection of aero-engine disc forgings. x. *In Proceedings of the British Institute of NDT Conference*, Telford, UK(10–12 September):pp. 1–6, 2013.

[156] R. Halmshaw. Non-destructive testing. 2nd ed. *NDT and E Int.*, 25:234., 1992.

[157] N. Brierley, T. Tippetts, and P. Cawley. Data fusion for automated non-destructive inspection. *Proc. R. Soc. A*, 240, 2014.

[158] C.G. Windsor and L. Capineri. Automated object positioning from ground penetrating images. *Insights*, 40:482–488, 1998.

[159] Y. Zhang, A. Roshan, S. Jahari, S.A. Khiabani, F. Fathollahi, and B.K. Mishra. Understanding the quality of pan sharpening- a lab study. *Photogramm. Eng. Remote Sens.*, 82:747–755, 2016.

[160] B. Duraisamy. Track level fusion of extended objects from heterogeneous sensors. *In Proceedings of the International Conference on Information Fusion*, Heidelberg, Germany:5–8 July, 2016.

[161] R. Heideklang and P. Shokouhi. Application of data fusion in nondestructive testing (ndt). *In Proceedings of the 16th International Conference on Information Fusion*, Istanbul, Turkey(9–12 July):pp. 835–841, 2013.

[162] Multisensor data fusion: A review of the state-of-the art. Khaleghi, b. and khamis, a. and karray, f.o. and razavi, s.n. *Inf. Fusion*, 14:28–44, 2013.

[163] M. Friedrich, S.G. Pierce, W. Galbraith, and G. Hayward. Data fusion in automated robotic inspection systems. *Insight-Non-Destr. Test. Cond. Monit.*, 50:88–94, 2008.

[164] J. Moysan, A. Durocher, C. Gueudré, and G. Corneloup. Improvement of the non-destructive evaluation of plasma facing components by data combination of infrared thermal images. *NDT and E Int.*, 40:478–485, 2007.

[165] R.R. Williams, J. Abdallah, and S. Nazarian. Implementation of data fusion techniques in nondestructive testing of pavements and center for transportation infrastructure systems. *University of Texas at El Paso*, Texas, TX, USA, 2004.

[166] U.H. Billah, H.M. La, A. Tavakkoli, and N. Gucunski. Classification of concrete crack using deep residual networks. In *In Proceedings of the International Conference on Structural Health Monitoring (SHMII-9), St. Louis, MI, USA, 4–7 August*, pages 1–6, 2019.

[167] U.H. Billah, A. Tavakkoli, and H.M. La. Concrete crack pixel classification using an encoder decoder based deep learning architecture. *In Proceedings of*

the International Symposium on Visual Computing, Lake Tahoe, NV, USA(7–9 October):pp. 593–604, 2019.

[168] S. Gibb, H.M. La, and S Louis. A genetic algorithm for convolutional network structure optimization for concrete crack detection. *In Proceedings of the IEEE Congress on Evolutionary Computation*, Rio de Janiero, Brazil(8–13 July):pp. 1–8, 2018.

[169] Y. Fujita and Y. Hamamoto. A robust automatic crack detection method from noisy concrete surfaces. *Mach. Vis. Appl.*, 22:245–254, 2010.

[170] J.-H. Chen, M.-C. Su, R. Cao, S.-C. Hsu, and J.-C. Lu. A self organizing map optimization based image recognition and processing model for bridge crack inspection. *Autom. Constr.*, 73:58–66, 2017.

[171] J.-K. Oh, G. Jang, S. Oh, J.H. Lee, B.-J. Yi, Y.S. Moon, J.S. Lee, and Y. Choi. Bridge inspection robot system with machine vision. *Autom. Constr.*, 18: 929–941, 2009.

[172] G. Li, X. Zhao, K. Du, F. Ru, and Y. Zhang. Recognition and evaluation of bridge cracks with modified active contour model and greedy search-based support vector machine. *Autom. Constr.*, 78:51–61, 2017.

[173] Z. Liu, Y. Cao, Y. Wang, and W. Wang. Computer vision-based concrete crack detetion using u-net fully convolutional networks. *Autom Constr.*, 104:129–139, 2019.

[174] C.V. Dung and L.D. Anh. Autonomous concrete crack detection using deep fully convolutional neural network. *Autom. Constr.*, 99:52–58, 2019.

[175] P. Broberg. Surface crack detection in welds using thermography. *NDT and E Int.*, 57:69–73, 2013.

[176] S.K. Sinha and P.W. Fieguth. Automated detection of cracks in buried concrete pipe images. *Autom. Constr.*, 15:58–72, 2006.

[177] P. Wang and H. Huang. Comparison analysis on present image-based crack detection methods in concrete structures. *In Proceedings of the 3rd Congress on Image and Signal Processing*, Yantai, China(16–18 October):pp. 2530–2533, 2010.

[178] S. Alam, A. Loukili, F. Grondin, and E. Rozière. Use of the digital image correlation and acoustic emission technique to study the effect of structural size on cracking of reinforced concrete. *Eng. Fract. Mech.*, 143:17–31, 2015.

[179] S. Iliopoulos, D. Aggelis, L. Pyl, J. Vantomme, P. Van Marcke, E. Coppens, and L. Areias. Detection and evaluation of cracks in the concrete buffer of the belgian nuclear waste container using combined ndt techniques. *Constr. Build. Mater.*, 78:369–378, 2015.

[180] M. Hamrat, B. Boulekbache, M. Chemrouk, and S. Amziane. Flexural cracking behavior of normal strength, high strength and high strength fiber concrete

beams, using digital image correlation technique. *Constr. Build. Mater.*, 106: 678–692, 2016.

[181] C. Xu, J. Xie, G. Chen, and W. Huang. Crack detection of reinforced concrete bridge using video image. *J. Cent. South Univ.*, 20:2605–2613, 2013.

[182] J. Glud, J.M. Dulieu-Barton, O. Thomsen, and L. Overgaard. Automated counting of off-axis tunnelling cracks using digital image processing. *Compos. Sci. Technol.*, 125:80–89, 2016.

[183] M. Vidal, M. Ostra, N. Imaz, E. García-Lecina, and C. Ubide. Analysis of sem digital images to quantify crack network pattern area in chromium electrodeposits. *Surf. Coat. Technol.*, 285:289–297, 2016.

[184] X. Li, H. Jiang, and G. Yin. Detection of surface crack defects on ferrite magnetic tile. *NDT and E Int.*, 62:6–13, 2014.

[185] S. Kabir. Imaging-based detection of aar induced map-crack damage in concrete structure. *NDT and E Int.*, 43:461–469, 2010.

[186] S. Anwar and M. Abdullah. Micro-crack detection of multicrystalline solar cells featuring an improved anisotropic diffusion filter and image segmentation technique. *Eurasip J. Image Video Process.*, 15, 2014.

[187] D. Dhital and J.-R. Lee. A fully non-contact ultrasonic propagation imaging system for closed surface crack evaluation. *Exp. Mech.*, 52:1111–1122, 2011.

[188] X. Guo and V. Vavilov. Crack detection in aluminium parts by using ultrasound-excited infrasred thermography. *Infrared Phys. Technol.*, 61:149–156, 2013.

[189] T.M. Meksen, B. Boudraa, R. Drai, and M. Boudraa. Automatic crack detection and characterization during ultrasonic inspection. *J. Nondestruct. Eval.*, 29: 169–174, 2010.

[190] I. Abdel-Qader, O. Abudayyeh, and M.E. Kelly. Analysis of edge-detection techniques for crack identification in bridges. *J. Comput. Civ. Eng.*, 17:255–263, 2003.

[191] T. Yamaguchi, T. Mizutani, M. Tarumi, and D. Su. Sensitive damage detection of reinforced concrete bridge slab by "time-variant deconvolution" of shf-band radar signal. *IEEE Trans. Geosci. Remote Sens.*, 57:1478–1488, 2018.

[192] Y.-J. Cha, W. Choi, G. Suh, S. Mahmoudkhani, and O. Büyüköztürk. Autonomous structural visual inspection using region-based deep learning for detecting multiple damage types. *Comput. Civ. Infrastruct. Eng.*, 33:731–747, 2017.

[193] K. Gopalakrishnan, S.K. Khaitan, A.N. Choudhary, and A. Agrawal. Deep convolutional neural networks with transfer learning for computer vision-based data-driven pavement distress detection. *Constr. Build. Mater.*, 157:322–330, 2017.

[194] J. Camilo, R. Wang, L.M. Collins, K. Bradbury, and J.M. Malof. Application of a semantic segmentation convolutional neural network for accurate automatic detection and mapping of solar photovoltaic arrays in aerial imagery. *arXiv*, page arXiv:1801.04018, 2018.

[195] M. Teichmann, M. Weber, M. Zoellner, R. Cipolla, and R. Urtasun. Real-time joint semantic reasoning for autonmous driving. *In Proceedings of the IEEE Intelligent Vehicles Symposium*, Changshu, China(26–30 June):pp. 1013–1020, 2018.

[196] M.R. Jahanshahi and S.F. Masri. Adaptive vision-based crack detection using 3d scene reconstruction for condition assessment of structures. *Autom. Constr.*, 22:567–576, 2012.

[197] W.S.M. Brooks, D. Lamb, and S. Irvine. Ir reflectance imaging for crystalline si solar cell crack detection. *IEEE J. Photovolt.*, 2015(5):1–5, 2015.

[198] S. Bang, S. Park, H. Kim, and H. Kim. Encoder–decoder network for pixel-level road crack detection in black-box images. *Comput. Civ. Infrastruct. Eng.*, 34: 713–727, 2019.

[199] X. Zhang, D. Rajan, and B. Story. Concrete crack detection using context-aware deep semantic segmentation network. *Comput. Civ. Infrastruct. Eng.*, 34:951–971, 2019.

[200] D. Zhang, Q. Li, Y. Chen, M. Cao, L. He, and B. Zhang. An efficient and reliable coarse-to-fine approach for asphalt pavement crack detection. *Image Vis. Comput.*, 57:130–146, 2017.

[201] A. Zhang, K.C.P. Wang, B. Li, E. Yang, X. Dai, Y. Peng, W. Fei, Y. Liu, J.Q. Li, and C. Chen. Automated pixel-level pavement crack detection on 3d asphalt surfaces using a deep-learning framework. *Comput.-Aided Civ. Infrastruct. Eng*, 32:805–819, 2017.

[202] R. Janning, L. Schmidt-Thieme, A. Busche, and T. Horvath. Pipe localization by apex detection. *In Proceedings of the IET International Conference on Radar Systems*, Glasgow, UK(22–25 October):pp. 1–6, 2012.

[203] S. Lee, L.M. Chang, and et al. Automated recognition of surface defects using digital color image processing. *Automation in Construction*, pages pp. 540–549, 2006.

[204] Kuo-Wei Liao and Yi-Ting Lee. Detection of rust defects on steel bridge coatings via digital image recognition. *Automation in Construction*, pages pp. 294–306, 2016.

[205] Heng-Kuang Shen, Po-Han Chen, and Luh-Maan Chang. Automated steel bridge coating rust defect recognition method based on color and texture feature. *Automation in Construction*, pages pp. 338–356, 2013.

[206] Foad Kazemi Majd, Nasim Fallahi, and Vincenzo Gattulli. Detection of corrosion defects in steel bridges by machine vision. *In: Proceedings of the 1st Conference of the European Association on Quality Control of Bridges and Structures*, pages pp. 830–834, 2021.

[207] Yundong Li, Antonios Kontsos, and Ivan Bartoli. Automated rust-defect detection of a steel bridge using aerial multispectral imagery. *Journal of Infrastructure Systems*, pages pp. 1–25, 2019.

[208] M. Khatayazad, L. De Pue, and W. De Waele. Detection of corrosion on steel structures using automated image processing. *Developments in the Built Environment*, pages 1–12, 2020.

[209] M. Enikeev, I. Gubaydullin, and M. Maleeva. Analysis of corrosion process development on metals by means of computer vision. *Eng. J.*, 21(4):183–192, 2017.

[210] F. F. Feliciano, F. R. Leta, and F. B. Mainier. Texture digital analysis for corrosion monitoring. *Corrosion Science*, page pp. 138–147, 2015.

[211] M.J. Swan. Color indexing. *Int. J. Comput. Vis.*, page pp. 11–32, 1991.

[212] P.H. Chen, Y.C. Chang, L.M. Chang, and P.C. Doerschuk. Application of multiresolution pattern classification to steel bridge coating assessment. *J. Comput. Civ. Eng.*, pages pp. 244–251, 2002.

[213] P.H. Chen, Y.C. Chang, and L.M. Chang. Artificial intelligence application to bridge painting assessment. *Automation in Construction*, pages pp. 431–445, 2003.

[214] P.H. Chen, Y.C. Yang, and L.M. Chang. Automated bridge coating defect recognition using adaptive ellipse approach. *Automation in Construction*, pages pp. 632–643, 2009.

[215] P.H. Chen, H.K. Shen, C.Y. Lei, and L.M. Chang. Support-vector-machine-based method for automated steel bridge rust assessment. *Automation in Construction*, pages pp. 9–19, 2012.

[216] P.H. Chen, Y.C. Yang, and L.M. Chang. Illumination adjustment for bridge coating images using bemd-morphology approach (bma). *Automation in Construction*, pages pp. 475–484, 2010.

[217] P.H. Chen, Y.C. Yang, and L.M. Chang. Box-and-ellipse-based anfis for bridge coating assessment. *J. Comput. Civ. Eng.*, pages pp. 389–398, 2010.

[218] H.K. Shen, P.H. Chen, and L.M. Chang. Automated steel bridge coating rust defect recognition method based on color and texture feature. *Autom. Constr.*, page pp. 338–356, 2013.

[219] B.N. Nelson, P. Slebodnick, E.J. Lemieux, W. Singletona, M. Krupab, K. Lucasb, D. Thomasc, and A. Seelingerc. Wavelet processing for image de-noising

and edge detection in automatic corrosion detection algorithms used in shipboard ballast tank video inspection systems. *Proc. SPIE*, pages pp. 134–145, 2001.

[220] H. Son, N. Hwang, C. Kim, and C. Kim. Rapid and automated determination of rusted surface areas of a steel bridge for robotic maintenance systems. *Automation in Construction*, pages pp. 13–24, 2014.

[221] S. Ghanta, T. Karp, and S. Lee. Wavelet domain detection of rust in steel bridge images. *IEEE Int. Conf. Acoust. Speech Sig. Process. (ICASSP)*, pages pp. 1–6, 2011.

[222] Z.W. Wang, M. Zhou, G. Slabaugh, J. Zhai, and T. Fang. Automatic detection of bridge deck condition from ground penetrating radar images. *IEEE Trans. Autom. Sci. Eng.*, 8:633–640, 2010.

[223] P. Gamba and S. Lossani. Neural detection of pipe signatures in ground penetrating radar images. *IEEE Trans. Geosci. Remote Sens*, 38:790–797, 2000.

[224] C. Yuan, S. Li, H. Cai, and V.R. Kamat. Gpr signature detection and decomposition for mapping buried utilities with complex spatial configuration. *J. Comput. Civ. Eng.*, 32, 2018.

[225] M.R. Shaw, S.G. Millard, T.C.K. Molyneaux, M.J. Taylor, and J.H. Bungey. Location of steel reinforcement in concrete using ground penetrating radar and neural networks. *NDT and E Int.*, 38:203–212, 2005.

[226] A. Simi, G. Manacorda, and A. Benedetto. Bridge deck survey with high resolution ground penetrating radar. *In Proceedings of the 2012 14th International Conference on Ground Penetrating Radar (GPR)*, Shanghai, China(4–8 June): pp. 489–495, 2012.

[227] L. Capineri, P. Grande, and J.A.G. Temple. Advanced image-processing technique for real-time interpretation of ground-penetrating radar images. *Int. J. Imaging Syst. Technol*, 9:51–59, 1998.

[228] G. Borgioli, L. Capineri, P. Falorni, S. Matucci, and C.G. Windsor. The detection of buried pipes from time-of-flight radar data. *IEEE Trans. Geosci. Remote Sens.*, 46:2254–2266, 2008.

[229] S. Delbo, P. Gamba, and D. Roccato. A fuzzy shell clustering approach to recognize hyperbolic signatures in subsurface radar images. *IEEE Trans. Geosci. Remote Sens.*, 38:1447–1451, 2000.

[230] C. Maas and J. Schmalzl. Using pattern recognition to automatically localize reflection hyperbolas in data from ground penetrating radar. *Comput. Geosci.*, 58:116–125, 2013.

[231] H. Chen and A. Cohn. Probabilistic robust hyperbola mixture model for interpreting ground penetrating radar data. *In Proceedings of the 2010 International Joint Conference on Neural Networks (IJCNN)*, Barcelona, Spain(18–23 July): pp. 1–8, 2010.

[232] B. Chaudhuri and G. Samanta. Elliptic fit of objects in two and three dimensions by moment of inertia optimization. *Pattern Recognit. Lett.*, 12:1–7, 1991.

[233] S. Birkenfeld. Automatic detection of reflexion hyperbolas in gpr data with neural networks. *In Proceedings of the World Automation Congress*, Kyoto, Japan(19–23 September):pp. 1–6., 2010.

[234] H. Ahmed, H. M. La, and K. Tran. Rebar detection and localization for bridge deck inspection and evaluation using deep residual network. *Automation in Construction*, 120:1–18, 2020.

[235] L.E. Besaw and P.J. Stimac. Deep convolutional neural networks for classifying gpr b-scans. *In Proceedings of the Conference on Detection and Sensing of Mines, Explosive Objects*, Baltimore, MD, USA(20–24 April):pp. 1–10, 2015.

[236] H. Harkat, A. Ruano, M. Ruano, and S.B. Dosse. Gpr target detection using a neural network classifier designed by a multi-objective genetic algorithm. *Appl. Soft Comput.*, 79:310–325, 2019.

[237] P. Martinez, M. Al-Hussein, and R Ahmad. A scientometric analysis and critical review of computer vision applications for construction. *Autom. Constr.*, 107, 2019.

[238] A survey of automation-enabled human-in-the-loop systems for infrastructure visual inspection. Agnisarman, s. and lopes, s. and madathil, k.c. and piratla, k. and gramopadhye, a. *Autom. Constr.*, 97:52–76, 2019.

[239] Q. Chen, B.G. De Soto, and B.T. Adey. Construction automation: Research areas, industry concerns and suggestions for advancement. *Autom. Constr.*, 94: 22–38, 2018.

[240] H. Ahmed, C. P. Le, and H. M. La. Pixel-level classification for bridge deck rebar detection and localization using multi-stage deep encoder-decoder network. *(Submitted to Automation in Construction)*, 2022.

[241] H. Ahmed, H. M. La, and A. Tavakkoli. Use of deep encoder-decoder network for sub-surface inspection and evaluation of bridge decks. *In: Proceedings of 13th International Workshop on Structural Health Monitoring (IWHSM)*, pages pp. 832–841, 2021.

[242] Yu He, Kechen Song, Qinggang Meng, and Yunhui Yan. An end-to-end steel surface defect detection approach via fusing multiple hierarchical features. *IEEE Transactions on Instrumentation and Measurement*, pages pp. 1493–1515, 2020.

[243] Wenyan Wang, Chunfeng Mi, Ziheng Wu, Kun Lu, Hongming Long, Baigen Pan, Dan Li, Jun Zhang, Peng Chen, and Bing Wang. A real-time steel surface defect detection approach with high accuracy. *IEEE Transactions on Instrumentation and Measurement*, pages pp. 5005610–5005620, 2022.

[244] Kun Liu, Nana Luo, Aimei Li, Hasan Sajid Ying Tian, and Haiyong Chen. A new self-reference image decomposition algorithm for strip steel surface defect detection. *IEEE Transactions on Instrumentation and Measurement*, pages pp. 4732–4742, 2020.

[245] H. Ahmed, S. T. Nguyen, D. La, C. P. Le, and H. M. La. Multi-directional bicycle robot for bridge inspection with steel defect detection system. *Accepted to the 2022 IEEE International Conference on Intelligent Robots and Systems (IROS)*, 2022.

[246] H Ahmed and H. M. La. Steel defect detection in bridges using deep encoder-decoder networks. *In: Proceedings of 13th International Workshop on Structural Health Monitoring (IWSHM)*, pages pp. 842–849, 2021.

[247] H. M. La, N. Gucunski, S.-H. Kee, and L.V. Nguyen. Data analysis and visualization for the bridge deck inspection and evaluation robotic system. *Visualization in Engineering*, 3(1):1–16, 2015.

[248] H. M. La, N. Gucunski, S.H. Kee, and L.V. Nguyen. Visual and acoustic data analysis for the bridge deck inspection robotic system. In *The 31st International Symposium on Automation and Robotics in Construction and Mining (ISARC)*, pages 50–57, July 2014.

[249] Kaiming He, Xiangyu Zhang, Shaoqing Ren, and Jian Sun. Deep residual learning for image recognition. In *Proceedings of IEEE Conference on Computer Vision and Pattern Recognition*, pages 770–778. IEEE, 2016.

[250] Liang-Chieh Chen, George Papandreou, Iasonas Kokkinos, Kevin Murphy, and Alan Yuille. Deeplab: Semantic image segmentation with deep convolutional nets, atrous convolution, and fully connected crfs. In *arXiv preprint: 1606.00915*, pages 1–8. arXiv, 2017.

[251] S. Gibb and H.M. La. Automated rebar detection for ground-penetrating radar. *In Proceedings of the 12th International Symposium on Visual Computing*, Las Vegas, NV, USA(12–14 December):815–825, 2016.

[252] G. Huang, Z. Liu, L. van der Maaten, and K. Q. Weinberger. Densely connected convolutional networks. In *In Proceedings of IEEE International Conference on Computer Vision and Pattern Recognition (CVPR)*, pages pp. 4700–4709, 2017.

[253] V Badrinarayanan, A Kendall, and R Cipolla. Segnet: A deep convolutional encoder-decoder architecture for image segmentation. In *IEEE Transactions on Pattern Recognition and Machine Intelligence*, pages vol. 39, no. 12, pp. 2481–2496, 2017.

[254] K. He, X. Zhang, S. Ren, and J. Sun. Spatial pyramid pooling in deep convolutional networks for visual recognition. *IEEE Transactions on Pattern Analysis and Machine Intelligence*, pages 1904–1925, 2015. doi: https://doi.org/10.1007/978-3-319-10578-9_23[Accessedon22June2022].

[255] New zealand bridge inspection and maintenance manual. `https://www.nzta.govt.nz/assets/resources/bridge-inspection-maintenance-manual/docs/4-structural-steel.pdf`, 2001. Accessed: 2022-08-08.

[256] Maria João Correia, Hugo Perneta, Manuela Salta, Laurent Gaillet, Hugo Patrício, and Franck Schoefs. Duratinnet: Maintenance and repair of transport infrastructure technical guide. steel structure- part iii, deterioration. *Lisbon, Portugal. European Union.*, 2012.

[257] G. D. Shanafelt and W. B. Horn. Guidelines for evaluation and repair of damaged steel bridge members. *National Cooperative Highway Research Program Report 271. Washington, DC. Transportation Research Board*, 1984.

[258] Mingxing Tan and Quoc Le. Efficientnet: Rethinking model scaling for convolutional neural networks. In *arXiv preprint: 1707.03718*, pages 1–8. arXiv, 2017.

[259] Radosavovic Ilija, Raj Prateek Kosaraju, Ross Girshick, Kaiming He, and Poitr Dollar. Designing network design spaces. In *arXiv preprint: 2003.13678*, pages 1–8. arXiv, 2020.

[260] Abishek Chaurasia and Eugenio Culurciello. Linknet: Exploiting encoder representations for efficient semantic segmentation. In *arXiv preprint: 1707.03718*, pages 1–8. arXiv, 2017.

[261] F. F. Feliciano, R. Leta, and F. B. Mainier. Texture digital analysis for corrosion monitoring. *Corrosion Science*, pages 138–147, 2015.

[262] F. Bonnin-Pascual and A Ortiz. Corrosion detection for automated visual inspection. *Development of Corrosion Protection*, INTECH:619–632, 2014.